HYDROTHERMAL SYNTHESIS, PHYISCO-CHEMICAL CHARACTERIZATION OF OMEGA ZEOLITE

A THESIS

SUBMITTED TO THE

UNIVERSITY OF POONA

FOR THE DEGREE OF

DOCTOR OF PHILOSOPHY

(IN CHEMISTRY)

BY

SUBHASH PANDURANG MIRAJKAR

CATALYSIS DIVISION

NATIONAL CHEMICAL LABORATORY

PUNE - 411 008, INDIA.

MAY 1996

DEDICATED TO MY BELOVED BROTHER

(Sharad P. Mirajkar)

AND

MY LATE PARENTS

CERTIFICATE

Certified that the work incorporated in the thesis "**HYDROTHERMAL SYNTHESIS, PHYSICO-CHEMICAL CHARACTERIZATION OF OMEGA ZEOLITE**" submitted by Mr. Subhash Pandurang Mirajkar, for the degree of Doctor of Philosophy, was carried out by the candidate under my supervision in the Catalysis Division, National Chemical Laboratory, Pune, India. Materials obtained from other sources have been duly acknowledged in the thesis.

B. S. Rao

[B.S. RAO]

(Research Guide)

ACKNOWLEDGEMENTS

I wish to express my sincere gratitude to Dr. B.S. Rao, Scientist E-II, National Chemical Laboratory, Pune, for his invaluable guidance and help rendered throughout the course of this investigation without which I would not have completed this thesis successfully.

I am deeply indebted to Dr. A.V. Ramaswamy, Head, Catalysis Division, for providing me all facilities to conduct research.

I am grateful to Dr. V.P. Shiralkar for his stimulating discussions, personal help and invaluable suggestions during the course of my research work without which it would have been very difficult for me to present this thesis.

I am indebted to Dr. S.G. Hegde, Dr. S. Sivasanker, Dr. Veda Ramaswamy and Mr. Puyam Singh of their help during the study. I am also thankful to all other scientific and non-scientific staffs and friends in the Catalysis Division, NCL, Pune, for extending their co-operation in all ways to complete my research work successfully.

It would be unfair if I forget Dr. C. Naccache, CNRS, France, for providing me the MAS NMR spectra for my samples.

I would be failing in my duty if donot thank my family members, my uncle, my wife, Swathi, and sons, Suhan and Sanket for their love, unfailing support, tremendous patience and faith in education and constant encouragement during the course of my research career whithout which, it would have been impossible for me to complete and present this thesis in a final form successfully.

I thank the Director, NCL, Pune, Dr. P. Ratnasamy, for permitting me to submit this work in the form of a thesis and constant encourangement throughout the course of my research.

[S. P. MIRAJKAR]

CONTENTS

Chapter I

General Introduction

1.1 INTRODUCTION

A Swedish mineralogist, A.F. Cronstedt[1] first in 1756 reported the occurrence of natural mineral for which he coined the term 'zeolite' from the Greek words "Zeo"; to boil and "lithos", stone. Damour[2] noticed that zeolites could be reversibly dehydrated without alteration of the structure and morphology. The role of water as a mineralizing agent, aided by alkaline conditions, drew the attention of mineralogists to hydrothermal reactions and synthesis. In 1962, the commercialization of these natural zeolites namely chabazite, erionite, mordenite and clinoptilolite commenced for various applications[3]. The zeolites are interesting materials because of their uniform pore size (Fig. 1.1). It was McBain, who proposed the term "Molecular sieves" to describe a class of materials that exhibited selective adsorption properties[4]. Molecular sieves separate components of a mixture on the basis of molecular size and shape differences. However, Barrer[5] was the first to show the molecular sieve behavior of zeolites and their potential in molecular sieving separation. Zeolites have found widespread use as adsorbents, ion exchangers, detergent builders and catalysts.

Zeolites are broadly defined as microporous, crystalline hydrated aluminosilicates with framework structure enclosing cavities and channels which are occupied by large ions and water molecules both of which have considerable freedom of movement permitting ion-exchange and reversible dehydration. Structurally, they possess a framework based on an infinitely extending three- dimensional network of SiO_4 and AlO_4 tetrahedra linked through oxygen atoms forming a rigid three-dimensional structure. The negative charge on the AlO_4 tetrahedra is compensated by cations resulting in an electrically neutral framework. Thus an empirical formula for zeolites can be given as,

$$M_{x/n}\,[(AlO_2)_x\,(SiO_2)_y].\,zH_2O$$

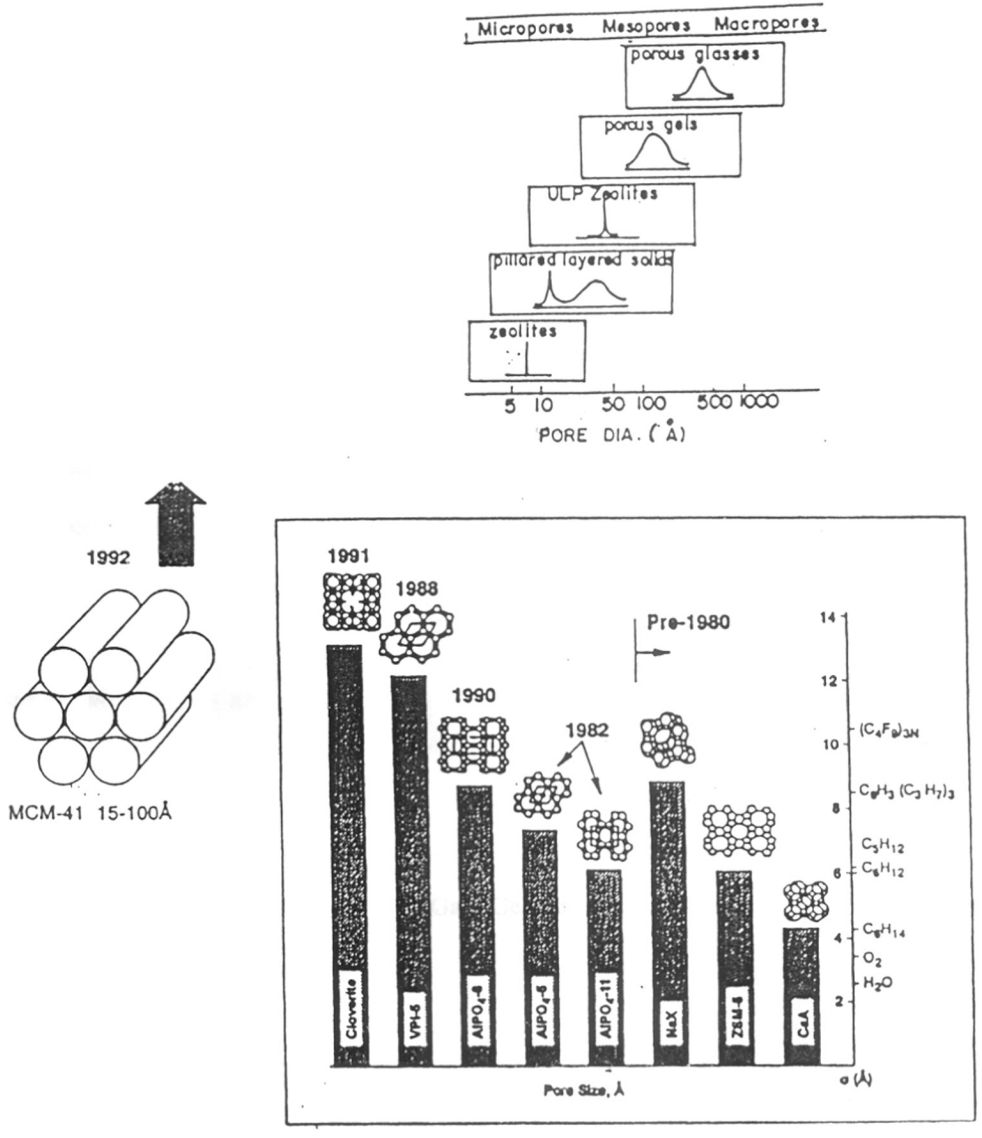

FIG. 1.1 : CORRELATION BETWEEN PORE SIZE OF MOLECULAR SIEVES AND THE DIAMETER (Å) OF VARIOUS MOLECULES

Where 'n' represents the charge on the exchangeable cation M, z is the number of water molecules. The framework composition is represented by square bracket and (x+y) is the total number of tetrahedra in the unit cell. In general (y/x) > 1 and controls the physico-chemical properties of zeolites.

1.2 ZEOLITE STRUCTURE

The primary building unit (PBU) of the zeolite structure is a tetrahedron of four oxygen atoms surrounding a central Si or Al atom. These tetrahedra are connected through their shared oxygen atoms to give rise to wide range of secondary building units (SBU). In turn, these SBUs are interconnected to give polyhedra which continue in various combinations to form various three dimensional structures of zeolites, which are shown in Fig. 1.2.

1.3 NOMENCLATURE

There is no systematic nomenclature developed for molecular sieve materials. The International Zeolite Association Structure Commission and IUPAC have assigned structural codes to the known synthetic and natural zeolites[6,7]. Designations consisting of three capital letters have been used to identify structure types. The codes for the zeolite identification have generally been derived from the names of the type species and do not include numbers and characters other than Roman letters. Structure type codes do not depend on the chemical composition, distribution of various possible T atoms (Si^{4+}, Al^{3+}, P^{5+}, Ga^{3+}, Ge^{4+}, B^{3+}, Be^{2+}, Ti^{4+} etc.), cell dimensions or crystal symmetry.

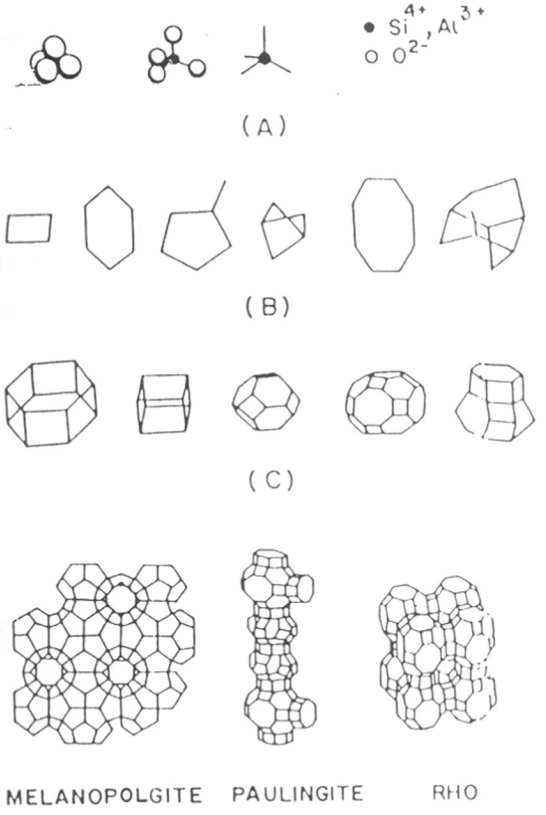

FIG. 1.2 : (A) PRIMARY UNITS, (B) SECONDARY UNITS,
(C) TERTIARY UNITS AND (D) ZEOLITE STRUCTURES

1.4 CLASSIFICATION

Classification of zeolites has been made on the basis of their morphology[8], crystal structure[9-11], chemical composition[12], effective pore diameter[13,14] and natural occurrence. The classification based on morphology was made by Bragg[8]. This classification was further modified on the basis of secondary building units present in the crystal structure by Meier[9] and Barrer[10].

On the basis of their chemical composition or silica to alumina ratio, zeolites are classified as (1) "low", (2) "intermediate", (3) "high" silica zeolites, (4) "silica" molecular sieves as shown in Table 1.1. Thermal stability increases from low silica zeolites to high silica molecular sieves. The high silica zeolites are hydrophobic in nature while low silica zeolites are more hydrophilic. The acidity tends to increase in strength with increase in Si/Al ratio. The cation concentration and ion exchange capacity which is proportional in Al content decreases with increase in Si/Al ratio. The structure of the low silica zeolites are formed predominantly with 4, 6 and 8 rings of tetrahedra. In intermediate silica zeolites, the onset of 5 rings in omega and mordenite zeolites is observed. In the high silica zeolite structure predominants of 5 ring tetrahedra are found.

Zeolites are also classified according to the pore opening, defined as the number T (or TO_4) units that shape the channel. Barrer[13] has made such a classification of zeolite into five groups. A modified classification into three groups, according to the largest ring present in the structure of each zeolite (Table 1.2) was proposed by Sand[14]. Recently, Davis *et al.*[15] discovered a very large pore aluminophosphate molecular sieve called VPI-5 containing 18 membered ring pore openings. Very recently, an extra large pore gallophosphate molecular sieve containing 20-membered ring pore opening, called cloverite has been discovered[16].

Table 1.1 : Classification of zeolites according to chemical composition*

Class	Si/Al ratio		Examples
"Low" Silica	1.0-1.5		A, X, Sodalite
"Intermediate" Silica	2.0-5.0	(a)	Natural Zeolites : Erionite, Chabazite, Clinoptilolite, Mordenite
		(b)	Synthetic zeolites : X, Y, L, Large-port Mordenite, Omega.
"High" Silica	10-several thousand	(a)	By thermochemical framework modification : highly siliceous variants of Y, mordenite erionite.
		(b)	By direct synthesis : ZSM-5, ZSM-11, EU-1, EU-2, Beta etc.
Silica molecular sieves	Several thousand to ∞		silicalite

*Ref. 12

Table 1.2 : Classification of zeolites according to the largest pore opening*

Small port (8 membered)	Intermediate port (10 membered)	Large port (12 membered)
Zeolite A	ZSM-5	Cancrinite
ZK-5	ZSM-11	Faujasite
Bikitaite	ZSM-23	Linde X,Y,L
Brewsterite	ZSM-22 (Theta-1)	Gmelinite
Chabazite	ZSM-48 (EU-2)	Mazzite
TMA-E	ZSM-50 (EU-1)	Mordenite
Edingtonite	Dachiardite	Offretite
Erionite	Epistilbite	Omega
Gismondine	Ferrierite	ZSM-12
Merlinolite	Stilbite	Beta
Levynite	Heulandite	NCL-1
Laumontite		
Natrolite		
Paulingite		
Phillipsite		
Rho		
Thomsonite		
Yugawarolite		

*Ref.14

1.5 ZEOLITE SYNTHESIS

Zeolites occur in nature in vugs and vesicles of basaltic lava, in specific kind of rocks subjected to moderate geological temperature, pressure and in altered and reacted volcanic ash deposits. The formation of such natural zeolites with volcanic glass and saline water as reactants must have occurred in temperature range 300-350K and at pH > 13, requiring several years of crystallization[17,18].

Reports of synthesis upto 1937 have been documented in the review of hydrothermal reactions by Morey and Ingerson[19]. Systematic hydrothermal studies began in 1940's by R.M. Barrer[20], following the major demonstration of separations utilizing molecular action and sorption by zeolites.

Zeolites are synthesized in hydrothermal condition by combination of certain basic oxides like K_2O and Na_2O with Al_2O_3 and SiO_2. These zeolite can be synthesized in many varieties, structure, composition and properties. Generally, zeolite crystallization is a nucleation controlled process, occurring in homogeneous alkaline, aqueous gels, in the temperature range of 348K to 523K. Different silica and alumina sources can be used in formulating a gel, and final product obtained is often dependent on the source chosen and the history of it.

In 1960's the organic quaternary cations (templates) were introduced in synthesis of zeolite[21]. The specific function of these organics is highly dependent on the details of the experiment. Normally, addition of organics to a reaction mixture can lead to four variations: (i) A different zeolite structure is obtained, (ii) crystallization rate is enhanced (or inhibited) (iii) same framework but a change in chemical composition is obtained (iv) a change in texture is observed. The manner in which such templates affect the zeolite crystallization is a complex process. Alkali metal cations also play an important role in the formation of crystallite size and morphology of the zeolite during the synthesis.

The actual mechanism of zeolite crystallization is not well understood because of the complexity of the interactions occuring in the hydrothermal magma. Sand[22] has summarized the simultaneous reactions that can occur during synthesis as

* precipitation of a gel phase.
* dissolution of the gel.
* nucleation of zeolite(s).
* continued crystallization and crystal growth of the zeolite(s).
* dissolution of the initial metastable phase(s).
* nucleation of the more "stable" metastable phase or phases.
* continued crystallization and crystal growth of the new crystalline phase(s) while the initial crystals are dissolved.
* dissolution of metastable phase(s).
* nucleation of the equilibrium phase(s).
* crystallization and crystal growth of the final crystalline phases.

From the experimental evidence, two mechanisms have been suggested for the transformation of gels into zeolites. Kerr[23,24] reported on the crystallization of zeolites A and X in specific systems in which he postulated the growth of crystals from solution. McNicol *et al.*[25] concluded that the nucleation and crystal growth of the zeolite takes place within the gel phase. It has been evidenced for example by crystallizing zeolites from clear solutions under hot stage with the help of microscope[26]. The nucleation and subsequent crystallization can occur readily in the solution. However, in solution phase transformation into crystallization starts at the liquid-solid interface. There are other physical variables such as order of mixing, rates of addition of aluminate to silicate solution and vice versa and the rate of agitation.

1.6 MODIFICATION OF ZEOLITES

To use the zeolites in different reactions it is necessary to modify them as per requirement and also to improve thermal stability and acidic strength.

1.6.1. Isomorphous substitution

The modification of zeolites by isomorphous substitution imparts additional properties to zeolite which may lead to interesting catalytic applications. The first isomorphous replacement in the lattice was reported by Goldsmith[27] in which Si^{4+} was replaced by Ge^{4+}. Recently isomorphous substitution of Si by elements such as B[28-30], Fe[29], Ga[29], Ti[31], V[32] etc. has been largely studied and has been shown to result in difference in the catalytic properties. Barrer[33] classified four types of isomorphous replacement in zeolites. (1) Cation exchange (2) Introduction of isomorphous element in the zeolite framework (3) Isomorphous replacement of isotopes and 4) Replacement of intracrystalline salts and molecular water. Tielen *et al.*[34] reviewed the catalytic applications of T-atom substitutions. Thereafter a series of Union Carbide patents and papers have described large numbers of new aluminophosphate molecular sieves (AlPO) containing equal amount of Al^{3+} and P^{5+} ions in the lattice. Metallo aluminophosphates (MeAlPO) have been reported[35,36] by isomorphous substitution by Co^{2+}, Fe^{3+}, Mg^{2+}, Zn^{2+}, Be^{2+}, B^{3+}, Ga^{3+}, Cr^{3+}, Ti^{4+}, V^{4+} and Mo^{3+} in the framework of AlPO. In other class of molecular sieves silicoalumino phosphates (SAPO) in which Si is substituted for Al or P or for both in AlPO framework.

Isomorphous substitution can be achieved either by direct hydrothermal synthesis or by post synthesis methods. The tetrahedral occupancy of the substituted metal ion can be characterized by techniques such as ion exchange capacities, XRD, IR, MAS-NMR, ESR, UV-VIS, XPS, Photoacoustic spectroscopy and by catalytic test of hydrocarbon conversion reactions.

1.6.2. Cation exchange

This property is a function of the amount of aluminium present in the framework of zeolite. Most of the zeolites are synthesized in a cationic form in which the positively charged cations balance the negatively charged framework system. These extraframework cations can be replaced by other cations[11]. The rate and degree of cation exchange depends on the following factors

1) The type of cation being exchanged, the size and charge.
2) The nature, size and strength of any cation co-ordination complex
3) The temperature of the ion exchange treatment
4) The thermal treatment of zeolite, before and after exchange.
5) The structural properties of the zeolite and its silica/alumina ratio.
6) The locations of the cations in the zeolite structure.
7) The concentration of the cation exchange solution.
8) The previous treatment of the zeolite.

1.6.3. Metal loading

In many reactions eg. involving hydrogenation or oxidation, it is necessary to have additional components in the catalyst to perform the total or partial catalytic functions. Such components are frequently metals, their oxides, or sulfides similar to those used in non-zeolite amorphous catalyst systems. The loading is done by ion exchange of zeolite from solution, impregnation from solution, adsorption from the gas phase and co-mulling during the catalyst formation of the solid metal component in its solution. Metals which are desirable for the introduction into the zeolite include the common hydrogenation and oxidation components such as Ni, Co, Pt, Ag, Pd, Mo, W, Cr etc.

1.7 ACIDITY IN ZEOLITES

Acidity in zeolite is a very important parameter and can be modified as per the need. Substitution of trivalent metal atoms such as Al, Ga, Fe, B etc. for Si in the zeolite framework generates the potential for acidic activity. When the charge compensating cation is hydrogen atom (proton) the zeolite framework exhibits the capacity to act as a proton donor as Brönsted acid[37-39].

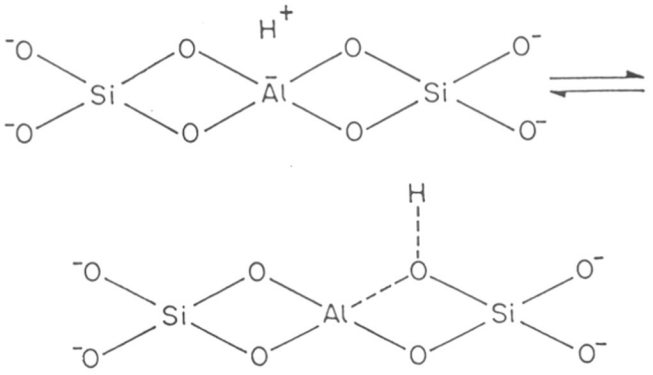

When the zeolite is heated to 823K , Si-O-Al bond breaks giving rise to Lewis acid site and water.

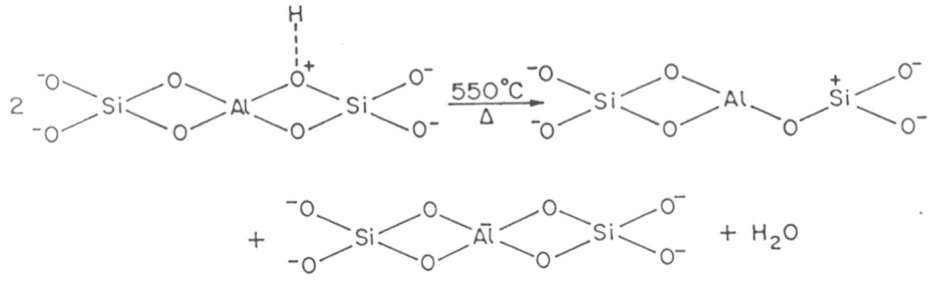

In zeolites both Lewis and Brönsted acid sites coexist. Dissociation energy calculations[40] show that between the bridging and terminal hydroxyl groups the former was found to be more acidic than the latter. This conclusion is supported by lower vibrational frequency of the bridging hydroxyl groups[41].

1.8 SHAPE SELECTIVITY IN ZEOLITES

The actual pore size within a given ring structure can be varied within limits by the cation present in the system. Weisz and Frilette[42] were the first to describe the shape selectivity. The pore size and shape may affect the selectivity of a reaction in four ways.

1.8.1. Reactant shape selectivity

When the operative size of the zeolite is such that it admits only certain smaller molecules from the reactants and excludes larger molecules (Fig.1.3a), and hence in a reaction mixture, only the smaller molecules react effectively.

1.8.2. Product shape selectivity

When some of the compounds formed within the pores are too bulky to diffuse out as products. The bulky product molecules will either be converted to smaller molecules and diffuse out or they will block the catalyst pores resulting in the deactivation of the catalyst. For example, p-xylene is produced preferentially in modified zeolites over the more bulky o- and m- isomers due to the pore diameter restrictions. Thus, the formation of products in this are diffusion reaction interaction[43] thereby favoured (Fig. 1.3 b) and creating a selectivity towards the product of certain dimension.

1.8.3. Restricted transition state shape selectivity

This occurs when certain reactions are prevented because of corresponding trnsition state requires more space than is available in the zeolite pore. Diffusing reactants and products in this situation are not hindered nor are reactions involving smaller transition state (Fig.1.3 c).

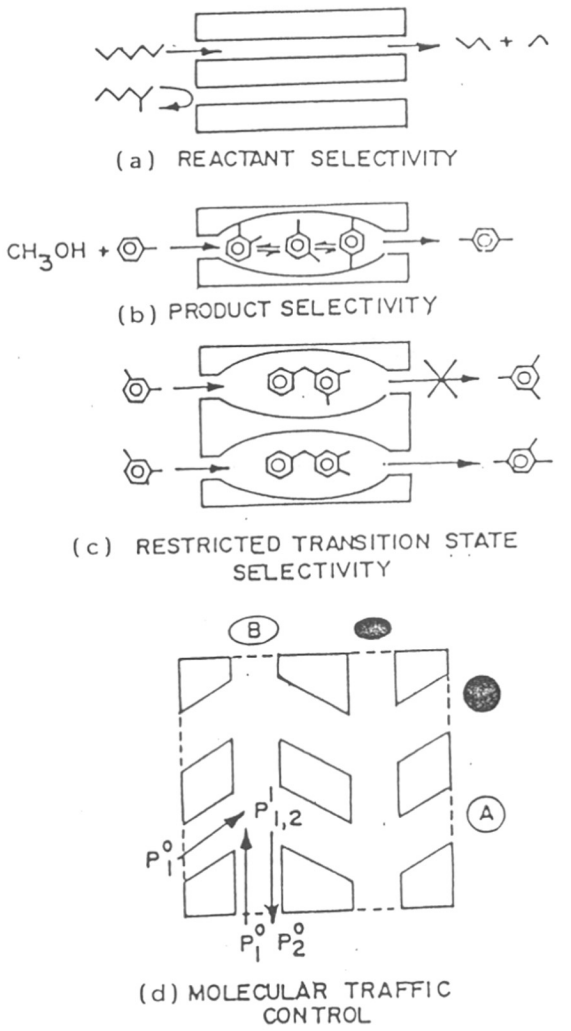

FIG. 1.3 : SHAPE SELECTIVITY IN ZEOLITES

1.8.4 Molecular traffic control

A new type of shape selectivity in zeolites, containing intersecting channel of different diameters has been proposed by Derouane and Gabelica[44]. In the case of zeolites with more than one type of intersecting channels, the reactants enter preferentially through one set of channels and the products diffuse out through the other, thus minimizing counter diffusion (Fig. 1.3 d). Several model reactions have been used to determine the shape selectivity of zeolites quantitatively.

(1) Constraint Index[45] (2) Refined constraint Index[46] (3) Spaciousness Index[47] (4) o-p-index in m-xylene isomerization[48] (5) DEB distribution in EB disproportionation[49].

1.9 STRUCTURAL FEATURES OF ZEOLITE OMEGA

The zeolite omega was initially synthesized by Union Carbide Corporation[50a]. The crystal structure of zeolite omega was first proposed by Barrer and Villiger[51] in 1969. Its framework structure is apparently same as that of the mineral mazzite and the synthetic zeolite ZSM-4[52-53] .

The framework structure of omega consists of gmelinite cages (Fig. 1.4). These cages are joined in column by shared 6-ring faces, the columns running parallel to the c-axis. The columns of gmelinite cages are also joined laterally to produce restricted cavities between pairs of cages. The lateral joining of six such columns creates wide channels running parallel to c axis.

The topology of zeolite omega consists of 1-dimensional channel structure. There are two kinds of channels; a circular 12-member channel with a diameter of 7.4 Å and elliptical 8-member channel with diameter 5.6 x 3.4Å. These channels are interconnected by small windows which do not allow diffusion of any molecules through them. Thus the pore architecture of zeolite omega is well-suited for tailoring the adsorption applications.

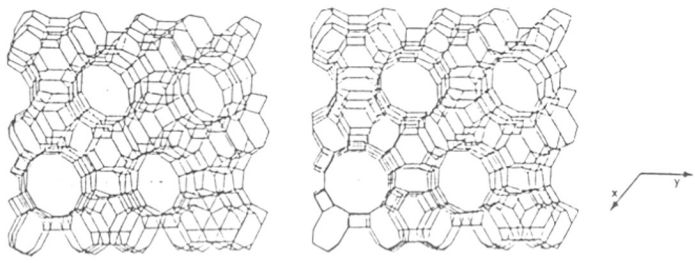

framework viewed along [001]

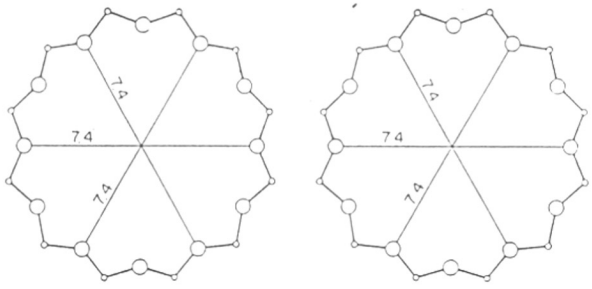

12-ring viewed along [001]

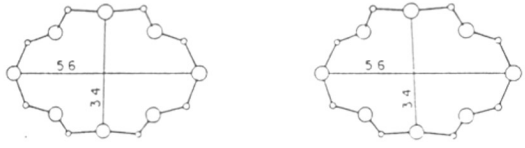

8-ring viewed along [001]

FIG. 1.4 : STRUCTURE OF ZEOLITE OMEGA

The framework density is 16.1 T / 1000 $Å^3$, which is typical for large pore zeolite. The silica/alumina ratio is also low indicating the possibility of several extra framework cations. However, due to the absence of any cage-like structures, the extraframework cations are not localized at any characteristic sites but they are present in the channels. Usually the water molecules are bonded to the extraframework cations. Cumulative structural data of zeolite omega are tabulated in Table 1.3. When gallium is incorporated in the framework, the crystal structure remains unaffected as far as symmetry[54] is concerned. Even though, omega is a zeolite with high acidity, not much work has been carried out to evaluate its potential use as a catalytic material.

1.10 PHYSICO-CHEMICAL CHARACTERIZATION OF ZEOLITES

1.10.1. X-Ray diffraction (XRD)

Among the different spectroscopic techniques employed for the structural evaluation of zeolites, the X-ray diffraction is one of the most important and useful techniques to identify (1) zeolite structure[55] (2) purity of the zeolite (3) % crystallinity (4) unit cell parameters (5) crystallite size and (6) to understand the kinetics of mechanism of crystallization. As the powder pattern is the finger print of the individual zeolite structure, phase purity and % crystallinity of the synthesized catalyst can be compared with the reference catalyst. The use of unit cell volume studies in confirming the structural incorporation of the elements other than Al, can be correlated with the change in unit cell volume[56].

1.10.2. Infra-red spectroscopy (IR)

Infra-red spectroscopy is one of the important tools. Various types of informations, on the nature of the active sites of the catalyst, the structural transformation in the catalyst, the identification of surface groups, the surface acidic properties of catalyst and the identification of the intermediates in the surface transformations can be obtained by the application of this

Table 1.3 Cumulative structural data of omega zeolite*

CHEMICAL COMPOSITION	
Typical Oxide Formula	$(Na, TMA)_2O : Al_2O_3 : 7SiO_2 : 5H_2O$
Typical Unit Cell content	$Na_{6.8}TMA_{1.2}[(AlO_2)_8(SiO_2)_{28}]21H_2O$
Variation	Si/Al = 2.5-6.0
	Na/Al = 0.5-1.5, TMA/Al = 0.7
CRYSTALLOGRAPHIC DATA	
Symmetry	Hexagonal
Density	2.16 g/cc
Space group	P 6_3/mmc
Unit Cell Volume	2160 Å^3
Unit Cell Constants	a = 18.15 Å, c = 7.59 Å
STRUCTURAL PROPERTIES	
Framework : Stereo 2.15	14-hedron of gmelinite-type linked by oxygen bridges in columns ∥ to c-axix
Secondary Building Units	S4R and D12R
Void volume	0.38 cc/cc
Cage type	14-hedron (II)
Framework dendity	1.65g/cc
Channel System	One-dimensional ∥ to c, 7.5 Å
Free Apertures	12 rings, 7.5 Å ∥
Cation Locations	TMA in 14-hedron cages; Na^+ at 0, 1/2, 1/4 between cages

* Ref. 50b

technique. Flanigen[57] and Ward[58] discussed the IR studies in the framework hydroxyl regions. Maroni[59] *et al.* and Janin[60] *et al.* have discussed the use of different probe molecules to study the acidity of zeolites by diffuse reflectance and transmission techniques. Baker[61] *et al.* studied the extraframework cations with far IR spectroscopy. The IR spectrum in the range of 200 - 1300 cm^{-1} is used to characterize and to differentiate various zeolite framework structure. These vibrations can be divided into structure sensitive (external linkages) and structure insensitive (internal tetrahedra) bands. Flanigen[62] reported the following positions of these bands.

Structure sensitive vibrations

- asymmetric stretch	1050 - 1150 cm^{-1}
- symmetric stretch	750 - 820 cm^{-1}
- double ring vibrations	500 - 650 cm^{-1}
- pore opening vibrations	300 - 420 cm^{-1}

Structure insensitive vibrations

- asymmetric stretch	950 - 1250 cm^{-1}
- symmetric stretch	650 - 720 cm^{-1}
- T-O bending	420 - 500 cm^{-1}

Crystallization of the zeolite during the synthesis can be studied by monitoring the changes in important IR vibration frequencies and their comparison with those of the reactants.

Structural incorporation of B, Fe, Ga, etc. in place of Al causes shift in the bands position due to the Brönsted acidity which correlates well with resultant acidity[63,64]. The IR absorption bands at around 3600 - 3700 cm^{-1} confirms the presence of the silanol[65,66] and/or bridged hydroxyl groups in the zeolites and their Brönsted acidity can be compared.

1.10.3. Nuclear magnetic resonance spectroscopy (NMR)

The great promise of this technique in investigating structural properties of zeolite catalyst was recognized immediately after the development of high resolution solid state NMR technique. Lippmaa *et al.*[67] were the first to demonstrate that ^{29}Si MAS-NMR (Magic Angle Spinning) spectra were sensitive to the nature and chemical environment of the atoms. This powerful technique is very useful in understanding the structural and physicochemical properties of the zeolites. Nagy and Derouane[68] reported the application of various NMR nuclei to study the zeolites. Much attention has been focussed on ^{29}Si and ^{27}Al MAS-NMR spectra in order to investigate (a) Si/Al ordering[69], (b) crystallographically equivalent and non-equivalent Si and Al ions in various sites[70,71], (c) framework Si/Al ratio[72], (d) the coordination number of Si and Al[73,74], (e) spectral correlation with Si-O-T bond angles[75] and Si-O bond lengths[76].

Solid state MAS-NMR spectroscopy for ^{29}Si, ^{27}Al can show evidence[69,70] for tetrahedrally coordinated atoms from the zeolite lattice and the concomitant deposition of octahedral Al, present in the pores of the zeolite. Thus, considerable knowledge has been obtained during the last few years about the structure of the zeolites from the study of their ^{29}Si, ^{27}Al, ^{71}Ga MAS-NMR spectra[77,78].

1.10.4. Thermal analysis

When crystalline zeolites are heated to elevated temperatures in air, they ultimately break down due to structural collapse resulting in the recrystallization to some non-zeolitic species and then formation of amorsphous solid. The different thermo-analytical curves (TG, DTA and DTG) are useful in evaluating thermal properties[79]. The shape and splitting of low temperature endotherm helps to identify the location of water molecules and also helps in studying the kinetics of dehydration of water molecules. Zeolites in general possess high

thermal stability. It is well known that thermal stability of zeolite framework structure increases with the increase in Si/Al ratio[80,81]. Breck[82] has summarized the thermal properties of various zeolites and reported that omega is stable upto 1023 K. The thermal behaviour of zeolite omega has been studied by Araya *et al.*[83]

1.10.5. Sorption and diffusion properties

Zeolites are microporous crystalline materials with ability to sorb selective molecules inside the channels and cavities. In zeolites usually, intracrystalline surface area constitute about 97 % of the total surface area. In 1846 Damour demonstrated that water could be reversibly removed from a zeolite without altering its crystalline framework. The reports[84,85] of sorption of gases and vapors by dehydrated zeolites started appearing since 1896. Barrer and co-workers[86,87] had extensively studied sorption of various gases and vapors on natural and synthetic zeolites. The selective adsorption of molecules in zeolite depends on

1. Molecular size of adsorbate
2. Polarizabilty and polarity of the adsorbate
3. Organophilicity and hydrophilicity of the zeolite host structure
4. Degree of unsaturation of organic adsorbate and
5. Polarizing power of the host cation

Studies on the sorption characteristics on zeolites can provide information about their (a) void volumes (b) size of pore opening, which depends on the ring size, (c) level of crystallinity and crystal size, (d) acidity, (e) diffusion properties and crystal blockage, if any.

Nitrogen sorption isotherm at low temperature, 77 K are useful in determining the micropore volume, pore size distribution and surface area of composite materials containing molecular sieves[90,91]. Adsorption and diffusion properties play an important role on the rate of chemical

reaction at the catalytic active sites. Barrer *et al.*[92] have given a detailed review on diffusion in zeolites. The diffusion in zeolites may be divided into three types viz., **Configurational, Knudsen** and **Bulk diffusion**.

1.11 CATALYSIS OVER ZEOLITES

Zeolites have advantages over conventional heterogeneous catalysts in many applications involving acid, acid-base, base, oxidation, reduction and polyfunctional catalysis. The main feature of the zeolite and molecular sieves to make them very useful as heterogeneous catalysts are

* Well defined crystalline structure.
* Good thermal stability.
* High internal surface area.
* Ion exchange properties.
* Ease of regeneration to initial activity.
* Well defined micropore system and shape selectivities.
* Ability to sorb and concentrate hydrocarbon.

The catalytic sites in aluminosilicate zeolites are mainly the Brönsted acid protons. As-synthesized zeolite can be converted into catalytically active H-form by different approaches. The first is the simple ion exchange of cations by protons from acidic solutions. But in this method, significant dealumination leading to the collapse of crystal structure occurs and hence, not preferred. The second method involves the replacement of cations (often Na) by ammonium ions, from solution containing ammonium salts followed by the thermal decomposition of ammonium form to the protonic form and ammonia. The strength and concentration of the acidic sites can also be modified by isomorphous substitution of trivalent Al and Si in the framework by other elements.

Zeolite catalysis play and important role in petrochemical and petroleum conversion process[93,94]. The number of processes like selectoforming[95], M-forming[96], M-2 forming[97], Cyclar[98] and Aromax[99] have been developed using zeolite catalyst and commercialized by Mobil Oil Co. and British Petroleum Co. A list of commercial processes based on zeolites is given in Table 1.4. Zeolite catalyst also play an important role in the synthesis of organic intermediates and excellent reviews are available on the application of zeolite catalysis in organic synthesis[100,101]. Zeolite catalysts in organic synthesis like alkylation[102-106], isomerization[107-113], electrophilic substitution of arenes[114,115], cyclization reaction (including heterocyclic ring formation), nucleophilic substitution and addition[116] is well established in two and multi-step synthesis.

1.12 AIM OF THE THESIS

Isomorphous substitution of Al^{3+} by Ga^{3+} in the framework modifies the physico-chemical and catalytic properties of the zeolite. The aim of the present investigation was the hydrothermal synthesis of Al- and Ga-omega followed by characterization and catalytic activities. The present study includes the following aspects :

1. Hydrothermal synthesis and crystallization kinetics of Al-omega and isomorphous substitution of Ga^{3+} in place of Al^{3+} in the omega framework.
2. Physico-chemical characterization of Al- and Ga-omega and their modified cationic forms using different analytical tools.
3. Ammonia sorption isotherms and analysis of sorption data in terms of various sorption models and evaluation of thermodynamic parameters such as chemical affinity and isosteric heats.
4. Catalytic evaluation of both Al- and Ga- isomorph of omega zeolite in different cationic forms in phenol alkylation with methanol and conversion of n-hexane reactions.

Table 1.4 : Industrial processes based on shape selective zeolite catalysts

Name of the process	Purpose
Selectoforming	Octane boosting
M-Forming	-do-
Catalytic Cracking	-do-
MDDW	Distillate dewaxing
MLDW	Lube dewaxing
M-2 Forming, CYCLAR	Gas to Aromatics
MOGD	Light olefins to gasoline and distillate
MTG	Methanol to Gasoline
MTO	Methanol to Olefins
MVPI, MLPI, MHTI	Xylene Isomerization
XYLOFINING	-do-
MTDP	Toluene disp.
ALBENE	Ethylbenzene synthesis
Para selective reaction	p-Xylene synthesis
	p-Ethyltoluene
	p-Diethylbenzene
	p-Cymene
	p-Diisopropylbenzene

Developed at National Chemical Laboratory, Pune and in commercial operation (cf. Annual Report 1989-90).

REFERENCES

1. Cronstedt, A.F., Kongl Vetenskaps Acad. Handl. Stockholm, **17**, 120 (1756).
2. Damour, A., Ann. Mines, **17**, 191 (1840).
3. Breck, D.W., "Molecular Sieve Zeolites", Adv. Chem. Ser., 101, American Chemical Society, Washington DC, 1971, Chapter IV, p. 251.
4. McBain, J.W., "The Sorption of Gases and Vapours by Solids", Pub. Rutledge and Sons, London, Chapter 5 (1932).
5. Barrer, R.M., Proc. Roy, Soc. (London), A 167, 393 (1938); Trans. Far. Soc., **40**, 559 (1944).
6. Barrer, R.M., Pure and Appl. Chem., **51**, 1091 (1979).
7. Meier, W.M. and Olson, D.H. Atlas of Zeolite Structure Types, London Butterworths (1987).
8. Bragg, W.L., The Atomic Structure of Minerals, Cornell University Press, Ithaca, New York (1937).
9. Meier, W.M. Molecular Sieves, Soc. of Chem. Ind. London, p.10 (1968).
10. Barrer, R.M., "Hydrothermal Chemistry of Zeolites", London Academic Press (1982).
11. Breck, D.W., "Zeolite Molecular Sieves: Structure, chemistry and use", London, Wiley (1974).
12. Flanigen, E.M., "In proceedings of the 5th International Conference of Zeolites", (Rees, L.V.C. Eds.) Naples, Italy, June 2-6, p.760 (1980).
13. Barrer, R.M., "Molecular sieves", Society of Chem. Ind., London, p.10 (1968).
14. Sand, L.B. Econ., Geol., p. 191 (1967).
15. Davis, M.E., Saldarriaga, C., Montes, C., Graces, J. and Crowder, C., Nature, **331**, 968 (1988).

16. Estemann M., McCusker L.B., Baerlocher C., Merrouche A. and Kessler H., Nature, **352**, 320 (1991).

17. Mumpton, F.A., Min. Soc., Am. Washington (1977).

18. Sand, L.B. and Mumpton, F.A., (Eds), Natural Zeolites, Occurance, Properties, Use, Pergamon Press, Oxford (1978).

19. Morey, G and Ingerson, E., Econ. Geol., **32**, 607 (1937).

20. Barrer, R.M. and Balchetz, L., J. Soc. Chem. Ind., London, **64**, 132 (1941).

21. Barrer, R.M. and Denny, P.J., J. Chem. Soc., 971 (1961).

22. Sand, L.B., Pure and Appl. Chem., **52**, 2105 (1980).

23. Kerr, G.T., J. Phys. Chem., **70**, 1047 (1966).

24. Kerr, G.T., J. Phys. Chem., **72**, 1385 (1968).

25. McNicol, B.D., Pott, G.T. and Loos, R.K., J. Phys. Chem., **76**, 3388 (1972).

26. Guth, J.L. and Caullet, P., J. Chim. Phys., **83**, 155 (1986).

27. Goldsmith, T.R., Min. Mag., **29**, 952 (1952).

28. Becker, K., John, H., Steinberg, K., Weber, M. and Nestler, K., "Catalysis on Zeolites", (Kallo, D. and Minachev, Kh. M., Eds), Akademia Kiado, Budapest, p. 515 (1988).

29. Naccache, C. and Ben Tarrit, Y. "Zeolite Science and Technology", (Ribeiro, F.R., Rodrigues, A.E., Rollmann, L.D. and Naccache, C., Eds.) Martinus Nijhoff, The Haque, p. 373 (1984).

30. Minachev, Kh.M., Khariamov, V.V. and Garanin, V.I. "Catalysis on zeolites", (Kallo, D. and Minachev, Kh.M. (Eds), Akademia Kiado, Budapest, p. 489 (1988)

31. Perego, G., Bellussi, G., Corono, C., Tanamasso, M. and Buonomo, F., "Stud. Surf. Sci. and Catal., **28**, 129 (1986).

32. Kornatowski, J., Sychev, M. Goncharuk, V. and Bauer, W.H., Stud. Sur. Sci. and Catal., **65**, 581 (1991).

33. Barrer, R.M., Baynham, J.W., Bultitude, F.W. and Meier, W.M., J. Chem. Soc., 195 (1959).

34. Tielen, T., Geelen, M. and Jacobs, P.A. in Proc. Int. Symp. zeolite catalysis, Eds, P. Fejes and D. Katto (Siofok, Hungary), p.1-18 (1985).

35. Wilsen, S.T., Lok, B.M., Messina, C.A., Cannan, T.R. and Flanigen, E.M., J. Am. Chem. Soc., **104**, 1146-1147 (1982).

36. Wilson, S.T. and Flanigen, E.M., ACS Symp. Ser., **298**, 329 (1988).

37. Ward, J.W., "Zeolites Chemistry and Catalysis", C. Rabo, J.A. Eds), ACS Monograph, Ch. 2, **171**, 118 (1976).

38. Breck, D.W. "Zeolite Molecular Sieves", John Wiley and Sons, New York, 449 (1974).

39. Jacobs, P.A. " Carboniogenic activity of zeolites", Chapter II, Elsevier Sci. Pub. Co., Amsterdam, Oxford, New York, **168**, 33 (1977).

40. Mortier, W.J. Saur, J., Lercher, J.A. and Noller, H.J., Phys. Chem., **88**, 905 (1984).

41. Hegde, S.G., Kumar, R., Bhat, R.N. and Ratnasamy, P., "Zeolites", **9**, 231 (1989).

42. Weisz, P.B. and Frilette, V.S., J. Phys. Chem., **64**, 382 (1960).

43. Weisz, P.B., Stud. Sur. Sci. and Catal., **7A**, 3, (1981).

44. Derouane, E.G. and Gabelica, Z., J. Catal., **65**, 486 (1980).

45. Frilette, V.J., Haag, W.O. and Lego, R.M., J. Catal., **67**, 218 (1981).

46. Martens, J.A., Tielen, M., Jacobs, P.A. and Weitkamp, T., Zeolites, **4**, 98 (1984).

47. Weitkamp, J. Ernst, S. and Karge, H.G., Erdol Kohle-Erdgas-Petrochem., **37**, 457 (1984).

48. Dewing, J.J., J. Mol. Catal., **61**, 173 (1990).

49. Weitkamp, J. Ernst, S., Jacobs, P.A. and Karge, H.G., Erdol Kohle-Erdgas-Petrochem., **39**, 33 (1984).

50a. Flanigen, E.M., and Kellberg, E.R., Dutch Pat. 6, 710, 729 (1967) (To Union Carbide).

50b. Breck D.W., "Zeolite Molecular Sieves", John Wiley and Sons, New York, 167 (1974).

51. Barrer, R.M. and Villiger, H., Chem. Comm., 659 (1969).

52. Galli, E., Cryst. Struct. Commun., **3**, 339 (1974).

53. Rinaldi, R., Pluth, J.I. and Smith, J.V., Acta Crystallogr. B. **31**, 1603 (1975).

54. Newsam, J.M., R.H. Jarman and Jacobson, A.J., Mat. Res. Bull., **20**, 125 (1985).

55. Von Ballmoos, R., 'Collection of simulated XRD powder patterns for zeolites', Butterworths, London (1984).

56. Meyer, B.L., Ely, S.R., Kutz, N.A., Kuduk, J.A. and Bossche, E.V., J. Catal., **91**, 352 (1985).

57. Flanigen, E.M. 'Zeolite Chemistry and Catalysis', ACS monograph (Rabo, J.A. Eds.), **171**, 118 (1976).

58. Ward, J.W., 'Zeolite Chemistry and Catalysis', ACS monograph (Rabo, J.A., Eds.), **171**, 118 (1976).

59. Maroni, V.A., Martin, K.A. and Johnson, S.A., ACS Symp. Ser., **368**, 85 (1988).

60. Janin, A., Lovalley, J.C., Macedo, A. and Raatz, F., ACS Symp. Ser., **368**, 117 (1988).

61. Baker, M.D., Godher, J. and Ozin, G.A., ACS Symp. Ser., **368**, 136 (1988).

62. Flanigen, E.M., Khatani, H. and Szymanski, H.A., Adv. Chem. Ser., **101**, 201 (1971).

63. Chu, C.J.W. and Chang, C.D., J. Phys. Chem., **89**, 1569 (1985).

64. Kutz, N., Heterogeneous catalysis - II, Shapiro, B.L. Eds., Texas A and M University Press, College Station, 121 (1984).

65. Topsoe, N., Pedersen, R. and Derouance, E.G., J. Catal., **70**, 41 (1981).

66. Jacobs, P.A. and Martier, W.Y., Zeolites, **2**, 226 (1982).

67. Lippmaa, E., Magi, M., Samosor, A., Engerlhardt, G. and Gummer, A.R., J. Am. Chem. Soc., **102**, 4889 (1980).

68. Nagy, J.B. and Derouane, E.G., ACS Symp. Ser., **368**, 2 (1988).

69. Lippmaa, E., Magi, M., Samoson, A., Tarmak, M. and Engelhardt, G., J. Am. Chem. Soc., **103**, 4992 (1981).

70. Fyfe, C.A., Gobbi, G.C., Klinowski, J., Thomas, J.M. and Ramdas, S., Nature, **296**, 530 (1982).

71. Fyfe, C.A., Gobbi, G.C., Klinowski, J. and Thomas, J.M., J. Phys. Chem., **86**, 1247 (1982).

72. Engelhardt, G., Lohose, U., Lippmaa, E., Tarmak, M. and Magi, M., Z. Anarg. Allg. Chem., **482**, 49 (1981).

73. Mastikhim, V.M. and Zamaraev, K.I., Z. Phys. Chemie., **152**, 332 (1987).

74. Muller, D., Gessnev, W., Behrens, H.S. and Schelev, G., Chem. Phys. Lett., **79**, 159 (1981).

75. Thomas, J.M., Fyfe, C.A., Ramdas, S., Klinowski, J. and Gobbi, G.C., J. Phys. Chem., **86**, 3061 (1982).

76. Ramdas, S. and Klinowski, J., Nature, **308**, 521 (1984).

77. Fyfe, C.A., Thomas, J.M., Klinowski, J., Gobbi, G.C., Angew. Chem., **95**, 257 (1983).

78. Nagy, J.B., Gabelica, Z. and Derouane, E.G., Chemistry Letters, **7**, 1105 (1982).

79. R.M. Barrer, and Langley, D.A., J. Chem. Soc., **3804**, 3811, 3817 (1958).

80. Rabo, J.A., "Zeolite Chemistry and Catalysis", Eds. Beringer, F.M., Am. Chem. Soc., Washington, D.C., p. 285 (1976).

81. Bremer, H., Marke, W., Schodel, R. and Vogt, F., Adv. Chem. Ser., **121**, 249 (1973).

82. Breck, D.W., Zeolite Molecular Sieve, Structure, Chemistry and Use, Wiley Interscience, New York, 449 (1974).

83. Araya, A., Barber, T.J., Lowe, B.M., Sinclair, D.M. and Varma, A., Zeolites, **4**, 263 (1984).

84. Friedel, G., Bull. Soc., Fr. Mineral Crystallogr., **19**, 14, 96 (1896).

85. Rabinowitch, R. and Wood, W.C., Trans. Faraday Soc., **32**, 947 (1936).

86. Barrer, R.M., Proc. Roy. Soc., A **167**, 39Z (1938).

87. Barrer, R.M., Quart. Review, London, 3239 (1949).

88. Barrer, R.M. and Breck, D.W., Trans Faraday Soc., **59**, 2569 (1963).

89. Barrer, R.M., Zeolites and Clay Minerals as Sorbents and Molecular Sieves, Academic Press, Inc., London.

90. Hong-Xin. Li. Martins, J.A., Jacobs, P.A., "Innovation in zeolite mater. sci.,", Gribet, P.J (Eds.), 75 (1987).

91. Tapp. N.J. Milestone, N.B., Bibby, D.M., Ibid, p. 393.

92. Barrer, R.M., Adv. Chem. Ser., **102**, 41 (1971).

93. Weisz, P.B., Pure Appl. Chem., **52**, 2091 (1980).

94. Chen , N.Y. and Garwood, W.E., Catal. Rev. Sci. Engg., **28**, 185 (1986).

95. Chen, N.Y., Mazink, J., Schwartz, A.B. and Weisz, P.B., Oil Gas J., **66**, 154 (1968).

96. Heinemann, H., Catal. Rev. Sci. Engg., 15(1), 53 (1977).

97. Chen, N.Y. and Yan, T.Y., Ind. Eng. Chem., Proc. Res. Dev., **25**, 151 (1986).

98. Johnson, J.A., Weiszmann, J.A. Hider, G.R. and Hall, A.P.H., Paper presented at NPRA Annual Meeting., San Antorio, Texas, March (1984).

99. Tamm, P.W. Mohr, D.H. and Wilson, C.R., Catalysis (1987), (Ward, J.W. (Eds), Elsevier Sci. Pub., Amsterdam, The Netherlands, p. 335 (1988).

100. Holderich, W., Hesse, M. and Naumann, F., Angew. Chemie, **27** (2), 226 (1988).

101. Van Bekkum, H. and Kouwenhoven, H.W., Red. Trav. Chim., Pays-as, **108**, 283 (1989).

102. Pradhan, A.R, and Rao, B.S., J. Catal. **132**, 79 (1991).

103. Prasad, S. and Rao, B.S., J. of Mol. Catal., **62**, L17-L22 (1990).

104. Blanka, Witcherlova and Jiri, Ccjka., J. Catal., **146**, 523, (1994).

105. Reddy, K.S.N, Rao, B.S., Shiralkar, V.P., Appl. Catal., A. General, **95**, 53 (1993).

106. Bandyopadhyay, R., Singh, P.S., and Rao, B.S. Communicated to React. Kinet. Catal. Lett.

107. Bandyopadhyay, R., Singh, P.S., and Shaikh, R.A., Communicated to Applied Catal.

108. Martens, J.A., Perez-Pariente, J., Sastre, E., Corma, A., Jacobs, P.A., Appl. Catal., **45**, 85 (1988).

109. Csicsery, S.M., J. Catal., **108**, 433, (1987).

110. Kim, M.H., Chen, C.Y., Davis, M.E., ACS Symp. Ser. **517**, 222, (1993).

111. Matsuda, T., Yogo, K., Mogi, Y., Ki Ku Chi, E., Chem. Lett. 1085 (1990).

112. Weitkamp, J., Neuber, N., Stud. Surf. Sci. **60**, 291, (1991).

113. Jacob, P.A. and Martens, J.A., Stud. Surf. Sci. Catal., **58**, 445 (1981).

114. Schumacher, I., and Wang. K., US Pat. 4 426 543 (1984).

115. Wortel, Th. M., Oudijn, D., Vleugel C.J., Rielofsen, D.P. and Bekkum, van H., J. Catal., **60**, 110 (19790.

116. Hatada, K., Ono, Y., and Keii, T., Adv. Chem. Ser., 121, Ch.45 (1973).

CHAPTER II

SYNTHESIS, CRYSTALLIZATION KINETICS AND CHARACTERIZATION OF ZEOLITE OMEGA AND ITS GALLIUM ANALOG

2.1. INTRODUCTION

Zeolites are synthesized hydrothermally (373-473 K) in highly alkaline (pH=10-12) solutions containing aluminum, silicon, alkali or alkaline earth metals and an organic templating species (when used).

Zeolite omega and ZSM-4 are two synthetic isotypes of mineral mazzite. The aluminosilicate framework consists of columns of gmelenite cages bridged by oxygen atoms to give a twelve membered cylindrical main channel system along the crystallographic c-axis[1-3]. The zeolite omega is usually crystallized at 363-423 K from aluminosilicate hydrogels containing a mixture of sodium hydroxide and tetramethylammonium hydroxide(TMAOH) ions[4-11]. The replacement of Al or Si in the zeolite structure by other elements, generally referred as "isomorphous substitution", modifies its physico-chemical characteristics. The isomorphous replacement of Al by other trivalent cations in the zeolite framework has been reviewed by Barrer[12], Szostak[13] and others[14]. The gallium analog of zeolite possesses physical and chemical properties different from their aluminum analogs[15]. The gallium analogs of ZSM-5[16], EU-1[17], mordenite[18], Y[19] and mazzite[20-21] have already been documented.

In this chapter systematic investigations on crystallization kinetics of aluminum omega, synthesis of gallium omega and characterization by different techniques are discussed in detail.

2.2 EXPERIMENTAL

(A) Synthesis of Al-omega

The reagents used for the hydrothermal synthesis of Al and Ga-omega are listed in Table 2.1 with their commercial specifications. A solution containing 1.17 g of sodium aluminate and 2.0 g of sodium hydroxide in 10 g of distilled water mixed with 1.6 g of tetramethylammonium hydroxide. This solution was slowly added with vigorous stirring to 18.0 g of silica sol. The thick paste formed was converted into uniform slurry by continuous stirring for two hours. The gel slurry having the following composition in terms of oxide mole ratio was transferred to a stainless steel autoclave (Fig 2.1) and heated up to 383 to 413 K for 5 to 20 days.

$$6.78\ Na_2O : Al_2O_3 : 17\ SiO_2 : 0.43(TMA)_2O : 251\ H_2O$$

Table 2.1 Reactants used for the omega zeolites and their specifications.

Sl No.	Reactants	Supplied by	Analysis
1.	Tetramethylammonium hydroxide (TMAOH)	Fluka	25 % in methanol
2.	Gallium nitrate	Aldrich	99.9 %
3.	Sodium hydroxide	S.D.Fine Chemicals, India.	99 %
4.	Sodium aluminate	-	43.8 % Al_2O_3, 39.0% Na_2O
5.	Silica sol	-	28.9 % SiO_2

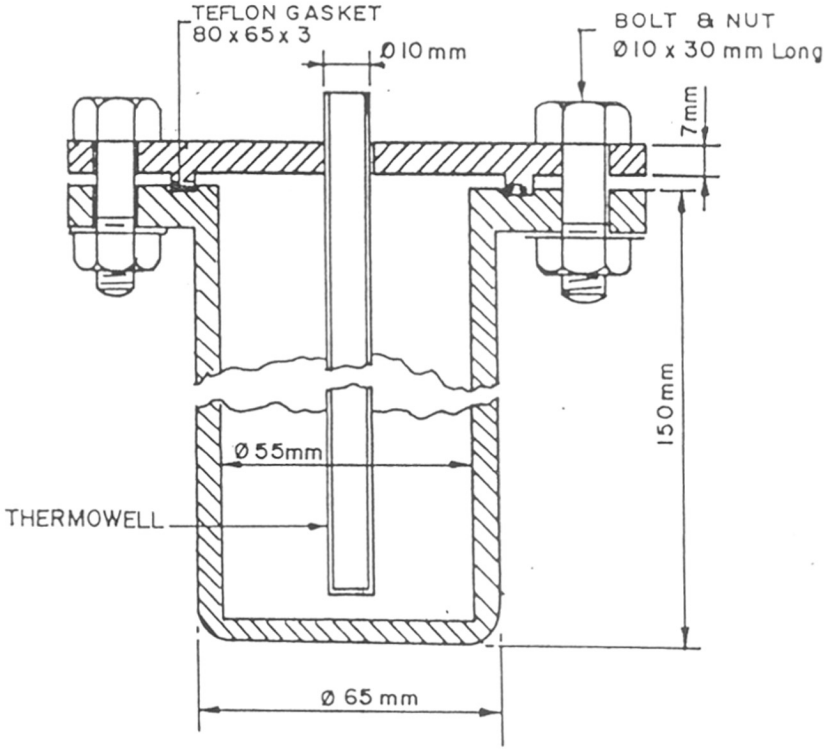

FIG. 2.1 : STAINLESS STEEL (316) AUTOCLAVE WITH TEFLON GASKET FOR HYDROTHERMAL SYNTHESIS

The sampling was carried out at different crystallization times to monitor the progress in crystallization. The autoclave was removed from the oven and quenched under cold water. The crystalline white solid was filtered, washed and dried at 393 K in the air for 6 h. The material was then calcined in presence of air at 873 K to expel the template.

(B) Synthesis of Ga-omega (isomorphous substitution)

The gallosilicate analog was prepared with the same oxide mole composition except that anhydrous gallium nitrate was used in place of sodium aluminate which required further addition of a calculated quantity of sodium hydroxide to maintain the sodium content in the Al-omega gel.

A solution containing 2.55 g of gallium nitrate and 2.73 g of sodium hydroxide in 10 ml of distilled water was mixed with 1.6 g of tetramethylammonium hydroxide. This solution was slowly added with vigorous stirring to 18.0 g of silica sol. The thick paste formed was converted into uniform slurry by continuous stirring for two hours. The same procedure as described above for Al-Omega was followed by heating, cooling, washing and drying to obtain the white crystalline gallium isomorph of zeolite omega.

Analysis of mother liquor after filtration did not show the presence of aluminum in Al-omega and gallium in Ga-omega synthesis. The yield based on total Al_2O_3 and Ga_2O_3 inputs is > 95% for both Al-omega and Ga-omega.

2.3 CHARACTERIZATION

2.3.1. X-ray diffraction (XRD)

The synthesized samples were analyzed by X-ray powder diffraction for quantitative and qualitative phase identification, with the Rigaku (D/Max-III VC) X-ray diffractometer using a Ni-filtered CuKα radiation (λ= 1.5406 Å) with graphite monochromator and Si as internal standard. The sample was continuously rotated during the scan. The most crystalline sample in aluminum omega and gallium omega was assumed to be 100% crystalline and was used as reference standard for measurement of crystallinity. The degree of crystallization of the solid product was estimated from XRD peak intensities(2θ range 4-36) using the following formula.

$$\%\text{Crystallinity} = \frac{\text{Peak area of intense peaks of the product}}{\text{Peak area of intense peaks of the standard}} \times 100$$

2.3.2. Scanning electron microscopy (SEM)

The morphology and crystal habit of synthesized sample were studied using a JEOL JSM 5200 scanning electron microscope by coating the sample with an evaporated Au film on an aluminum sample holder.

2.3.3. Infrared (IR) spectroscopy

The infrared spectra were recorded in the region between 400-1300 cm^{-1} on a Pye-Unicam, SP 300 spectrometer using nujol mull technique.

2.3.4. Solid state MAS-NMR spectroscopy

The solid state MAS NMR spectra (^{29}Si, ^{27}Al and ^{71}Ga) were recorded at 298K on a Bruker-MSL-300 FT NMR spectrometer. For ^{29}Si spectra, a 2s pulse and recycle time of 3s were found to be sufficient and the chemical shift was measured with respect to tetramethylsilane (TMS) as an external reference. For ^{27}Al spectra 3s pulse and 0.25s recycle time were found to be adequate and the aqueous solution of $AlCl_3$ served as an external reference. For ^{71}Ga a 3s pulse and a 0.3s recycle time were found to be sufficient and $[Ga(H_2O)_6]^{3+}$ was used as an external reference.

2.3.5. Thermal analysis

Simultaneous thermoanalytical curves (DTA and TG) were obtained in air with Setaram TG-DTA 92 analyzer under the following conditions.

Weight of the sample = 40 mg

Heating rate = 10 K min^{-1}

Atmosphere = flowing air

Finely powdered α-alumina was used as a reference material.

2.3.6. Sorption measurements

Sorption measurements were carried out using a conventional gravimetric system consisting of a McBain balance (sensitivity $\approx$ 70 cms, gm^{-1}). The experimental setup is shown in (Fig. 2.2). About 50-70 mg of zeolite sample was pressed to a pellet and weighed into an aluminum bucket which was then suspended to silica spring. The assembly was then evacuated by means of a two stage rotary pump and oil diffusion pump to vacuum of 10^{-6} Torr. The sample was heated slowly to 673 K under vacuum, till a constant weight was obtained. The temperature of the sample was then lowered to 298K and the sorbate vapor was admitted to the sample at constant temperature and pressure. The amount sorbed was measured from the extension of the spring which was recorded after 2 h at each equilibrium pressure using a cathetometer.

2.3.7. Chemical analysis

The chemical compositions of fully crystalline Al-omega and Ga-omega zeolites in the anhydrous form were determined both by XRF (non-destructive) and gravimetric (destructive) methods. For nondestructive method, X-ray spectrometer 3070 was used. For gravmetric (destructive) method a known quantity of zeolite sample was heated at high temperature in platinum crucible in duplicate for six hours to constant weight. Dry zeolite powder was moistened with sulphuric acid and 5 ml of hydroflouric acid was added. The contents were heated over a hot-plate till most of the silica had been expelled. Hydroflouric acid treatment was repeated thrice and at the end, the sample was evaporated to dryness. From the loss in weight silica was estimated. The residue was fused with potassium pyrosulphate and the melt was dissolved in dilute hydrochloric acid and made upto a known volume. The sodium, aluminum and gallium were estimated using atomic absorption spectrometer (Hitachi Z 8000). The ion exchange properties of Ga-omega were evaluated by saturating the calcined (organic free) gallosilicate sample with 1N NaCl solution and then by exchanging with potassium. Ion exchange was done under reflux at 368 K for 4 h. The procedure was repeated to ensure complete exchange.

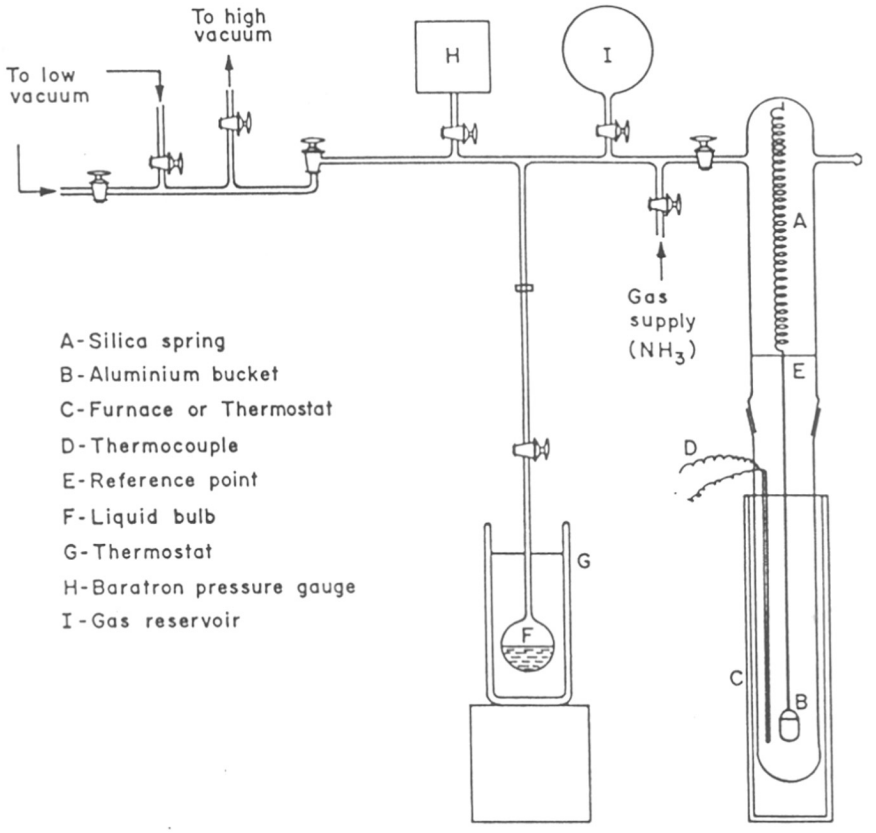

FIG.2·2: GRAVIMETRIC ADSORPTION UNIT

2.4 RESULTS AND DISCUSSION

2.4.1. X-ray diffraction and crystallization kinetics

Fig.2.3 and 2.4 show the XRD patterns of Al and Ga-omega zeolites with progressive crystallization at 398 K at different time intervals. The XRD pattern of Al-omega (Fig. 2.3.e) is in close agreement with the reported data. There is also close similarity between the XRD pattern for Al-omega (Fig. 2.3.e) and Ga-omega (Fig. 2.4.e). Table 2.2 clearly indicates lowering of 2θ values for the XRD reflections in Ga-omega as compared to those in Al-omega and this may be the consequence of incorporation of comparatively larger gallium species in place of framework aluminum. A similar expansion is also reported in the isomorphous substitution of Ga into the framework of mordenite[18]. The unit cell volume calculated from XRD data for Ga-Omega (2225 $Å^3$) is higher than that for Al-omega (2210 $Å^3$) as summarized in Table 2.2. This observation is also consistent with Ga-O bond length being larger than Al-O bond length.

The crystallization kinetics were studied by comparing the extent of crystallization of the gel mixture at different interval of synthesis time and at different temperatures. The degree of crystallization was evaluated[22] by the ratio of sum of the areas of intense XRD peaks (2θ range 4-36) of the sample under consideration to that of the most crystalline sample obtained during the study.

The crystallization kinetic curves at 383, 398 and 413 K are shown in Fig. 2.5. The curves show sigmoidal or S-shaped nature, indicating different rates of crystallization at different synthesis times. It is defined that the initial portion (induction period) to correspond to the time needed to form crystallization centers as nuclei. This is followed by a rapid formation of the crystalline structure. Lastly , the rate of crystallization decreases as process approaches to completion indicated by a near-constancy (100%) in percentage crystallization. The curves show that the kinetics of crystallization depends on the temperature, as expected.

As the main period of crystallization (% crystallinity from 30 to 75) is almost linear, the crystallization was treated as a first order reaction. The formation of nuclei during the induction period is assumed to be an energetically activated process and since nucleation is the rate determining step during the induction period, the activation energy for nucleation (En) was calculated from

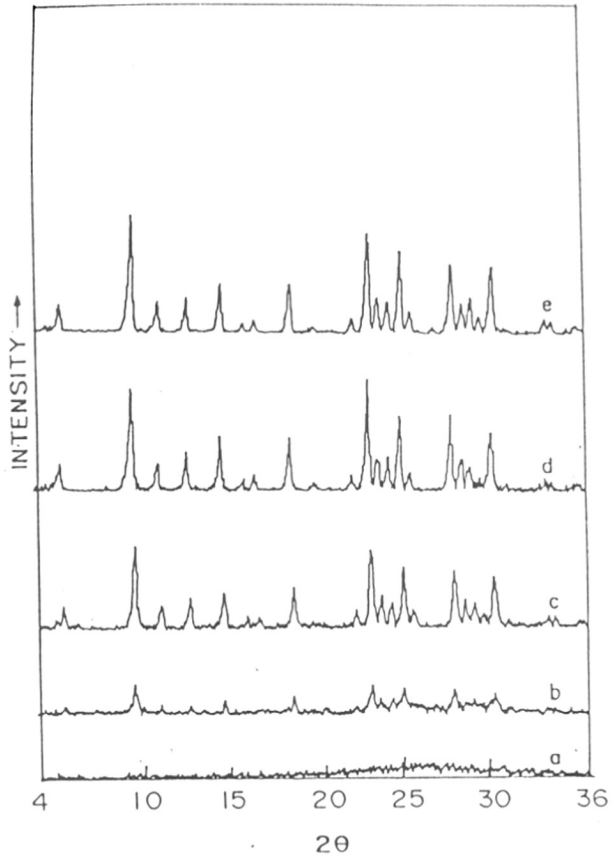

FIG. 2.3 : X-RAY DIFFRACTION PATTERNS OF Al-OMEGA ZEOLITES WITH DIFFERENT DEGREE OF CRYSTALLI NITY (a) 0%, (b) 26%, (c) 72%, (d) 93% AND (e) 100%

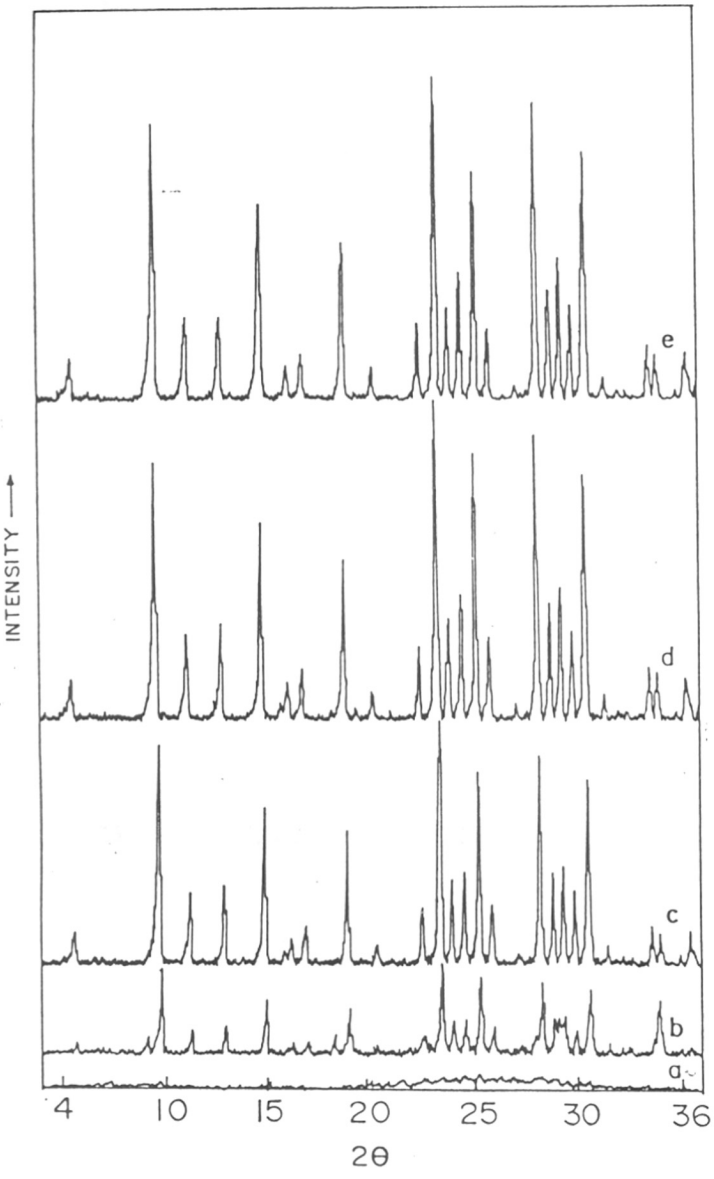

FIG. 2.4 : X-RAY DIFFRACTION PATTERNS OF Ga-OMEGA ZEOLITES WITH DIFFERENT DEGREE OF CRYSTALLINITY (a) 0%, (b) 21%, (c) 70%, (d) 93% AND (e) 100%

Table 2.2 : 'd' Spacings and relative intensities for omega samples.

Al-omega (uc volume = 2210 Å^3)				Ga-omega (uc volume = 2225 Å^3)	
Literature*		Present study		Present study	
d (Å)	(I/I_{max}) X 100	d (Å)	(I/I_{max}) X 100	d (Å)	(I/I_{max}) X 100
9.090	86	9.089	100	9.134	100
7.870	21	7.891	17	7.916	19
6.860	27	6.878	58	6.888	23
5.940	32	5.955	47	5.979	63
4.695	32	4.690	29	4.708	21
3.794	58	3.79	87	3.805	66
3.708	30	3.704	35	3.714	14
3.620	25	3.621	33	3.628	33
3.516	53	3.518	78	3.526	37
3.456	20	3.428	25	3.441	12
3.130	38	3.141	68	3.162	71
3.074	21	3.082	35	3.094	22
-	-	3.034	30	3.043	36
-	-	2.979	17	2.988	25
2.921	63	2.924	60	2.924	60

*Ref. 22

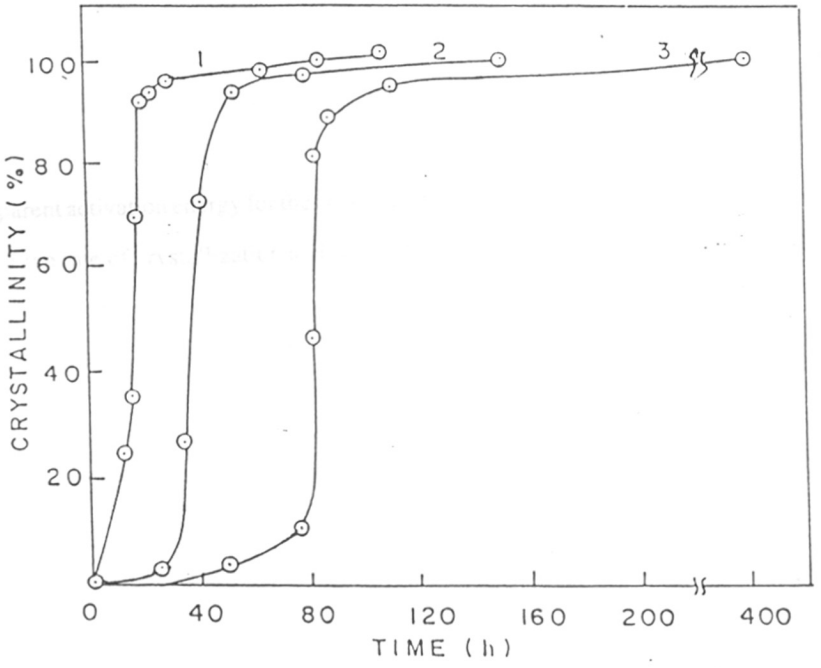

FIG. 2.5 : KINETICS OF CRYSTALLIZATION OF Al-OMEGA AT (1) 413 K, (2) 398 K AND (3) 383 K

temperature dependance of the rate of nucleation. The rate of nucleation has been assumed to be inversely proportional to the nucleation period. Apparent activation energy for nucleation was calculated from the Arrhenius equation which expresses the temperature dependance of the rate of nucleation.

$$\frac{d \ln (1/\theta)}{d (1/T)} = \frac{- En}{R} \qquad \ldots (1)$$

Where θ is the induction period, that is the time on the crystallization curve where the conversion to the crystallization is just starting. T is the absolute temperature and R is the molar gas constant.

The apparent activation energy for the crystal growth (Ec) was calculated from the temperature dependance of the rate of crystallization and was obtained from point on the crystallization curves where 50% crystallization is complete. The temperature dependance of the rate of crystallization may be represented as

$$\frac{d \ln (1/K)}{d (1/T)} = \frac{- Ec}{R} \qquad \ldots (2)$$

where K is the point on the crystallization curve (in hours) where 50% crystallization is complete. T is the absolute temperature and R is the molar gas constant.

The values for apparent activation energy of nucleation (En = 82.9 kJ $mole^{-1}$) and apparent activation energy of crystallization (Ec = 65.6 kJ, $mole^{-1}$) were obtained from the slopes of linear plots ln 1/θ vs 1/T and ln 1/K Vs 1/T respectively.

Number of reports[23-25] have described zeolite crystallization as a process that follows first order kinetic equation by Avrami-Erofeev equation and the activation energies for the processes of nucleation (En) and crystallization (Ec) have been evaluated by applying Arrhenius equation. However, recently Thompson[26] and other researchers[27] have suggested that these analytical treatments to crystallization curves and application of Arrhenius equation to crystallization kinetics cannot be applied to reveal details regarding the crystallization to determine activation energies from such analysis principally due to the insensitivity of measurements of the mass of zeolite by

conventional methods. Linear plots were, however, obtained when crystallization kinetics data were analyzed in terms of Avrami-Erofeev equation. Avrami-Erofeev parameters (m and k) obtained from the slopes and intercepts respectively are tabulated in table 2.3 only for comparative study.

Table 2.3 Avrami-Erofeev parameters for aluminosilicate omega synthesis using TMAOH

synthesis temp K	10^2 x k	m
413	5.827	4.83
398	2.444	7.10
383	1.208	20.67

2.4.2. Scanning electron microscopy

The progress in crystallization has also been monitored by scanning electron micrograph. Figure 2.6 (A to D) show the representative phases during the crystallization of aluminiosilicate at 398K. The well defined crystallites start appearing with the increase in the crystallinity of zeolite. Fig. 2.6 A and B show the SEM of 26% and 72% crystalline samples. Fig 2.6 C and 2.6 D show 100% crystalline samples at 398 and 413 K, respectively, indicate the absence of any amorphous material and also other crystalline phase impurities.

The scanning electron micrographs of Ga-omega samples with different crystallinity showed in Fig. 2.7 (E to H), indicate that, as the degree of crystallinity increases, well defined crystallites start appearing in place of amorphous material of irregular shape.

The salient features of the SEM photographs in Fig 2.7 (G and H) is the change in the crystal morphology for Ga-omega crystallized at 348K. These crystallites are of cylindrical shape with average size being 4 x 2 μm for 30 h at 398 K (Fig. 2.7 G) and 8 x 2 μm for 90 h at 398 K (Fig 2.7H) and shape is distinctly different from Al- omega crystallites. This shows a marked influence on the crystal morphology of isomorphous replacement of Al^{3+} by Ga^{3+} in the omega framework.

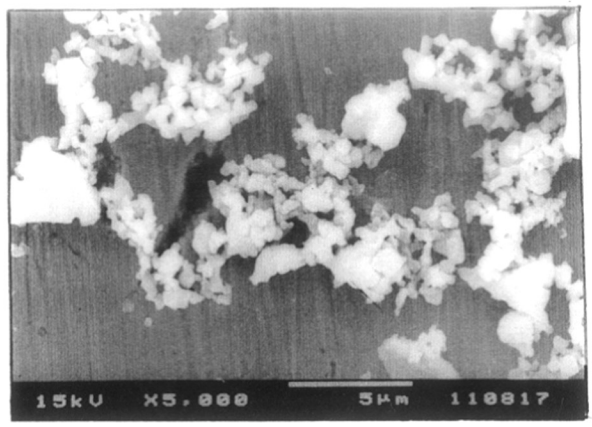

A

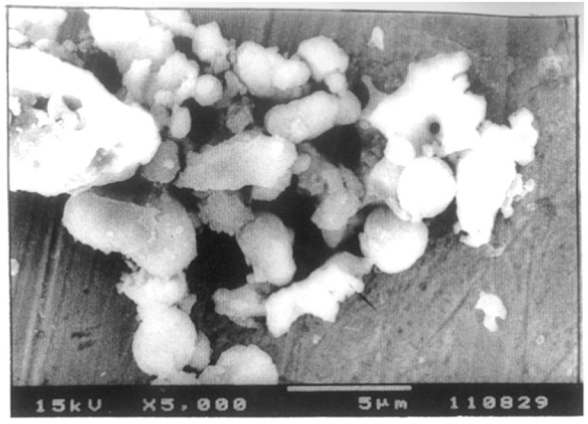

B

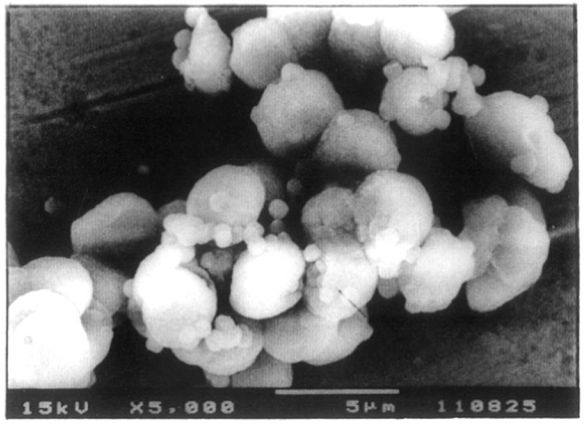

C

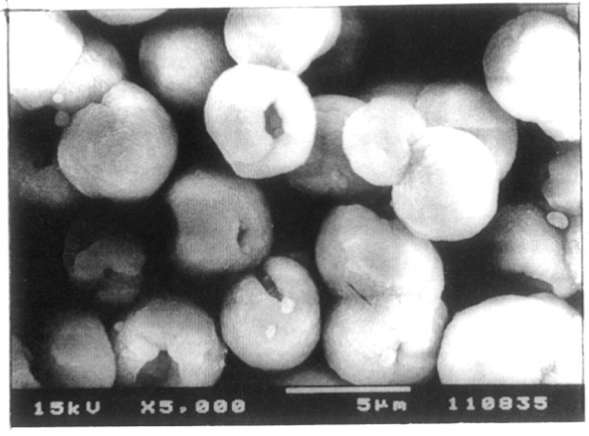

D

FIG. 2.6 : SEM PHOTOGRAPHS OF Al-OMEGA WITH DIFFERENT DEGREE OF CRYSTALLINITY (A) 26%, (B) 72%, (C) 100% AT 398 K AND (D) 100% at 413 K

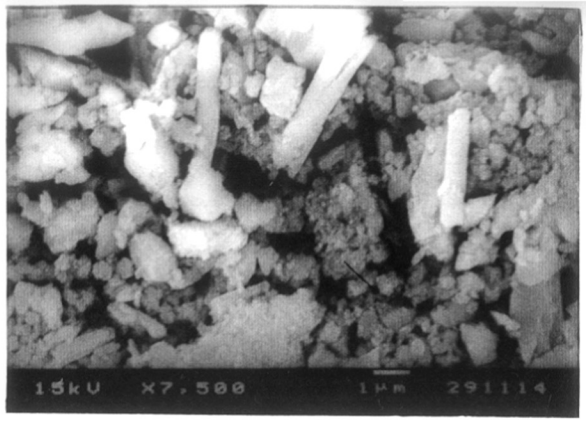

E

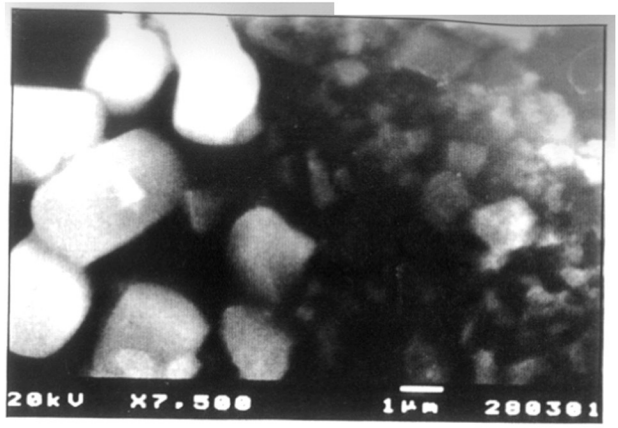

F

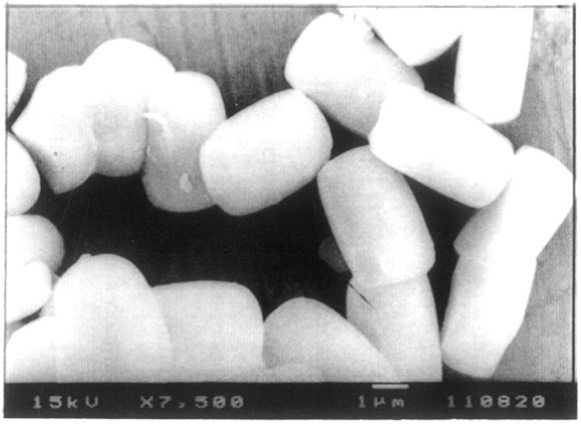

G

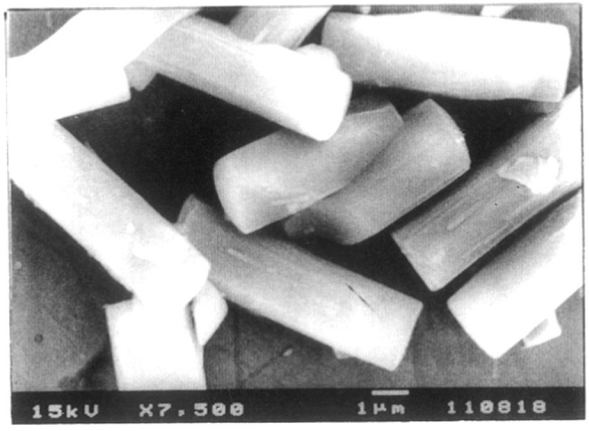

H

FIG. 2.7 : SEM PHOTOGRAPHS OF Ga-OMEGA SAMPLES WITH DIFFERENT DEGREE OF CRYSTALLINITY (E) 21%, (F) 70%, (G) 100% (20h) AND (H) 100% (90h) AT 398 K

Fig. 2.7 G and 2.7 H also show the influence of crystallization period on the size of crystallite. A similar change in crystal morphology has also been reported[28] in the synthesis of number of zeolites including omega. This shows that, along with the synthesis parameters such as the nature of the ingredients, gel composition and crystallization temperature, isomorphous species in the silica matrix exert an influence on the crystal morphology of the zeolite produced.

2.4.3. Framework IR spectra

Framework IR spectra in the region 400-1300 cm^{-1} are compared for Al-omega and Ga-omega in Fig. 2.8. A progress in crystallinity is also shown in Fig. 2.8 by the IR spectra of Al-omega obtained at different crystallization times. Fig. 2.8,l shows the IR spectra for almost amorphous (% crystallinity ~10) aluminosilicate gel. As the percent crystallinity of the product increases, a very broad band at 1060 cm^{-1}, due to the assymmetric stretch, becomes sharper and shifts towards lower wavenumber (1030 cm^{-1}) in fully crystalline Al-omega (fig. 2.8) zeolite. Similarly, a shoulder around 1105 cm^{-1} becomes more prominent around 1130 cm^{-1} in the fully crystalline sample.

A band around 852 cm^{-1} present in the amorphous sample disappears in crystalline Al-omega. A salient feature of Fig. 2.8 is the emergence of peaks at 820 and 620 cm^{-1} on account of absorption of structure sensitive bands due to the symmetric stretch and double ring respectively. Although the position of these bands does not shift, their intensities increase with the increase in percentage crystallinity, except for a band around 615 cm-1 corresponding to a double ring which becomes very weak in Ga-omega. Also, the position of the band assigned to pore opening around 450-460 cm-1 does not change with crystallinity. The framework IR characteristics for Al-omega summarized in Table 2.4 are in close agreement with the reported data[29]. Another interesting feature of Fig. 2.8 and Table 2.4 is the lower wavenumber value of all the structure sensitive bands in Ga-omega as compared to those of Al-omega. This is in accordance with the substitution of Al^{3+} species with the heavier Ga^{3+} species in the omega framework. Sometimes a doublet around 800 cm^{-1} in the Gallium analog in place of a singlet in the aluminum analog confirmed[30] the incorporation of Ga^{3+} ions in the framework of zeolite omega.

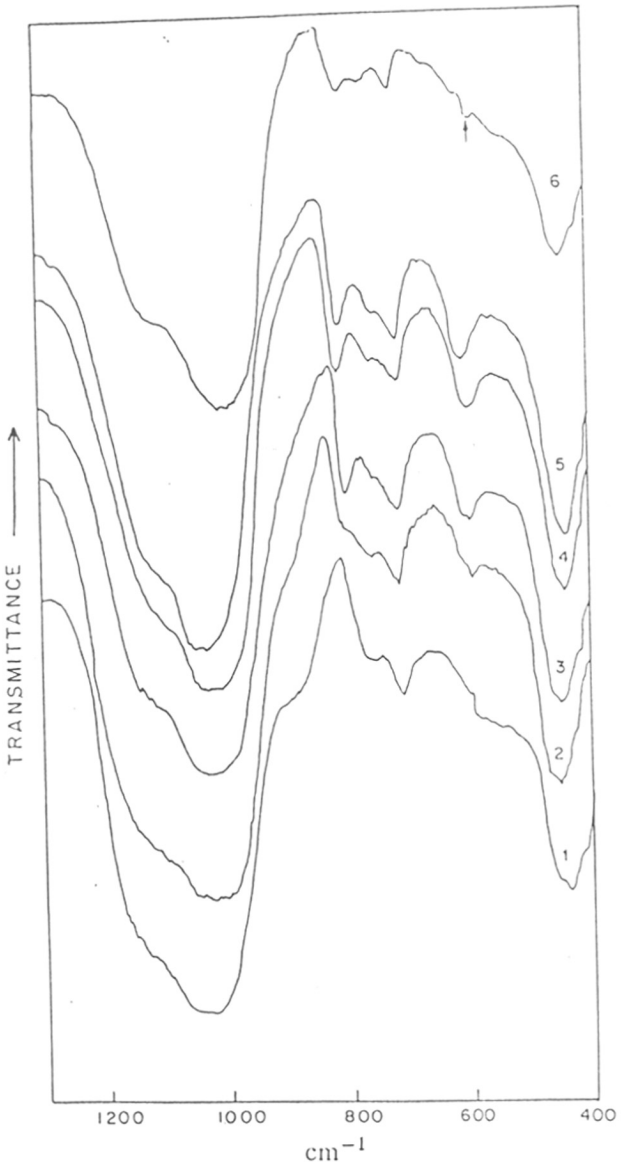

FIG. 2.8 : FRAMEWORK IR SPECTRA OF SAMPLES WITH DIFFERENT DEGREE OF CRYSTALLINITY Al-OMEGA (1) 0%, (2) 26%, (3) 72%, (4) 93%, (5) 100% AND (6) 100% Ga-OMEGA

Table 2.4 Framework IR vibrational bands of crystalline Al and Ga-omega

Al-omega (synthesized at 398 K)		Al-Omega* (Literature data)		Ga-omega (synthesized at 398 K)	
1130	sh	1130	sh	1139	sh
1037	vs	1024	vs	1025	vs
825	m	805	mw	815	m
770	sh	-	-	770	sh
730	mw	722	mw	730	mw
625	m	610	mw	615	vw
455	ms	451	ms	450	ms

* Ref [29]

vs - very strong, sh - shoulder, m - medium, mw - medium weak, ms - medium strong, vw - very weak.

2.4.4. Chemical composition

The chemical composition of fully crystalline Al-omega and Ga-omega in the anhydrous form determined by both the gravimetric (destructive) and XRF (non-destructive) methods are compared in table 2.5.

The silica to alumina ratio in the solid is found to be around 7.0 ± 0.25. The sodium occupancy, however, is only 70% of the total aluminum incorporation. This shows that the excess negative charge on 30% of framework AlO_4^- tetrahedra is balanced by protons produced upon the decomposition of templating species. The chemical composition of Ga-omega also shows the SiO_2/Ga_2O_3 ratio to be around 6.87-7.42. The sodium occupancy in Ga-omega is 90% of the total gallium content in the solid and it is higher than that in Al-omega. The aluminum content (as an impurity from raw materials) in Ga-omega is negligible ($SiO_2/Al_2O_3 > 1200$). Since Ga-omega exhibits XRD pattern characteristic of the omega framework with no report of Al-omega with SiO_2/Al_2O_3 ~1200, it is reasonable to assume the incorporation of Ga^{3+} ions into the omega framework. The substantial ion exchange capacities of calcined Ga-omega zeolite is a strong evidence for the presence of Ga ions in the zeolite framework.

2.4.5. Solid state MAS-NMR spectroscopy

Fig. 2.9 depicts ^{29}Si and ^{27}Al MAS NMR spectra of Al- and Ga-omega are almost identical exhibiting peaks at 92.85 ppm (Si-0Al), 97.99 ppm (Si-1Al), 104.05 ppm (Si-2Al) and 111.59 ppm (Si-3Al). These NMR data are in close agreement with those reported earlier[31,32]. The intensities of the peaks corresponding to (Si-1Al) and (Si-2Al) are more than that for (Si-0Al) and (Si-3Al). The ^{27}Al MAS NMR spectrum for Al-omega shows a sharp doublet in the range 62-56 ppm, corresponding to the tetrahedral aluminum atoms located in the two non-equivalent crystallographic sites of the framework corresponding to the four membered (S4R, site A) and six membered rings (S6R, site B) of the gmelinite columns[31,32]. The area under each of the peaks gives[31,32] almost the quantitative measure of the number of these sites and the ratio Al_A/Al_B is usually around 1.25. However, the ^{27}Al MAS NMR spectrum for Ga-omega shows the absence of any significant amount of aluminum in the samples. The ^{71}Ga MAS NMR spectrum of Ga-omega shows a signal at 156.9 ppm and thus

Table 2.5 Chemical composition of Al- and Ga-omega.

Chemical composition (anhydrous)	Al-omega		Ga-omega	
	XRF	Gravimetric	XRF	Gravimetric
% SiO_2	75.71	74.10	66.66	62.66
% Al_2O_3	17.75	18.37	0.09	0.09
% Ga_2O_3	-	-	25.82	28.71
% Na_2O	7.25	7.53	7.42	8.53
$SiO_2/[Al_2O_3 + Ga_2O_3]$	7.25	6.85	7.42	6.87
Surface Area, m^2g^{-1}	259		234	

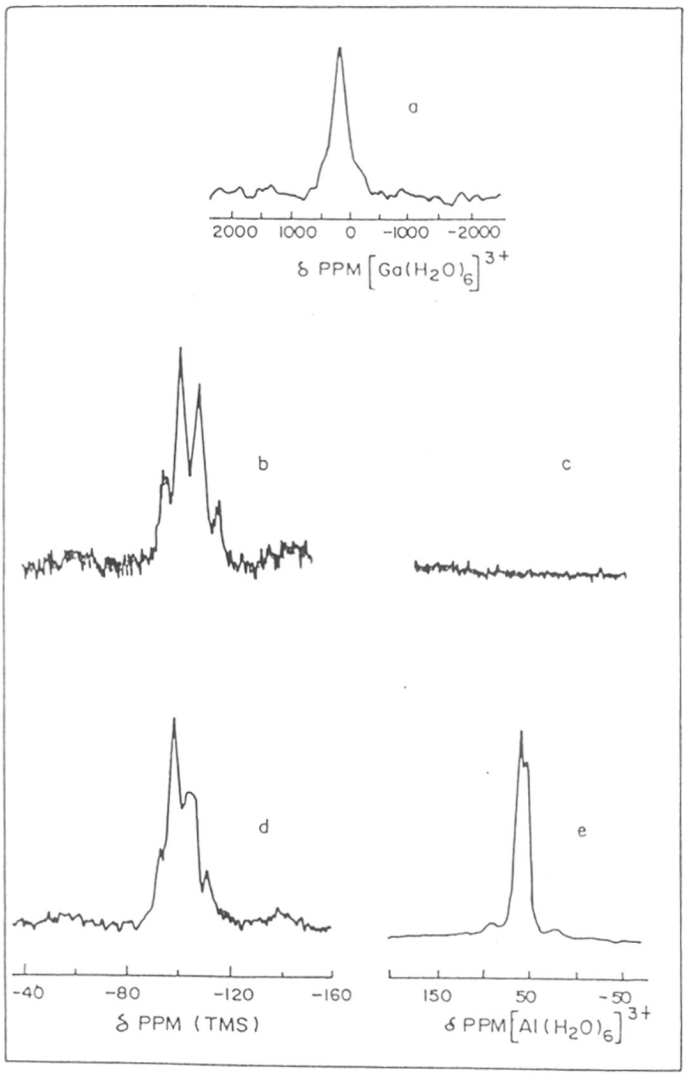

FIG. 2.9 : MAS NMR SPECTRA FOR Ga-OMEGA (a) ^{71}Ga, (b) ^{29}Si, (c) ^{27}Al AND FOR Al-OMEGA OF ^{29}Si AND ^{27}Al

confirms the tetrahedral coordination of Ga^{3+} species in the omega framework. The gallium signal peak is not sharp but rather broad, indicating that although the sample is highly crystalline, a distortion in the symmetry around Ga-nuclei may be present.

2.4.6. Thermal properties

Fig. 2.10 shows the DTA and TG curves for typical Al-omega and Ga-omega zeolites crystallized at the same temperature. Both the TG curves show a loss in weight up to 573 K (around 10 wt%) due to dehydration of physically sorbed water. It is then followed by a very slow loss in weight (around 1.5wt%) up to 833 K, probably due to the decomposition of physically occluded template molecules. A very sharp loss in weight (around 3.5 wt%) takes place over a very narrow temperature range (863-893 K) due to the oxidative decomposition of templating species associated with the framework aluminum tetrahedra to balance its negative charge. After 890 K, there is no more loss in weight, even up to 1273 K. The total loss up to 1273 K with Al-omega is 14.5-15 wt % and is rather higher than that (11.5 wt%) in Ga-omega.

The DTA curves reflect the TG changes. A broad and weak endotherm up to 573 K due to dehydration of physically sorbed water is followed by a weak and diffuse exotherm up to 773 K due to decomposition of physically occluded template species. A very sharp exotherm in the range 880-890 K is exhibited on account of the oxidative decomposition of templating species associated with the charge compensation on the framework aluminum tetrahedra. The Ga-omega sample also gives the maximum for this exotherm at 878K. It is seen from Fig. 2.10, a small exotherm for TMA-Al-omega at 1224 K due to structural collapse whereas Ga-analog indicated at temperature around 1127 K. The protonic forms of both Al- and Ga-omega zeolites showed low thermal stability which is discussed in Chapter III.

2.4.7. Sorption properties

Fig. 2.11 depicts the sorption uptake (P/Po=0.8, T=298 K) of samples of different crystallinity obtained from typical synthesis experiments (398 K) for Al-omega and Ga-omega. These curves typically show that sorption uptake increases as the degree of crystallinity increases. Water, being a polar molecule and comparatively smaller in size, is able to get occluded in cavities of samples

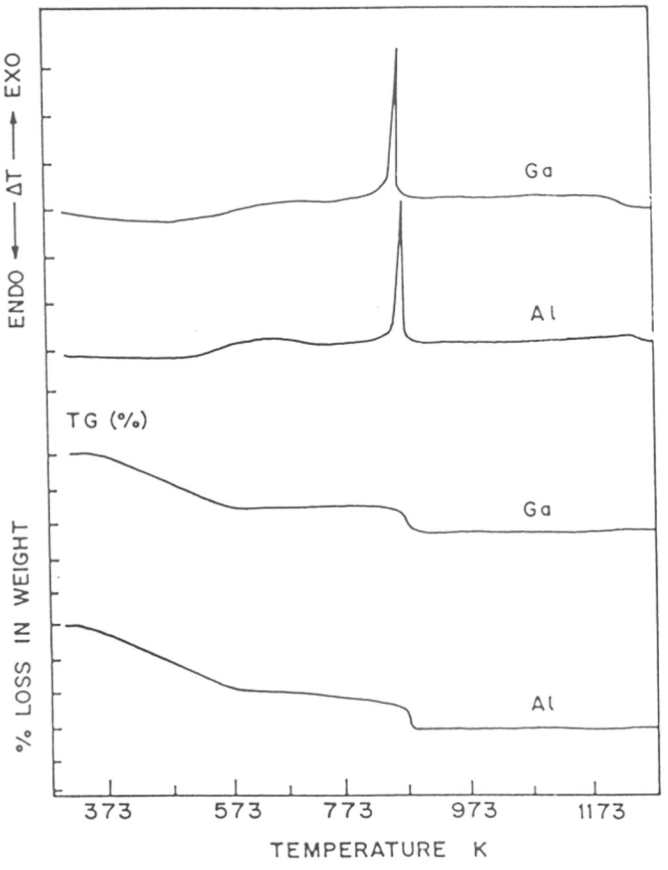

FIG. 2·10 : THERMO-ANALYTICAL (DTA AND TG) CURVES FOR Ga-OMEGA AND Al-OMEGA CRYSTALLIZED AT 398 K

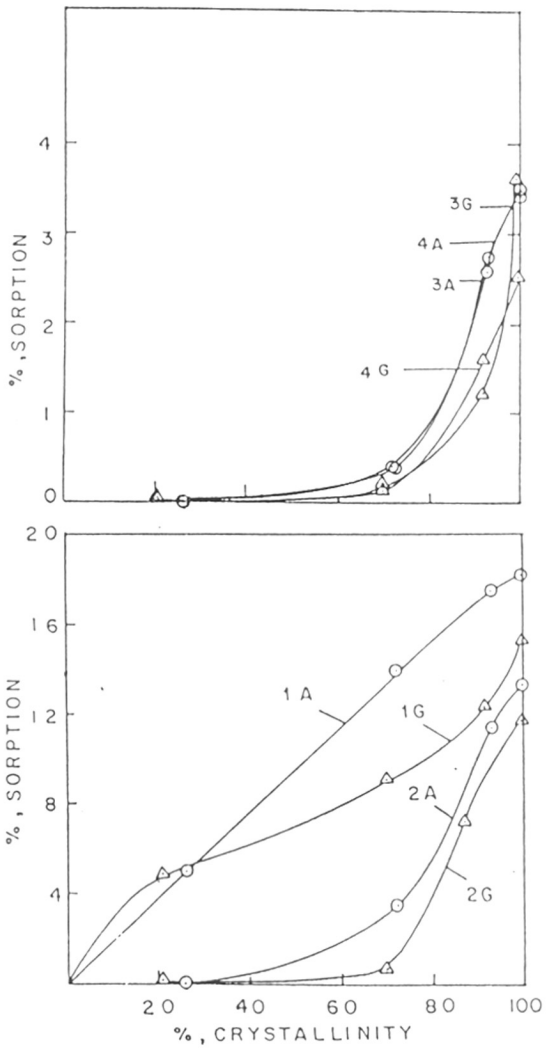

FIG. 2.11 : SORPTION UPTAKE (wt %) AS A FUNCTION OF DEGREE OF CRYSTALLINITY AT 398 K FOR Al-OMEGA (1 A), WATER (2 A), n-BUTYLAMINE, (3 A) n-HEXANE, (4 A) CYCLOHEXANE AND FOR Ga-OMEGA (1 G) WATER (2 G) n-BUTYLAMINE (3 G) n-HEXANE (4 G) CYCLOHEXANE

of low crystallinity. The sorption of water, however, gives the measure of the hydrophilic/hydrophobic character of the product or also the measure of incorporation of trivalent species like Al^{3+} and Ga^{3+} in the silica matrix. n-Hexane, cyclohexane and n-butylamine (n-BA) are comparatively larger in size and they were sorbed in the cavities of zeolite samples of crystallinity higher than 50%.

Table 2.6 summarizes the sorption uptake (at p/p_o = 0.8, T = 298 K) of water, n-hexane, cyclohexane and n-BA in fully crystalline samples of Al- and Ga- omega synthesized at different temperatures. The salient features of Table 2.6 are as follows :

The sorption uptakes are found to decrease with the increase in synthesis temperature. Since the gel SiO_2/M_2O_3 ratio and product SiO_2/M_2O_3 ratio (M = Al or Ga) are almost the same for all the samples; at least, water sorption uptake is not expected to change. The decrease in sorption uptake with the increase in synthesis temperature is consistent with the observed increase in the crystallite size. As the molecular size of the probe molecule increases, a decrease in sorption uptake with the increase in crystallite size becomes appreciable on account of their different packing in the zeolite voids. Ga-omega exhibits lower sorption uptake than its aluminum analog, on account of the larger crystallites of the former or may be due to the presence of occluded Ga_2O_3 species in the pores of the molecular sieve. Both the polar molecules like water and n-BA show higher sorption uptake than that for nonpolar molecules like n-hexane and cyclohexane. Polar molecules are expected to interact strongly with the sorption centers (extra-framework cations) and may also lead to a close packing and hence may exhibit enhanced sorption uptake.

Table 2.6 Adsorption (wt %) of Al- and Ga-omega zeolites, P/Po = 0.8 and T = 298 K

	Al-omega			Ga-omega		
Synthesis ---> Temperature (K)	383	398	413	383	398	413
Adsorbate						
Water	20.45	18.10	17.30	17.50	14.9	15.3
n-butylamine	17.19	13.22	10.10	15.50	11.69	9.60
n-hexane	6.70	4.91	2.09	4.70	2.95	1.80
cyclohexane	6.50	5.05	2.25	4.61	2.47	1.80

2.5. CONCLUSIONS

Zeolite Al-omega was synthesized hydrothermally using TMAOH (25 wt.% in methanol) in the temperature range of 383 - 413 K. The apparent activation energies for the process of nucleation and crystal growth are obtained from crystallization kinetics. Zeolite Ga-omega was also hydrothermally synthesized at 398 K using TMAOH as template. The incorporation of Ga into omega framework was confirmed by chemical analysis, XRD, framework IR and solid state MAS-NMR spectra. The unit cell volume obtained from the XRD data for Ga-omega (2225 $Å^3$) was found to be higher than that (2210 $Å^3$) for Al-omega zeolite. The IR spectra of Ga-omega shows a lower wavenumber for the structure sensitive vibrations, due to the incorporation of heavier Ga atoms, as compared to those of Al-omega. The ^{71}Ga MAS-NMR spectrum confirms the tetrahedral coordination of Ga^{3+} species in the omega framework. Al-omega exhibited spherical crystallites (3 μm), whereas a cylindrical morphology (3.5 x 8.5 μm) was obtained for Ga-omega. Chemical analysis shows that the Na occupancy in Ga-omega is higher than that in Al-omega. The Al- and Ga-omega are stable upto temperature of 1173 K. Sorption uptakes are found to be higher for Al-omega than for Ga-omega. This may be due to larger crystallite size or may be due to occlusion of Ga_2O_3 in the pores of the molecular sieves Ga-omega.

REFERENCES

1. Barrer,R.M. and Villigier, H.Z., Kristallogr., **128**, 352(1969).
2. Galli, E.: Cryst. Struct. Commun. **3**, 339 (1974).
3. Rinaldi, R., Pluth, J.J. and Smith, J.V.: Acta Crystallogr., B31, 1603 (1975).
4. Flanigen, E.M. and Kellberg, E.R.: Dutch Pat. 6, 710, 729 (1968.)
5. Aiello, R. and Barrer, R.M., J. Chem. Soc. A, 1470 (1970).
6. Cole, J.F. and Kouwenhoven, W., Adv. Chem. Ser., **121**, 583 (1973), Am. Chem. Soc., Washington DC.
7. Perrotta, A.J., Kibby, C., Mitchell, B.R. and Tucci, E.R., J. Catal., **55**, 240 (1978).
8. Ciric, J., French Pat. 1 502 289 (1967), US Pat. 3 923 639 (1975).
9. Ciric, J. and Reid, L.J., U.S. Pat. 3 433 589 (1969).
10. Dwyer, F.G. and Chu, P., J. Catal., **59**, 263 (1979).
11. Araya, A., Barber, T.J., Lowe, B.M., Sinclair, D.M., and Varma, A., Zeolites, **4**, 263 (1984).
12. Barrer, R.M.: Hydrothermal Chemistry of Zeolites, Academic Press, London, 251 (1982).
13. Szostak, R. and Thomas, T.L., J. Catal., **100**, 55 (1986).
14. Ball, W.J., Dwyer, J., Garforth, A.A. and Smith, W.J., Stud. Surf. Sci. Catal., **28**, 137 (1986).
15. Newsam, J.M. and Vaughan, D.E.W., New Developments in Zeolite Science and Technology, Murakami, Y. and Ward, J.W. (Eds.), 459 (1986).
16. Hayashi, S., Suzuki, K., Shin, S., Hayamizu, K. and Yamamoto, O., Bull. Chem. Soc. Jpn., **15**, 52 (1985).
17. Rao, G.N., Shiralkar, V.P., Kotasthane, A.N., Ratnasamy, P., Molecular Sieves, Vol. 1, Synthesis of Microporous Materials, Ch.13, Occelli, M.L. and Robson, H.E., (Eds.), Van Nostrand Reinhold, NY, 153 (1992).
18. Eapen, M.J., Reddy, K.S.N., Joshi, P.N. and Shiralkar, V.P., J. Incl. Phenom., **14**, 119 (1992).
19. Kuhl, G.H., J. Inorg. Nucl. Chem., **33**, 3261 (1971).
20. Newsman, J.M., Jarman, R.H. and Jacobson, A.J., Mat. Res. Bull., **20**, 125 (1985).

21. Vaughan, D.E.W. and Strohmaier, K.G., Molecular Sieves, Vol. I, Synthesis of Microporous Materials, Ch.8, Occelli, M.L. and Robson, H.E. (Eds.), Van Nostrand Reinhold, NY, 92 (1992).

22. Breck, D.W., Zeolite Molecular Sieves Structure, Chemistry and Use, John Wiley Interscience, NY, 364 (1974).

23. Shiralkar, V.P. and Clearfield, A., Zeolites, **9**, 363 (1989).

24. Kulkarani, S.B., Shiralkar, V.P., Kotasthane, A.N., Borade, R.B. and Ratnasamy, P., Zeolites, **2**, 313 (1982).

25. Joshi, P.N., Kotasthane, A.N. and Shiralkar, V.P., Zeolites, 598 (1990).

26. Thompson, R.W., Zeolites, **12**, 680 (1992).

27. Ouden, C., Den, J.J. and Thomson, R.W., Am. Chem. Soc. Ind. Eng. Chem. **31** (1), 369 (1992).

28. Fajula, F., Nicolas, S., Renzo, F.D., Gueguen, C. and Figueras, F., Zeolite Synthesis, ACS Symp. Series, Vol. 398, Occelli, M.L. and Robson, H.E. (Eds.), Van Nostrand Reinhold, NY, 493 (1988).

29. Szostak, R., Molecular Sieves: Principles of Synthesis and Identification, Van Nostrand Reinhold, 320 (1989).

30. Szostak, R. and Thomas, T.L., J. Catal., **101**, 549 (1986).

31. Massiani, P., Fajula, F. and Figueras, F., Zeolites, **8**, 322 (1988).

32. Chauvin, B., Massiani, P., Dutarte, R., Figueras, F. and Fajula, F., Zeolites, **10**, 174 (1990).

Chapter III

Physico - Chemical Characterization Of Modified Omega Zeolites

3.1 INTRODUCTION

The ability to undergo reversible cation exchange is one of the most important properties of zeolites. The adsorption and catalytic properties of zeolites are modified to a considerable extent by the replacement of Na^+ with other multivalent ions[1]. The variations in the physico-chemical properties of exchanged zeolites are generally determined by the measurement of sorption, thermal and diffusion properties[1,2]. From the sorption capacities for different probe molecules, the modifications in pore structure are determined. The sorption of nitrogen at 78 K not only gives[3] a measure of the surface accessible to molecules comparable in size with nitrogen or smaller but also the surface area of the sample.

The acidic and basic properties of solid surfaces are interesting aspects of surface structure and are important in the field of heterogeneous catalysis. The acidity of zeolite has been extensively evaluated by IR spectra of chemisorbed bases such as pyridine, piperidine and n-butylamine on zeolites[4-6]. Titration with organic bases such as n-butylamine using Hammet indicators has been reported[7,8]. The molecular size of these basic molecules, however does not permit them to penetrate comparatively smaller windows (2.6 Å) of sodalite cages in the zeolite[9]. Ammonia molecule on the other hand, penetrates the sodalite cavities of zeolites and interact strongly with acid centers as well as cations in the zeolite lattice. From the chemisorption of ammonia, the number and strength of acid centers are calculated[10-14] and the temperature needed to desorb the ammonia completely is taken as a measure of acid strength of the site.

Isosteric heats of adsorption of piperidine, pyridine, n-butylamine[15] and ammonia[8] also serve as a measure of zeolite acidity. Barrer has reported the adsorption of ammonia in zeolites[16,17]. Takahashi and co-workers[18-21] reported detailed studies on acidity determination with n-butylamine and differential heats of ammonia sorption in various oxide catalysts and Y-type zeolites exchanged with La^{3+}, Ca^{2+}, and H^+. Extensive studies have been reported by Coughlan and his workers[22-27] on ammonia sorption on various cation exchanged with A, X, Y, L type zeolites and mordenite.

On account of increased accessibility, large pore zeolites have always been the focus of catalytic activity for the catalyst chemists. Apart from faujasites (type X and Y), mordenite, LTL, zeolite omega and ZSM-4 synthetic isotypes of the mineral mazzite[28,29] are the large pore zeolites expected to catalyze hydrocarbon conversion reactions.

Zeolite omega is a large pore zeolite (7.5 Å) having hexagonal symmetry with a silica to alumina ratio in the "intermediate" range of (5 to 10). Structural details of zeolite omega are explained in chapter I. The difficulty of obtaining reliable information on the porosity of zeolite omega arises from the necessity of removing the encapsulated TMA ions by thermal treatment when performed in the presence of an inert gas, the decomposition of the organic cations is incomplete and a residue remains on the zeolite. In the presence of air or oxygen, substantial exothermic effects accompany the oxidative breakdown of the tetramethylammonium hydroxide, associated with the partial destruction of the framework[30].

The difference in the porosity of 11 Å aperture size predicted by Flanigen[31] and the actual porosity observed in case of synthetic acidic catalysts prepared from synthetic omega could not be resolved even when decomposition of TMA was carried out in the presence of an inert gas or in presence of an air. Similar observations were made by Chauvin *et al.*[32] The intracrystalline zeolite porosity is reflected in sorption uptakes which are in turn reflected in physico-chemical properties.

A systematic investigation of the thermal stability with the help of XRD, IR, TG, DTA results and sorption properties of both Al- and Ga-isomorphs in different cationic forms of zeolite omega with special emphasis on sorption kinetics with n-hexane, cyclohexane, water and benzene and also isotherms of ammonia sorption in the temperature range of 323-523 K is carried out. The results on the sorption uptakes based on sorption kinetics, analysis of sorption isotherms in terms of different isotherm models, evaluation of different thermodynamic parameters have been reported in the present study.

3.2 EXPERIMENTAL

3.2.1 Preparation of various cationic forms of omega zeolite and chemical analysis

The as-synthesized samples of Al-omega (Si/Al = ~4.45) and Ga-omega (Si/Ga = ~4.17) were obtained by hydrothermal crystallization as reported in Chapter II[33]. The as-synthesized zeolites were calcined carefully in the range 863-893 K for 6h. The temperature was raised to 573 K with a heating rate of 3 K min^{-1} and then to 893 K with a heating rate of 2 K min^{-1}. It was confirmed by DTA/TG that no occluded TMA was found in the calcined sample. The template- free samples thus obtained were ion exchanged with lanthanum nitrate and ammonium nitrate separately by following the conventional cation exchange procedure. The NH_4-Ga-omega sample was calcined in a controlled manner by slow heating at a rate of 2 K min^{-1} upto 748 K for long duration (10h). All the template free samples and cation exchanged samples were powdered, and sieved (200 mesh) and were stored over saturated ammonium chloride solution at room temperature. The unit cell compositions of these samples were calculated from wet chemical analysis estimated by gravimetric methods in combination with atomic absorption spectrometer and flame photometer. The unit cell compositions of zeolite samples are listed in Table 3.1.

3.2.2 X-ray diffraction

The influence of the thermal treatment on crystallinity of NH_4-Al-omega and NH_4-Ga-omega was studied by following procedure.

Both the samples were kept at the identical position in the calciner in silica crucible and calcined in air at a heating rate of 3 K min^{-1}. The calcination temperature was raised stepwise to 723, 773, 823 and 923 K. The temperature was maintained for 2 h at every step and samples were removed to check their thermal stability. The samples NH_4-Al-omega and NH_4-Ga-omega treated at 373 K were taken as standard (100 % crystallinity) for the calculation of percent relative crys-

Table 3.1 Unit cell composition of the zeolites

Sample	Unit cell composition	No. of unit cells/gm X 10^{-20}	Surface area (m^2/g)	Micro pore volume ($ml\ g^{-1}$)
Na-Al-omega	$Na_{6.54}H_{0.04}[(AlO_2)_{6.6}(SiO_2)_{29.4}]$	2.61	259	0.098
Na-Ga-omega	$Na_{6.6}H_{0.09}[(GaO_2)_{6.69}(SiO_2)_{29.31}]$	2.31	234	0.086
H-Al-omega(98.6)	$Na_{0.08}H_{6.52}[(AlO_2)_{6.6}(SiO_2)_{29.4}]$	2.79	290	0.106
H-Ga-omega(99.3)	$Na_{0.05}H_{6.64}[(GaO_2)_{6.69}(SiO_2)_{29.31}]$	2.45	246	0.093
La-Al-omega(62.2)	$Na_{2.5}La_{1.35}H_{0.05}[(AlO_2)_{6.6}(SiO_2)_{29.4}]$	2.51	210	0.077
La-Ga-omega(58.0)	$Na_{2.93}La_{1.35}H_{0.05}[(GaO_2)_{6.96}(SiO_2)_{29.31}]$	2.22	195	0.072

Values within the parantheses signify the percent exchange of cations.

tallinity. The X-ray powder diffraction patterns were recorded on Rigaku (model, D/MAX-III-VC, Japan) X-ray diffractometer using a Ni filtered CuKα - radiation (λ = 1.5406 Å) Si was used as internal standard for the analysis of the sample.

3.2.3. Infra-red spectroscopy

The framework IR spectra were recorded in the frequency range of 400-1300 cm^{-1} using KBr pellet technique. Also FTIR spectra of samples with/without pyridine sorption in the hydroxyl stretching vibration region 3000-4000 cm^{-1} and in the region of 1700 to 1400 cm^{-1} was recorded on **Nicolet 60 SXB FTIR** spectrophotometer following the procedure as described below.

The powder sample was pressed (5 ton/$inch^2$) into self supporting wafers (5-12 mg/cm^2) introduced into a conventional all silica in-situ transmittance FTIR cell which was connected to an evacuation gas manipulation manifold (**Micromeritis-Accusorb 2000 B**). The sample was activated at 673 K for 4 h in vacuum (10^{-6} Torr) and cooled to 323 K. Pyridine vapor (5 Torr) was then introduced and equilibrated for 1 h. It was then evacuated at 373 K and cooled down to 323 K before recording the spectrum (2 cm^{-1} resolution, 100 scans). Again the sample was evacuated at 423 K and the spectra were recorded after cooling it to 323 K.

3.2.4 Thermal analysis

Thermal analysis of all the omega zeolites were performed on an automatic derivatograph (SETARAM TG-DTA 92). The thermograms of the samples were recorded under following conditions.

Weight of the sample = 40 mg

Heating rate = 10 K min^{-1}

Pressure = Flowing air at atmospheric pressure

Finely powdered α - alumina was used as a reference material.

3.2.5 Adsorption measurements

The sorption measurements were carried out on an all glass gravimetric apparatus using a McBain-Baker type silica spring (sensitivity ~ 70cms g^{-1}) balance (Fig. 2.2, Chapter II). The temperature during isotherm measurements was maintained within ± 1 K using an Aplab temperature controller. The temperature accuracy throughout the sorption measurements was ± 1%. The sorption isotherms were measured at an interval of 50 K in the temperature range of 323 - 523 K using 50-70 mg sample, degassed in vacuum (10^{-6} Torr) at 673 K for 10h. The temperature was raised with the heating rate of 2 K, min-1 with simultaneous evacuation at 10^{-6} Torr. The temperature was then lowered to the isotherm temperature at which it was allowed to stabilize and maintained at least 2 h before the commencement of the measurement. The sorption isotherms were measured upto 400 Torr. The isotherm measurements were initially carried out at 523 K and then subsequently at lower temperature. In order to check the reversibility of the sorption, the desorption measurements were carried out. After each isotherm, the sample was evacuated at 10^{-6} Torr at 673 K for 10h. X-ray diffractograms were recorded for each sample before and after the sorption measurements in order to check the structural stability.

Prior to the measurement of sorption kinetics, the sample was activated under vacuum (10^{-6} Torr) at 673 K as mentioned above. The sample was cooled down to 298 K and was then contacted with vapors of liquid sorbates at relative pressure of 0.8. Equilibrium sorption was measured up to 2 h. A low temperature (78 K) nitrogen sorption was carried out using Omnisorb, 100CX.

Ammonia from cylinder (purity > 99.5%) was further purified by passing it over ignited calcium oxide, potassium hydroxide pellets and activated molecular sieve.

3.3 RESULTS AND DISCUSSION

3.3.1. X-ray diffraction

The XRD profiles of the thermally treated samples at different temperatures are shown in Fig.3.1 and Fig.3.2, for NH_4-Al-omega and NH_4-Ga-omega respectively and it is observed that there

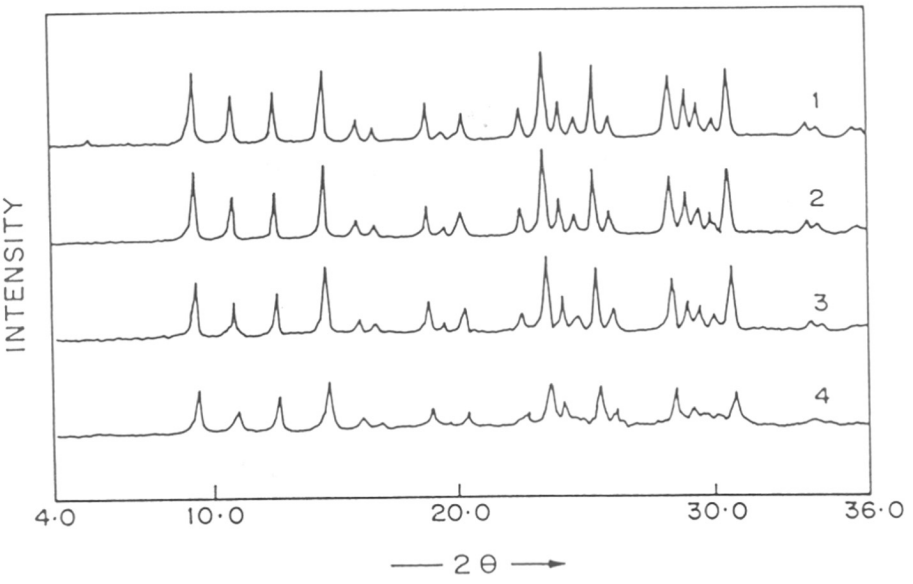

FIG. 3·1: X-RAY DIFFRACTOGRAM OF NH_4-Al-OMEGA AT 1) 373 K, 2) 723 K, 3) 823 K, 4) 923 K

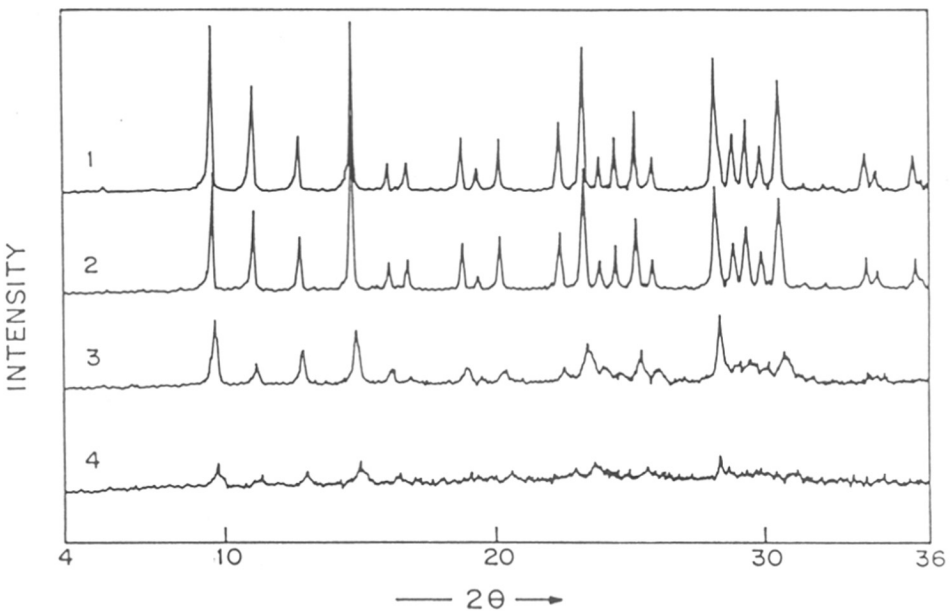

FIG. 3·2 : X-RAY DIFFRACTOGRAM OF NH_4-Ga-OMEGA AT 1) 373 K , 2) 723 K , 3) 773 K AND 4) 823 K

is a gradual decrease in the XRD peak intensities of NH_4-Al-omega with increase in calcination temperature. In case of NH_4-Ga-omega there appears to be abrupt decrease in crystallinity at 773 K and 823 K.

The salient features of the calcination treatment and the parameters derived from XRD data are summarized in Table 3.2. It is observed from the Table 3.2 that NH_4-Al-omega shows gradual decrease in percent relative crystallinity from 86 at 723 K to 59 at 923 K whereas NH_4-Ga-omega shows sharp decrease in percent relative crystallinity from 83 at 723 K to nearly amorphous at 923 K. This is also supported by the gradual decrease in unit cell volume of NH_4-Al-omega whereas for NH_4-Ga-omega the unit cell volume decreased suddenly at 773 K. Similar results on thermal stability are also reported on NH_4-Al-omega[30] and Na-Al-omega[34] in the literature.

The x-ray diffraction patterns of Al- and Ga-omega zeolites in Na^+, La^{3+} and H^+ forms calcined at 723 K for 6 h are shown in Fig. 3.3 and 3.4 respectively. The XRD pattern of Na-Al-omega (Fig. 3.3) confirms the reported data[35,36]. The XRD data for exchanged zeolite samples show that the crystallinity is retained in all the Al-omega samples.

The XRD pattern of Na-Ga-omega shows close similarity with the XRD pattern of Na-Al-omega. The XRD data for Ga-omega shows that the crystallinity is retained in a broad sense; whereas H-Ga-omega shows around ~78% crystallinity. This indicates that H-Ga-omega is thermally not as stable as Na^+ and La^{3+} exchanged Ga-omega.

3.3.2. FTIR SPECTROSCOPY

3.3.2a Framework region

The framework IR spectra of Al-omega samples of varying crystallinity and crystalline Ga-omega are already described in Chapter II. The IR spectra in the region of fundamental vibrations of framework for Na^+, H^+ and La^+ forms are compared with those of (TMA) forms for Al- and Ga-omega in Fig. 3.5 and 3.6 respectively. The specific IR absorptions are assigned (Table 3.3) to stretching, ring breathing, and bending vibrations of Si-O-M (M = Al or Ga) linkages as described

Table 3.2 Effect of temperature on crystallinity of NH_4-Al-omega and NH_4-Ga-omega zeolite

Sample	a,Å	c,Å	V,Å^3	Crystallinity %
NH_4-Al-omega (373)*	18.327	7.643	2223.2	100
NH_4-Al-omega (723)	18.317	7.647	2222.0	86
NH_4-Al-omega (773)	18.317	7.647	2222.0	86
NH_4-Al-omega (823)	18.308	7.637	2216.9	86
NH_4-Al-omega (923)	- -	- -	- -	59
NH_4-Ga-omega (373)	18.344	7.660	2232.1	100
NH_4-Ga-omega (723)	18.326	7.648	2224.4	83
NH_4-Ga-omega (773)	- -	- -	- -	64
NH_4-Ga-omega (823)	- -	- -	- -	40
NH_4-Ga-omega (923)	- -	- -	- -	- -

* Values within parenthesis indicate calcination temperature (K).

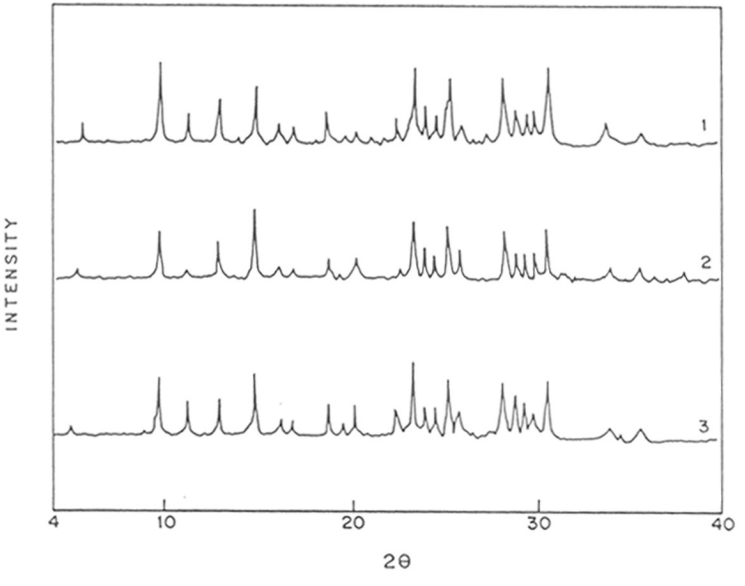

FIG. 3·3 : X-RAY DIFFRACTOGRAMS OF (1) Na-Al-OMEGA, (2) La-Al-OMEGA AND (3) H-Al-OMEGA

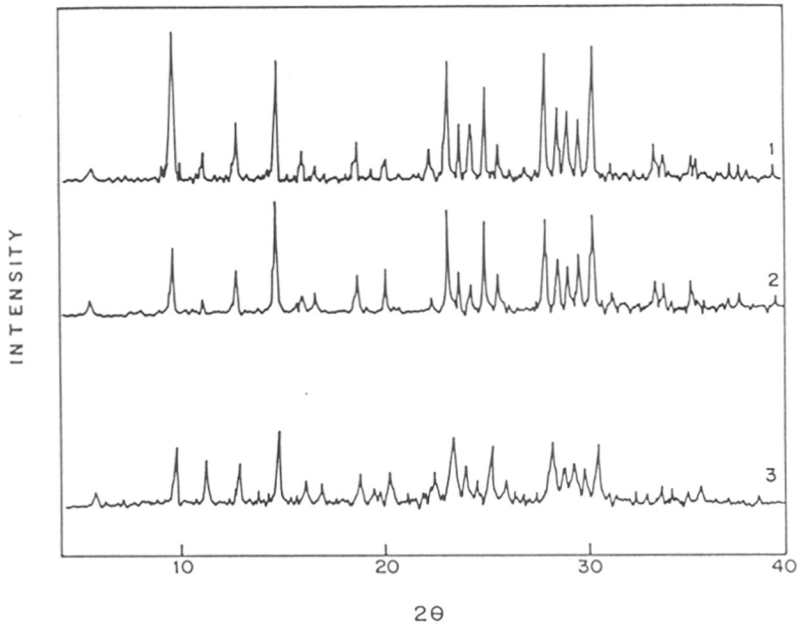

FIG. 3·4 : X-RAY DIFFRACTOGRAMS OF (1) Na-Ga-OMEGA ,(2) La-Ga-OMEGA AND (3) H-Ga-OMEGA

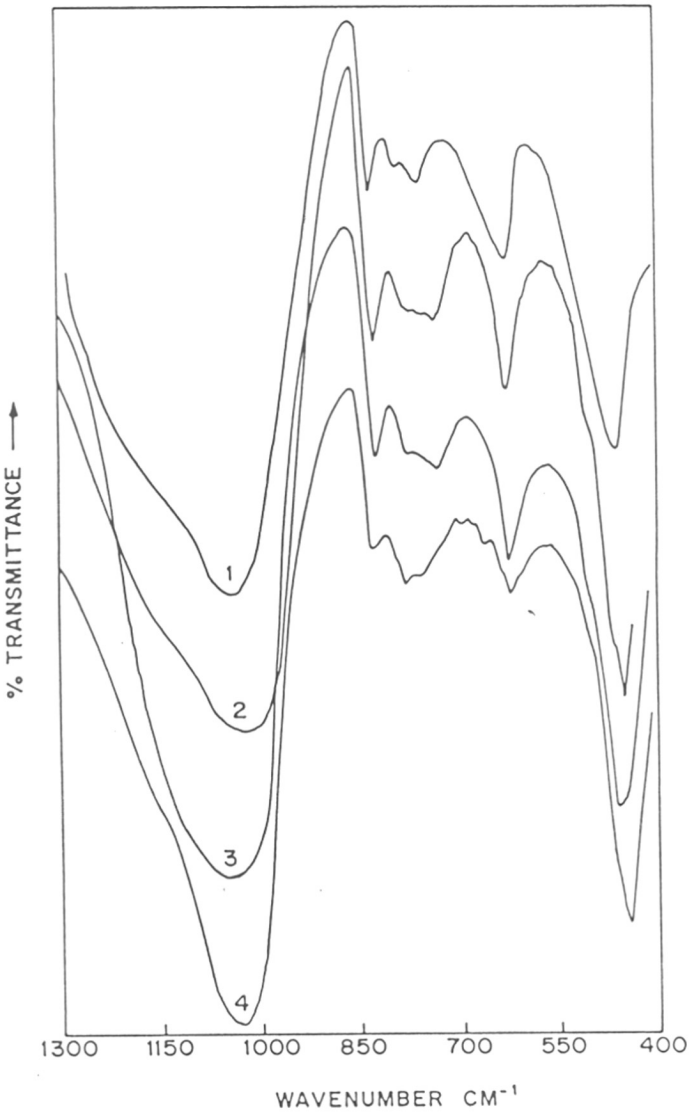

FIG.3·5 : IR SPECTRA OF CATION EXCHANGED
1) TMA-Na-Al-OMEGA, 2) Na-Al-OMEGA, 3) La-Al-OMEGA,
AND 4) H-Al-OMEGA

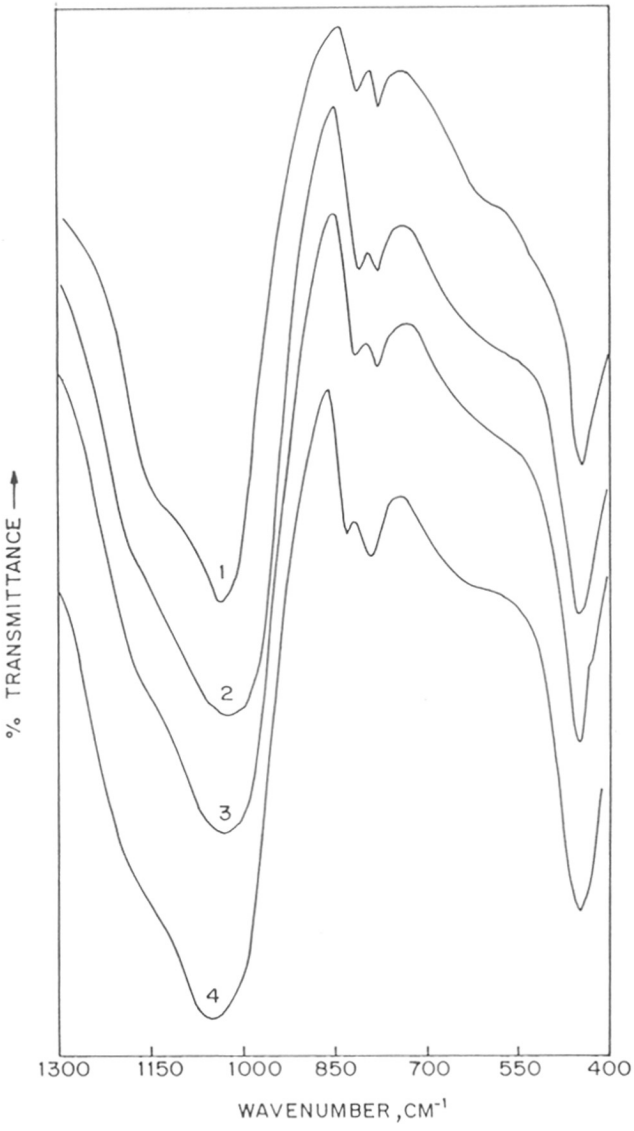

FIG.3·6: IR SPECTRA OF CATION EXCHANGED
1) TMA-Na-Ga-OMEGA, 2) Na-Ga-OMEGA, 3) La-Ga-OMEGA
AND 4) H-Ga-OMEGA

Table 3.3 IR bands of framework vibrations

Sample	Asymmetric stretching (cm^{-1})	Symmetric stretching (cm^{-1})	S-6 ring breathing (cm^{-1})	Bending vibrations (cm^{-1})
TMA-Al-omega	1037	825 m, 730 sh	625	450
Na-Al-omega	1037	821, 768, 733	622	447
La-Al-omega	1034	823, 773, 732	625	451
H-Al-omega	1034	823, 770, 735	620	448
TMA-Ga-omega	1025	815, 730	615	450
Na-Ga-omega	1027	816, 730	617 sh	447
La-Ga-omega	1023	817, 728	618 sh	450
H-Al-omega	1037	827, 734	625 sh	453

in literature[37]. Spectra of Al-omega zeolite in $(TMA)^+$, Na^+, H^+ and La^{3+} forms are identical indicating the structural stability of the zeolite on calcination and ion exchange. However, the spectra of Ga-omega samples on calcination and ion exchange (Fig. 3.6) show significant alterations in intensity and positions of framework IR spectral bands. The band at 1027 cm^{-1} due to asymmetric stretch in Na form is shifted to 1037 cm^{-1} on conversion to H- form. In addition, all other structure sensitive bands also shift to higher wavenumbers indicating more silicious nature of the framework in H^+ form. This indicates that Ga in the framework hydrolyses and comes out of the framework. Another significant observation is that all structure sensitive bands in TMA-Ga-omega are shifted to low wavenumbers compared to (TMA)Al which is attributed to the difference in force constant of Si-O-Al and Si-O-Ga bondage.

3.3.2.b Hydroxyl region

Infra Red spectra of H- forms of Al- and Ga-omega zeolites in the region of -OH stretching vibrations are shown in Fig. 3.7. Absorption bands are observed at 3740, 3660, 3615 and 3300 cm^{-1} (broad) for H-Al-omega and 3740, 3670, 3628 and 3350 cm^{-1} for H-Ga-omega samples. The bands at around 3740, 3620 and 3300 cm^{-1} are assigned to isolated silanols, bridging hydroxyl groups and hydrogen bonded -OH groups respectively. The difference in acidic bridging OH groups (Si-O-Al, 3615 cm^{-1}) of H-Al-omega compared to that of H-Ga-omega zeolite (Si-O-Ga, 3628 cm^{-1}) is due to the difference in the electronegativity of Al and Ga tetrahedral species[38]. In addition, the weak band at around 3660 cm^{-1} in both Al- and Ga-omega is due to extra lattice Al and Ga species[39,40].

3.3.2.c Absorbed pyridine

Infra red spectroscopy of absorbed pyridine has become widely used technique to determine nature of acidity of solid acids[40]. It has become possible because the ring vibration of liquid-like or physically absorbed pyridine at 1440 cm^{-1} shifts to 1450 cm^{-1} upon formation of coordinated species by adsorption on Lewis acid sites and to 1550 cm^{-1} upon formation of pyridinium ions by protonation at Brönsted sites. In Fig. 3.8, IR spectra of chemisorbed pyridine at 373, 473, 573 and 673 K on H-Al- and H-Ga-omega zeolites are presented. In both samples, in addition to bands due to hydrogen

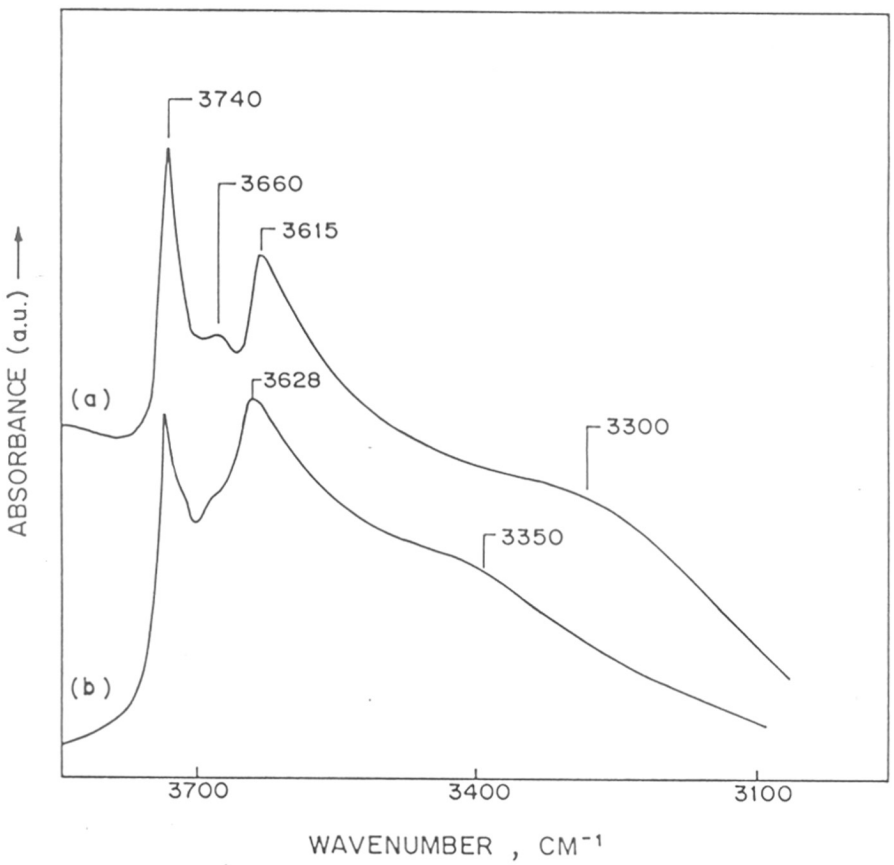

FIG.3·7: IR SPECTRA OF SURFACE HYDROXYL GROUPS ON a) H-Al-OMEGA AND b) H-Ga-OMEGA

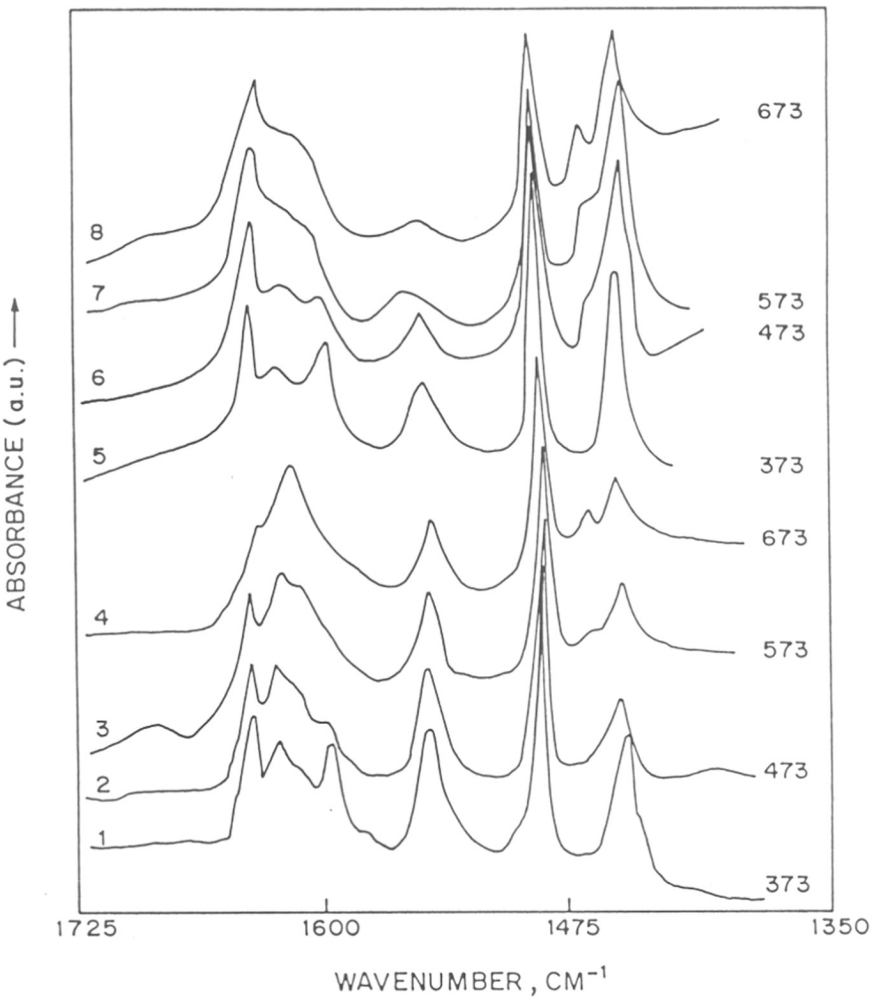

FIG. 3·8 : IR SPECTRA OF CHEMISORBED PYRIDINE ON H-Al-OMEGA (1 TO 4) AND H-Ga-OMEGA (5 TO 8) AT 373 (1,5); 473 (2,6); 573 (3,7); AND 673K (4,6) RESPECTIVELY

bonded pyridine at 1600 and 1445 cm^{-1}, the formation of pyridinium ions was indicated by the bands at 1635 and 1548 cm^{-1} and the bands at 1622 and 1455 cm^{-1} indicate the presence of coordinated pyridine due to Lewis acid sites. The band at 1490 cm^{-1} is common to both types of species. It should be noted that intensity of bands at 1550 cm^{-1} decreases more sharply than that of 1450 cm^{-1} band for H-Ga-omega compared to H-Al-omega on increasing the temperature of pyridine desorption. It indicates that Bronsted acid sites of H-Ga-omega are thermally less stable than those of H-Al-omega. At higher temperature of desorption, a new band appears around 1465 cm^{-1} for both H-Al- and H-Ga-omega zeolites. This band is attributed to the formation of a new pyridine Lewis site interaction[41].

3.3.3. Thermal properties

The thermal stability of the zeolites is technically important for economic reasons as these are used over a large number of cycles after regeneration by thermal activation around 773 K. The high temperature (> 1073 K) exotherm in DTA peak is considered as a measure of thermal stability of the zeolite.

The DTA, TG curves for Na-Al-omega and NH_4^+, H^+ and La^{3+} exchanged forms of the same are shown in Fig. 3.9. The TG curve for Na-Al-omega indicates two different stages of water loss (Table 3.4). The first one is between 319 - 518 K and second one is from 518 - 667 K and then remains almost constant upto 1273 K. The former weight loss amounting to ~ 80% of the total is mainly due to physically sorbed zeolitic water molecules. The second stage weight loss corresponds to the process of dehydroxylation. In case of NH_4-Al-omega, one more stage of weight loss is observed between 601 to 881 K due to oxidative decomposition of the ammonium form. The second stage weight loss seems to be delayed between 903 and 1078 K. This shows that protons are present in NH_4-Al-omega. Similar results are obtained for H-Al-omega. In case of La-Al-omega the hydroxylation takes place around 823 K. Similar results are obtained qualitatively for Ga-omega zeolites (Fig. 3.10) except lower thermal stability.

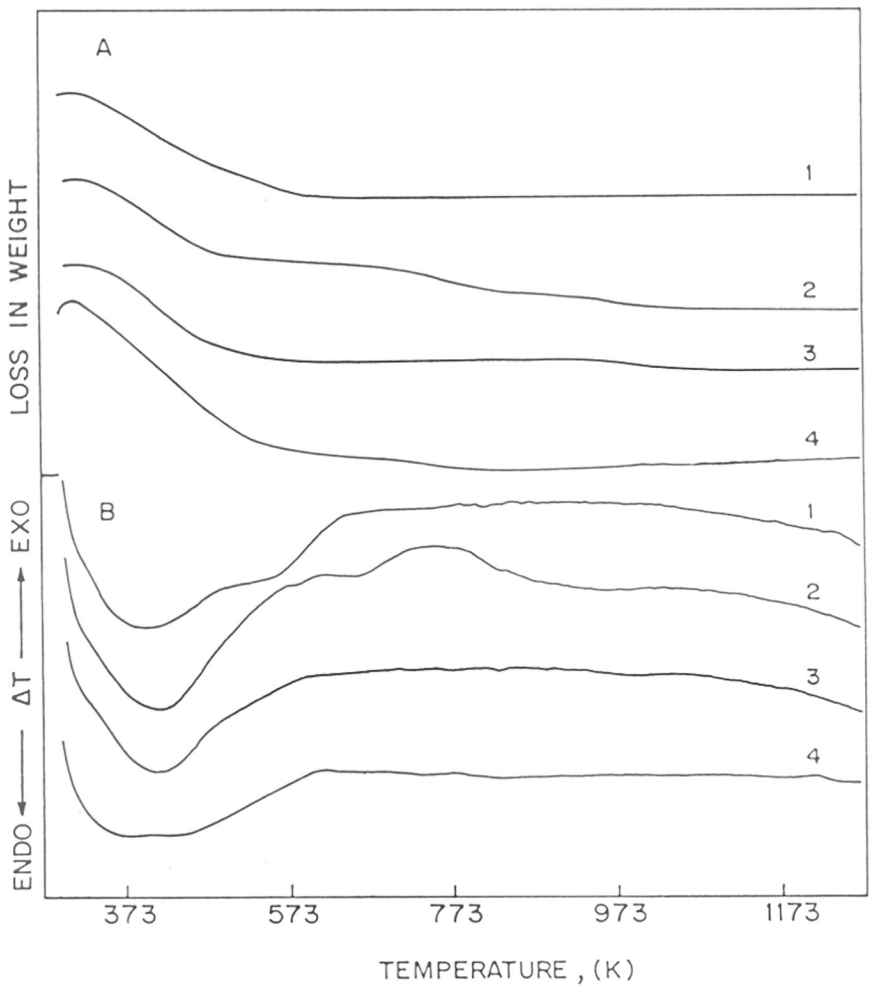

FIG. 3·9 : TG (A) AND DTA (B) CURVES OF 1) Na-Al-OMEGA, 2) NH_4-Al- OMEGA, 3) H-Al-OMEGA AND 4) La-Al-OMEGA

Table 3.4 Thermo analytical data for omega zeolites

Sample	% wt loss	Temp. (k)	Endo	Exo
Na-Al-omega	9.36	319 - 518	308 - 516	-
	2.62	523 - 667	518 - 667	-
	-	-	-	1224 - 1268
NH4-Al-omega	9.76	319 - 610	332 - 609	-
	3.36	651 - 881	-	656 - 943
	1.61	896 - 1071	-	1224 - 1260
H-Al-omega	11.36	322 - 617	324 - 619	-
	1.15	904 - 1078	907 - 1081	-
La-Al-omega	10.60	320 - 634	318 - 622	701 - 798
	0.58	708 - 787	-	1095 - 1243
			-	-
Na-Ga-omega	7.30	321 - 500	322 - 617	-
	2.43	503 - 622	-	-
	-	-	-	1127 - 1193
NH4-Ga-omega	8.63	317 - 552	316 - 626	-
	4.71	568 - 932	-	638 - 943
	-	-	-	1094 - 1155
H-Ga-omega	10.58	319 - 600	319 - 600	-
	0.09	1092 - 1158	-	-
	-	-	-	1087 - 1156
La-Ga-omega	11.50	316 - 768	308 - 618	1094 - 1146

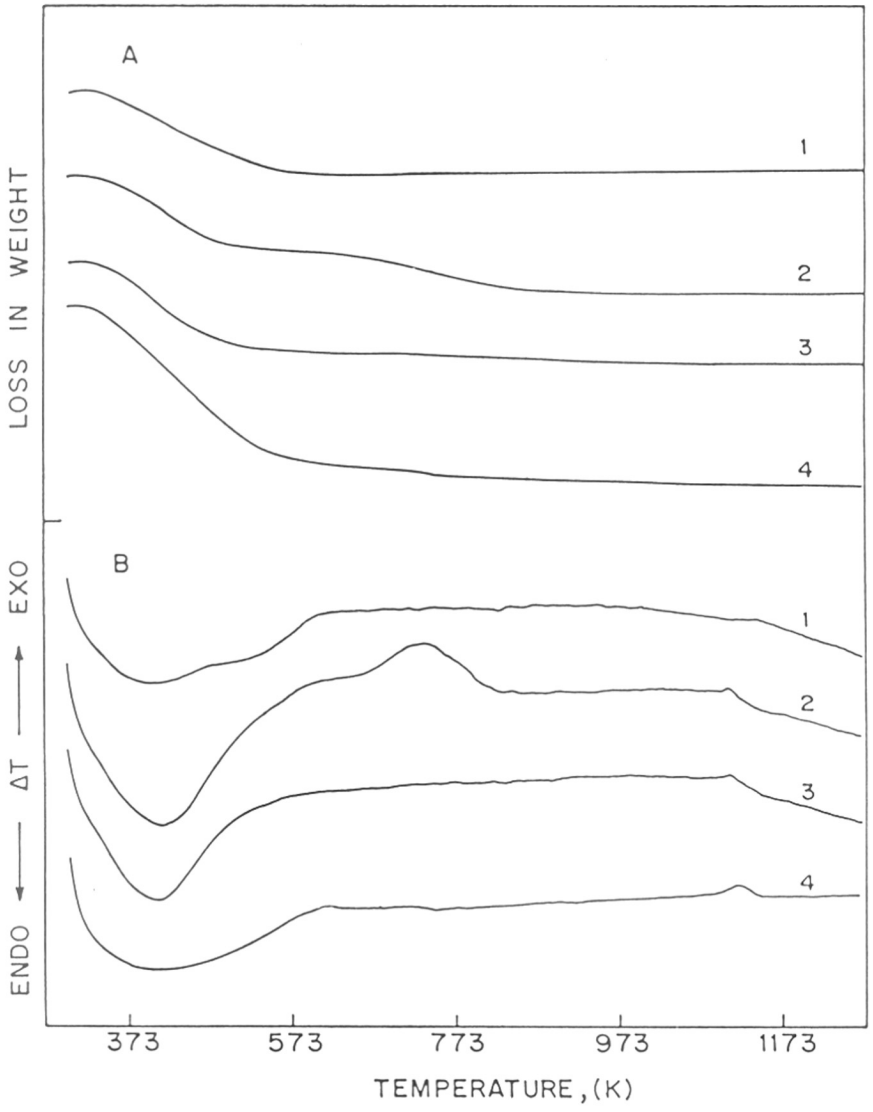

FIG. 3·10: TG (A) AND DTA (B) CURVES OF 1) Na-Ga-OMEGA 2) NH_4-Ga-OMEGA, 3) H-Ga-OMEGA AND 4) La-Ga-OMEGA

DTA curves from Fig. 3.9 and 3.10 for Al- and Ga-omega zeolites respectively indicate low temperature broad and diffuse endotherm in the range of 323 to 523 K. In case of Na-Al-omega a small endotherm is observed around 573 K indicating different environment of extraframework cations. A weak exotherm is observed around 748 K in case of NH_4-Al-omega which may be due to oxidative decomposition of NH_4- species. This exotherm is absent in the case of H-Al-omega. The low temperature endotherm is diffuse in nature in the case of Na-Al-omega. This is probably indicative of wide range of sorption centers. A high temperature exotherm is found in all the Al-analogs indicative of structural break down. The exotherm corresponding to decomposition in NH_4-Al-omega may also be accompanying a type of phase transformation leading to a dense phase formation.

Ga-analog exhibit almost same type of DTA curves. However, the salient feature of these DTA curves is lowering of high temperature exotherm in all the zeolites in the range of 1108 - 1128 K. These indicate lower thermal stability of Ga-omega as compared to Al-omega zeolite.

3.3.4. Adsorption measurements

3.3.4A Unit cell composition and sorption kinetics

Table 3.1 summarizes unit cell compositions of all the six catalysts i.e. Na-Al-omega and its gallium isomorph and the protonic forms and La^{3+} exchanged forms of both the catalysts. The % exchange in the protonic forms was $\simeq$ 99% in both the cases whereas that in La^{3+} exchange was about 60 $\pm$ 2 %. The Si/Al ratio in Al-omega was $\simeq$ 4.45 and Si/Ga ratio in Ga-omega was 4.17. This shows that gallium isomorph of omega zeolite contains more Ga^{3+} species in the unit cell lattice compared to Al^{3+} in the Al-omega. Alternatively a small fraction of Ga^{3+} is likely to be occluded in the non-lattice positions. In such a situation total nonframework species, i.e. $Na^+ + H^+$ would have been in deficit as compared to total Ga^{3+} in the solid. However, unit cell composition shows almost 1:1 equivalence between $(Na^+ + H^+)$ and Ga^{3+} in the solid. The unit cell composition also

show that in case of gallium isomorph of omega zeolite in the sodium form, of the total charge balancing species, protons are upto 5% present and which are exchanged with La^{3+} during lanthanum exchange.

In order to give the more realistic picture of various properties, the number of unit cells per gram are often found to be useful. Based on the unit cell composition, Table 3.1 also lists the number of unit cells per gram. A logical trend in the value of number of unit cells per gram is evident in case of cation exchange with lighter protons and heavier La^{3+} species compared to original Na^{+} species.

Low temperature (78 K) nitrogen sorption often serves as the criterion for the estimate of micropore void volume and specific surface area of the lattices of zeolites modified by various post-synthesis methods such as cation exchange. Table 3.1 also lists micropore volumes and specific surface area of these catalysts. In spite of slightly higher contents of tetrahedral species (Ga^{3+}) other than Si^{4+} in Ga-omega compared to Al^{3+} in Al-omega the former shows lower micropore volume and specific surface area compared to the latter one. Perhaps the larger Ga^{3+} occupies more void volume than Al^{3+} in the omega lattice leaving lower void space available for sorption. This observation is also supported by the changes observed in the void volume of protonic forms of both the isomorphs. The micropore volume and specific surface area increase from 0.098 ml g^{-1} to 0.106 ml g^{-1} and from 259m^2 g^{-1} to 290m^2 g^{-1} respectively for Na^{+} and H^{+} form of Al-omega. For Ga-omega the micropore volume increases from 0.086 ml g^{-1} to 0.093 ml g^{-1} and specific surface area increases from 234m^2 g^{-1} to 246m^2 g^{-1} Na^{+} and H^{+} forms respectively. The increase in the void volume and specific surface area in case of proton exchange of Al-omega is higher than that in Ga-omega.

The striking feature of Table 3.1 is the very low specific surface area of the La^{3+} exchanged samples of Al-omega and Ga-omega. Perhaps the larger La^{3+} species as well as much larger hydroxy cations of La^{3+} such $La(OH)^{2+}$/$La(OH)_2^{+}$ occupy position near the pore openings or in the channels thereby reducing the pore size to such an extent that nitrogen molecule exerts hindrance.

3.3.4B Sorption kinetics and equilibrium sorption uptakes

Table 3.5 summarizes the equilibrium sorption uptake from the sorption kinetics of four different probe molecules for water, n-hexane, cyclohexane and benzene at 298 K (P/Po = 0.8), for 2 h. Both Al and Ga isomorphs and cation exchanged omega zeolites show almost identical equilibrium sorption uptake with water (≈24 molecules u.c.$^{-1}$). However, with other probe molecules Ga-omega shows lower equilibrium uptake than Al-omega. The drastic reduction in the equilibrium sorption uptake for molecules larger than water such as n-hexane, cyclohexane and benzene may be due to occlusion of gallium species in the channels. This result supports the observations of low specific surface area of Ga-omega samples in case of low temperature nitrogen sorption data discussed in the earlier section.

3.3.5. Ammonia sorption isotherms and applications

1. Fig.3.11 depicts the families of ammonia sorption isotherms in all the six samples in the temperature range of 323 - 523 K upto 400 Torr. The salient feature of these isotherms is that they exhibit typically the shape of type I isotherm according Kiselev's classification[42]. The shape of the isotherm clearly shows that almost 90% of the total sorption capacity takes place in a very narrow range of pressure ~ 40 Torr followed by slowly rising plateau over a very wide range of pressure upto 400 Torr.

Table 3.6 summarizes the sorption capacities obtained experimentally and by applying different isotherm equations for all the samples at different temperatures and upto 400 Torr. As expected thermodynamically the sorption uptake decreases with the increase in temperature. In case of Na-Al-omega the uptake decreases from 14.1 molecules u.c.$^{-1}$ at 323 K to 5.50 molecules u.c.$^{-1}$ at 523 K whereas in H-Al-omega it decreases from 14.3 molecules, u.c.$^{-1}$ at 323 K to 6.6 molecules u.c.$^{-1}$ at 523 K. This means that although sorption uptake decreases with increase in temperature the hold up capacity increases at higher temperature from sodium form to protonic form. In fact, in case of lanthanum form, the hold up capacity is higher (6.9 molecules u.c.$^{-1}$) than protonic form and it is so almost at all the temperatures with almost identical sorption uptake at

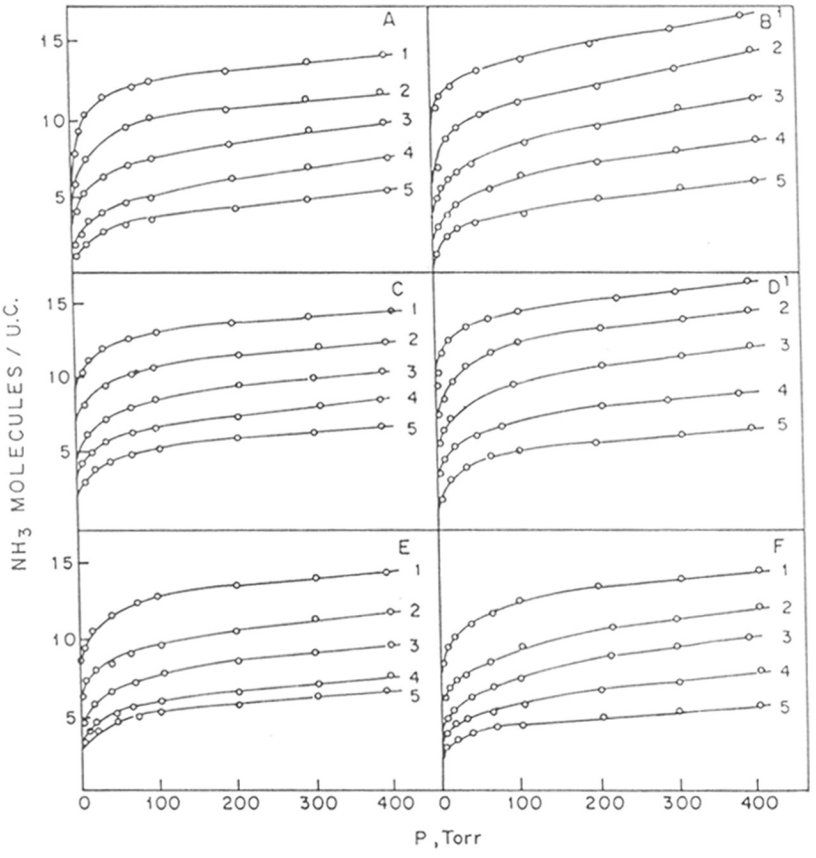

FIG. 3.11 : NH_3 SORPTION ISOTHERMS IN (A) Na-Al-OMEGA, (B) Na-Ga-OMEGA, (C) La-Al-OMEGA, (D) La-Ga-OMEGA, (E) H-Al-OMEGA, (F) H-Ga-OMEGA AT (1) 323 K, (2) 373 K, (3) 423 K, (4) 473 K, (5) 523 K

Table 3.5 Equilibrium sorption uptakes of omega samples at 298 K and P/P0=0.8

Sample	Amount sorbed, molecules / u.c.			
	Water	n-Hexane	Cyclohexane	Benzene
Na-Al-omega	23.85	1.27	1.55	1.87
	(18.63)	(4.75)	(5.67)	(6.35)
Na-Ga-omega	23.55	0.82	0.82	0.91
	(16.24)	(2.72)	(2.66)	(2.72)
La-Al-omega	24.26	1.23	1.32	1.87
	(18.24)	(4.42)	(4.62)	(6.08)
La-Ga-omega	23.66	0.57	0.37	0.30
	(15.67)	(1.80)	(1.14)	(0.85)
H-Al-omega	26.57	1.43	1.66	1.87
	(22.14)	(5.69)	(6.44)	(7.56)
H-Ga-omega	24.11	0.84	0.37	0.28
	(17.60)	(2.94)	(1.25)	(0.90)

Values within the parantheses indicate (wt %) sorption capacity

Table 3.6 Saturation capacities and affinity coefficients of omega zeolites

Sample	Temp.(K)	Molecules / u.c.					
		Experi-mental	Langmuir	BET	Freundlich	Dubinin	Affinity coefficient $B/\beta^2 X10^7$
Na-Al-omega	323	14.10	13.88	11.01	-	14.79	6.90
	373	11.80	11.49	8.74	-	12.16	9.65
	423	9.90	10.00	6.29	-	9.77	9.79
	473	7.60	7.81	4.80	-	7.41	11.82
	523	5.50	5.63	3.50	-	5.30	12.23
La-Al-omega	323	14.40	14.89	11.38	14.94	14.13	7.92
	373	12.45	13.33	9.52	12.58	11.48	7.85
	423	10.50	11.88	7.60	10.59	9.95	7.59
	473	8.65	10.02	6.00	8.66	7.94	7.05
	523	6.90	7.96	4.70	6.88	5.01	6.57
H-Al-omega	323	14.30	14.49	11.10	14.53	13.80	9.22
	373	11.60	12.35	8.41	11.54	10.72	8.07
	423	9.50	9.80	6.33	9.44	7.94	6.99
	473	7.40	8.06	5.18	7.07	6.76	5.99
	523	6.60	7.30	4.48	5.30	6.17	5.58
Na-Ga-omega	323	16.50	16.67	11.89	-	15.14	7.88
	373	14.20	14.70	9.78	-	12.88	8.58
	423	11.20	12.35	6.93	-	9.44	9.90
	473	8.60	8.95	4.90	-	7.76	11.73
	523	6.05	6.50	3.40	-	5.01	12.02
La-Ga-omega	323	16.38	17.11	12.73	16.79	15.31	9.36
	373	14.35	16.00	10.60	13.33	13.49	8.71
	423	12.00	13.79	8.59	11.22	10.72	8.01
	473	9.10	10.60	5.91	8.91	8.13	7.46
	523	6.70	7.71	4.60	6.68	5.89	6.58
H-Ga-omega	323	14.00	14.49	11.04	14.13	13.80	10.81
	373	11.80	12.99	7.83	11.88	10.47	9.10
	423	9.85	10.64	6.14	10.00	8.32	8.24
	473	7.50	8.26	4.78	7.38	6.92	7.36
	523	5.30	5.62	3.58	5.30	5.13	6.20

323 K. Similar observation is seen in case of Na-Ga-omega and La-Ga-omega but not in H-Ga-omega. The increase in hold up capacity at higher temperature may have some relation to the acidity behaviour of the zeolite.

3.3.5A Chemisorption/Sorption irreversibility

It was our general observation that all the zeolite samples studied retained a certain amount of ammonia upon desorption under vacuum. The desorption was carried out by lowering the relative pressure to zero Torr. Even at zero Torr pressure and after evacuation for 1 h. Some residual amount of ammonia was retained. The Table 3.7 lists the amount of ammonia retained irreversibly as a function of sorption temperature for all the six samples. For a comparative purpose Table 3.7 also gives uptake of ammonia at 400 Torr. Table 3.7 clearly demonstrates, commensurate to thermodynamic expectation that in general the amount retained decreases with increase in desorption temperature. The decrease is however, more sharp in case of sodium form of zeolites, moderate in case of La^{3+} exchanged zeolites and rather lower in case of protonic forms of both the isomorphs. Fig. 3.12 shows more clearly the variation in amount of ammonia retained with the increase in the temperature of desorption. The protonic form of Al-isomorph retained almost 20% of ammonia uptake even at 523 K of ammonia uptake at and 400 Torr. Where as its gallium counterpart retains ~15% at 523 K of its ammonia uptake at 400 Torr. At lower temperature (323 K) however all the zeolites retain almost 45-50% of their sorption uptake at 400 Torr indicating considerable character of irreversibility. The comparatively higher amount of ammonia retained at 523 K by protonic form of zeolites predicts rather stronger acidic character of these zeolites for any Brönsted acid site catalyzed reaction.

3.3.5B Dubinin Equation

Analysis of isotherm data in terms of various isotherm equations always gives some useful information as regards the physical state of a sorbed phase. An attempt is made here for testing the

Table 3.7 **Amount of ammonia retained irreversibly as a function of temperature**

	Molecules / u.c. at K				
Temperature -->	323	373	423	473	523
Sample					
Na-Al-omega	6.31	4.68	1.54	0.60	0.40
	(14.10)	(11.80)	(9.90)	(7.60)	(5.50)
La-Al-omega	7.28	5.43	3.60	2.60	1.84
	(14.40)	(12.45)	(10.50)	(8.65)	(6.90)
H-Al-omega	7.54	5.60	4.47	3.52	2.94
	(14.30)	(11.60)	(9.50)	(7.40)	(6.60)
Na-Ga-omega	8.05	5.10	1.91	1.10	0.50
	(16.50)	(14.20)	(11.20)	(8.60)	(6.05)
La-Ga-omega	7.38	5.33	3.22	2.30	1.72
	(16.38)	(14.35)	(12.00)	(9.10)	(6.70)
H-Ga-omega	6.59	5.20	3.70	2.80	2.05
	(14.00)	(11.80)	(9.85)	(7.50)	(5.30)

Values within paranthesis indicate sorption capacity at 400 Torr.

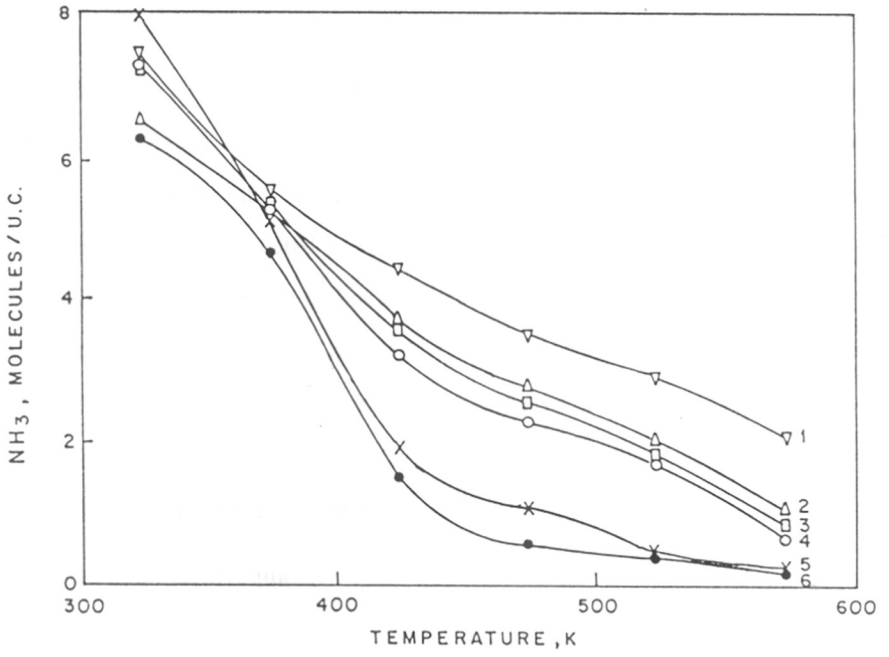

FIG.3.12 AMOUNT OF AMMONIA RETAINED IRREVERSIBLY AS A FUNCTION OF TEMPERATURE (1) H-Al-OMEGA, (2) H-Ga-OMEGA, (3) La-Al-OMEGA, (4) La-Ga-OMEGA, (5) Na-Ga-OMEGA AND (6) Na-Al-OMEGA

applicability of Polanyi's potential theory modified by Dubinin Radushkevich[43] for ammonia sorption in different omega zeolite lattices over the entire temperature range (323-523 K). The Dubinin-Radushkevich, equation is expressed as

$$\log W = \log Wo - B/2.303ß^2 [T \log P_o/P]^2 \quad ----(1)$$

where W, P, Wo, B possess their usual meaning and ß is the affinity co-efficient. Typical Dubinin plots are shown in Fig. 3.13 and 3.14, which show fairly linear plots over the entire temperature range for almost all the zeolites. The slopes of these linear plots decrease with the decrease in temperature. The co-efficient ß being inversely proportional to the temperature, increases with the decrease in temperature as listed in Table 3.6 earlier. Table 3.6 also lists the sorption uptake obtained from the intercept made by linear plots on Y axis. The linear Dubinin plots were also reported for ammonia sorptions in beta zeolites[44], CO_2 sorption in LTL zeolites[45] and for n-BA sorptions in FeY zeolites[46]. These sorption uptakes were found to be rather lower than those obtained experimentally at 400 Torr. The factor $B/ß^2$ related to the affinity co-efficient, does not show any specific trend with the temperature for all the omega samples.

3.3.5C BET Sorption Isotherm Equation

The multilayer sorption approach with a special value (a very high value) of heat of sorption (C) for the first layer leads to the type II isotherm according to Kiselev's classification and so called BET equation. When ammonia sorption data were analyzed in terms of BET equation, linear plots (shown in Fig. 3.15) were obtained upto a relative pressure of 0.15. Similar observations were made for CO_2 sorption in LTL zeolites[45]. The deviation occurring from linearity at higher pressure region may be due to multilayer formation and/or capillary condensation. BET plots display a small intercept on Y axis which increases with the increase in temperature indicating decrease in the value of C (heat of sorption for the first layer). The monolayer capacity obtained from slopes and intercepts of linear plots are listed in Table 3.6 and are rather reasonably lower than those obtained experimentally at 400 Torr. Perhaps the experimental values represent the sorption uptake which is more

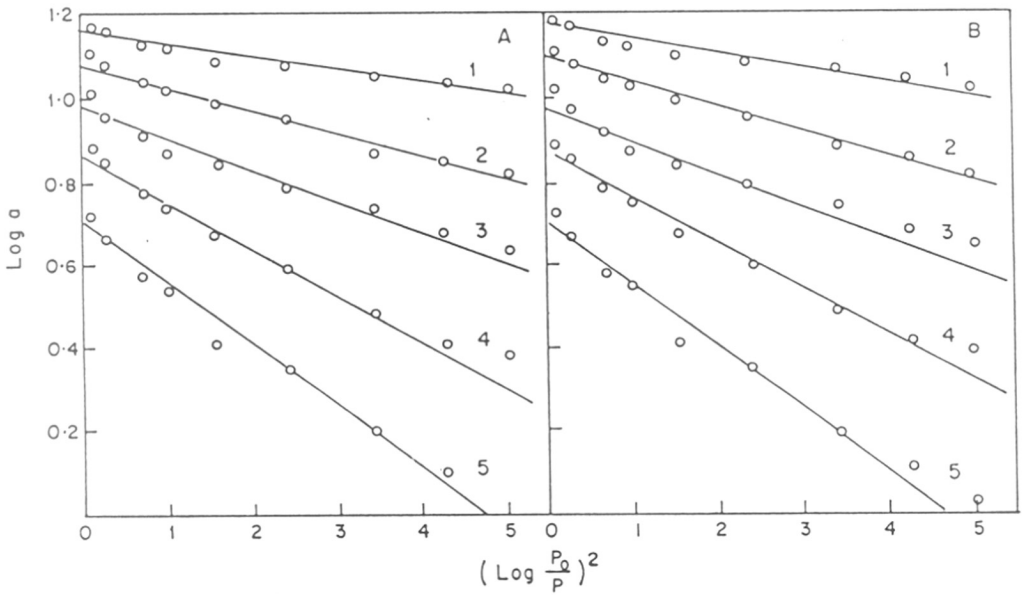

FIG.3·13:DUBININ PLOTS FOR NH_3 SORPTION OF (A) Na-Al-OMEGA, (B) Na-Ga-OMEGA AT (1) 323 K, (2) 373 K, (3) 423 K, (4) 473 K AND (5) 523 K

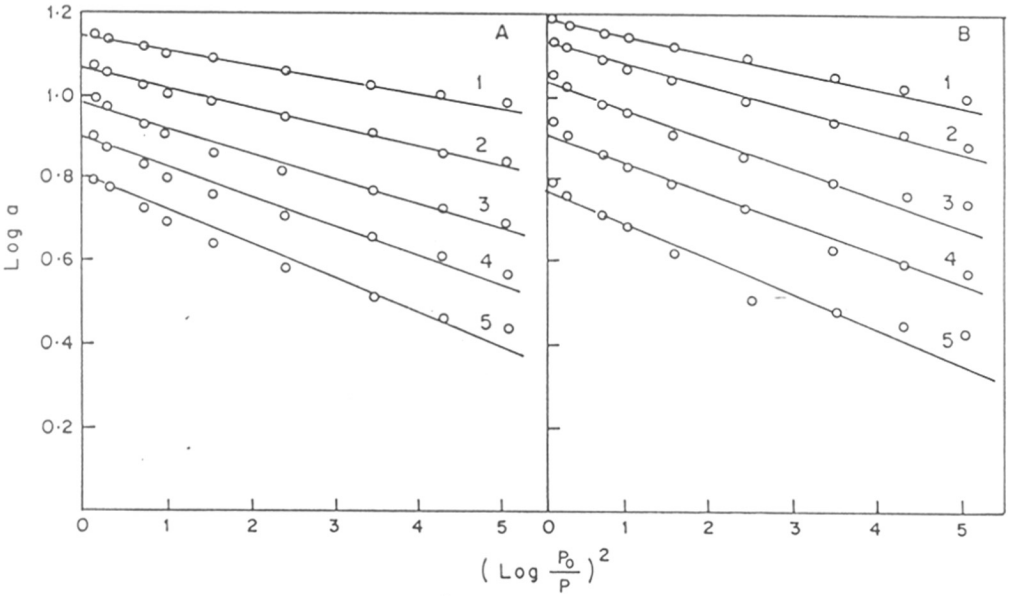

FIG.3·14:DUBININ PLOTS FOR NH_3 SORPTION OF (A) La-Al-OMEGA, (B) La-Ga-OMEGA (1) 323 K, (2) 373 K, (3) 423 K, (4) 473 K AND (5) 523 K

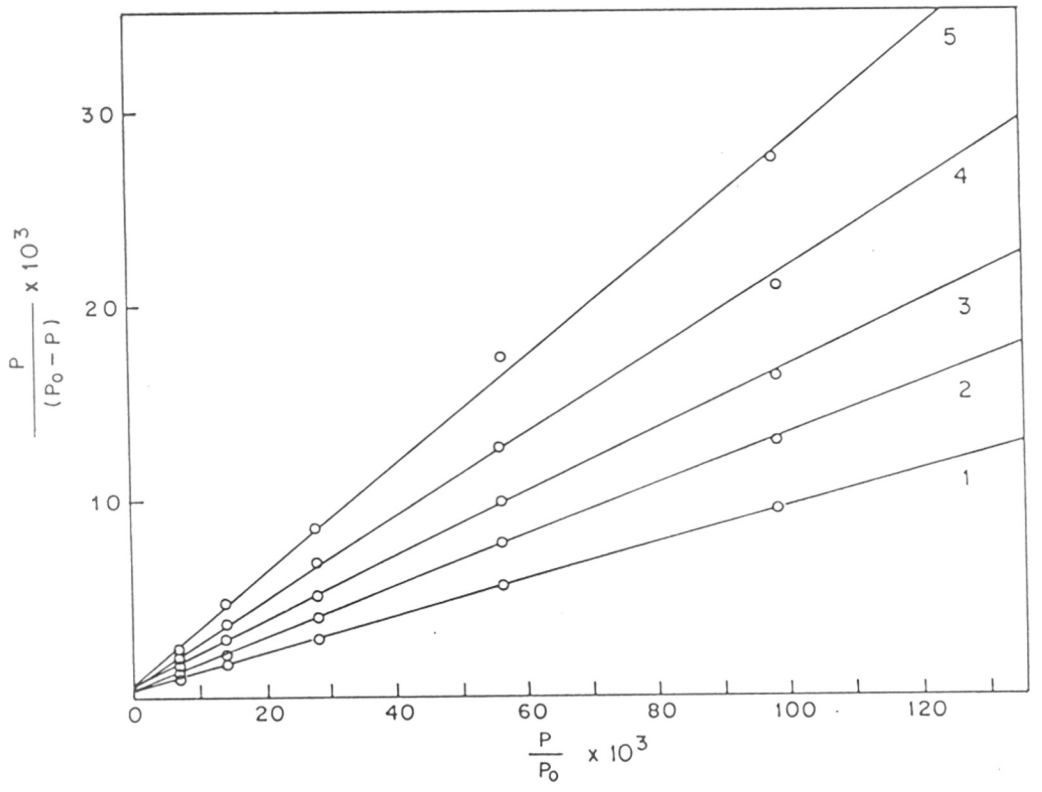

FIG.3·15:BET PLOTS FOR NH_3 SORPTION OF H-Go-OMEGA AT(1)323 K, (2) 373 K, (3) 423 K, (4) 473 K AND (5) 523 K

than that needed for the formation of monolayer on the sorbent surface. The CO_2 sorption data[47] in cation exchange Y zeolites failed to follow the BET sorption model on the other hand ammonia sorption in beta zeolites[44] shows satisfactory representation of BET sorption model.

3.3.5D Langmuir Sorption Equation

Langmuir sorption isotherm equation has been derived on the assumption of localized monolayer sorption on the centers of energetically homogeneous sorption centers with 1:1 correspondence between the sorption centers and sorbate molecules. When the ammonia sorption data in omega zeolites in the present studies were analyzed in terms of Langmuir equation, excellent linear plots were obtained for all the zeolites at all the temperatures. The typical Langmuir plots are shown in Fig. 3.16. These linear plots are found to yield a small intercept on Y axis and the value of this intercept increases with the increase in isotherm temperature. The reciprocal of the intercept may be related to the strength of the sorption centres and as the intercept decreases the more stronger interaction is involved in the sorption phenomenon. The saturation uptakes obtained from the reciprocals of the slopes of these linear plots are listed for comparative purpose in Table 3.6 and it shows that these capacities are marginally higher at lower temperatures and reasonably higher at high temperatures than experimental sorption uptakes. This observation seems to be logical as experimental uptakes are taken at 400 Torr whereas saturation uptakes are obtained almost at the plateau in the sorption isotherm. n-Butylamine sorption in EU-1 zeolites[48], FeY zeolites[46], ammonia sorption in beta zeolites[44] did yield linear plots, however, CO_2[47] and NH_3[49] sorption in cation exchanged Y zeolites failed to represent Langmuir equation.

3.3.5E Freundlich Sorption Equation

In a low or moderate pressure region, compared to saturation pressure, Langmuir equation reduces to Freundlich type equation, and it approximates a two dimensional film of the sorbate on the sorbent surface. Analysis of ammonia sorption data in different omega zeolites in the present studies yielded linear plots for all the zeolites at all the isotherm temperatures. The typical of these linear plots shown in Fig. 3.17 are characterized by a decrease in the slopes with decrease in isotherm

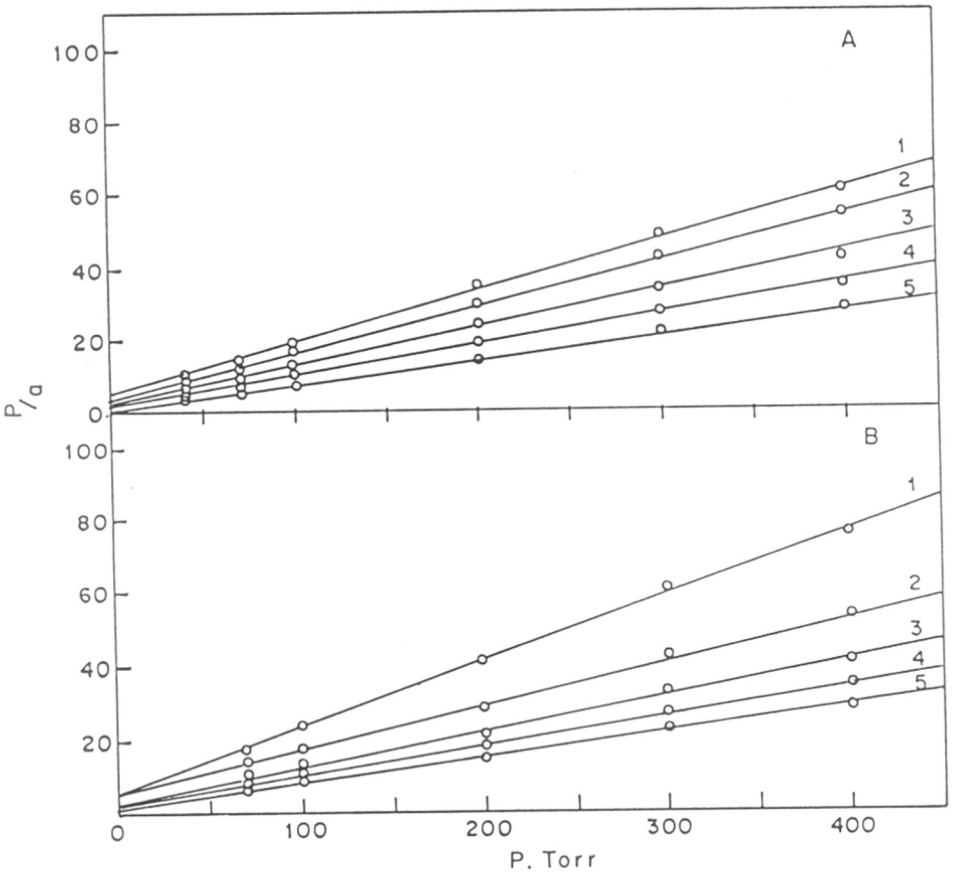

FIG.3·16: LANGMUIR PLOTS FOR NH_3 SORPTION OF (A) H-Al-OMEGA AND (B) H-Ga-OMEGA AT (1) 323 K, (2) 373 K, (3) 423 K (4) 473 K AND 523 K

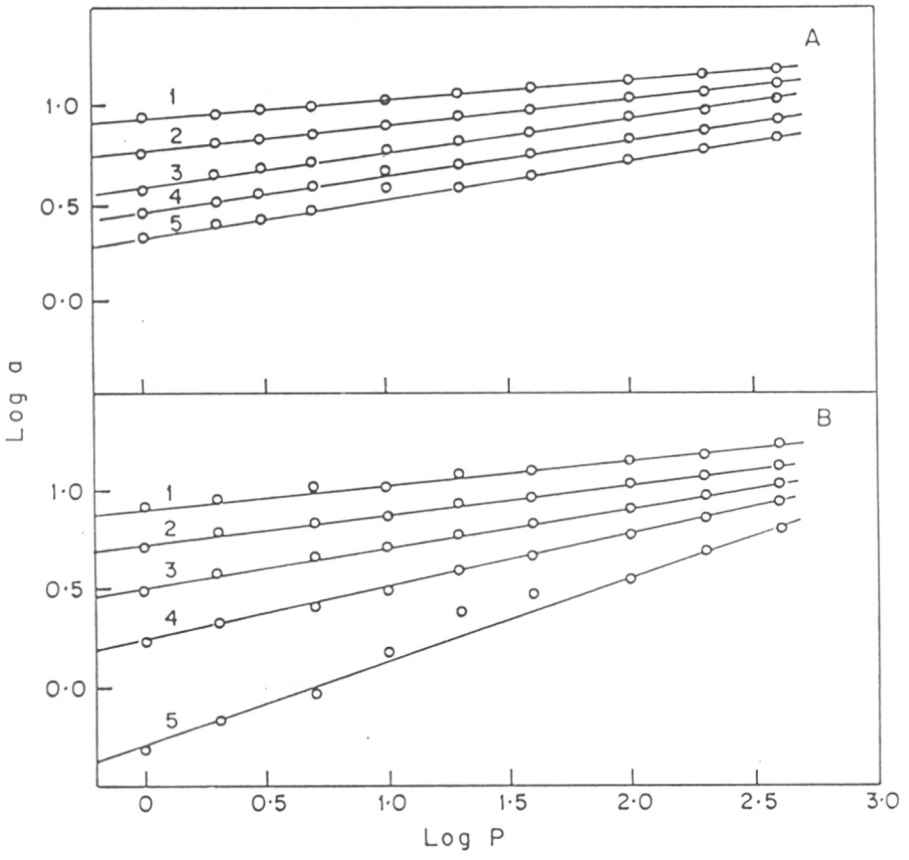

FIG.3·17: APPLICABILITY OF FREUNDLICH EQUATION FOR NH_3 SORPTION OF (A) La-Al-OMEGA, (B) La-Ga-OMEGA AT (1) 323 K, (2) 373 K, (3) 423 K, (4) 473 K AND (5) 523 K

temperature. The excellent linearity of these plots indicates the applicability of Freundlich equation to the ammonia sorption in omega zeolites. CO_2 sorption in LTL[45], n-BA sorption in FeY zeolites[46] could be satisfactorily represented by Freundlich approach, whereas n-BA sorption in EU-1[48], titanosilicates[50] failed to yield linear Freundlich plots. The sorption uptakes derived from these linear plots are compared in Table 3.6 and are reasonably found to be much closer to the experimental sorption uptake at 400 Torr.

3.3.5F Sips Isotherm Equation

The Sips[51] equation based on the localized sorption model with a sorbate-sorbate interaction usually takes care of any deviation from Langmuir approach. If the sorption is assumed to be a chemical reaction between the sorption center and the sorbate molecules, the Langmuir equation results with 1:1 correspondence between them and if some tolerance is made for the complicating factors, the Sips equation results. Mathematically Sips equation is expressed as

$$\log [\theta/(1-\theta)] = \log A + c \log P \text{ ---- (2)}$$

Where A and c are constants and P is an equilibrium pressure at coverage θ. θ was calculated by using the monolayer uptakes obtained by Langmuir equation. In order to check the applicability of Sips equation, the plots of log (θ/1-θ) against log P for all the omega zeolites were constructed for ammonia sorptions in the temperature range 323-523 K. Fig. 3.18 shows typical Sips plots for ammonia sorptions in omega zeolites in the lower pressure region (100 Torr) and a reasonable linearity confirms the applicability of Sips equation to the ammonia sorption data in omega zeolites in the low pressure region only. Similar observation was also reported for CO_2 sorption in LTL zeolites[45].

The deviation from unity of the value of C derived from the slopes of the linear plots give the extent of a deviation from Langmuir approach. All linear plots obtained in low pressure region

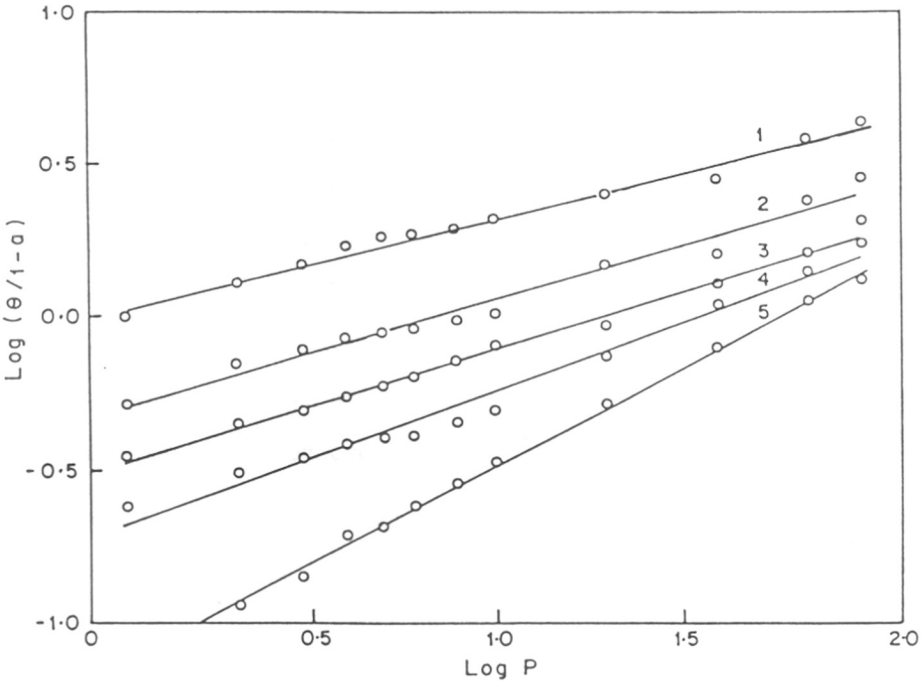

FIG.3·18:PLOTS OF SIPS EQUATION OF Na-Ga-OMEGA AT(1)323 K, (2) 373 K, (3) 423 K, (4) 473 K AND (5) 523 K

gave the value of C to be in the range of 0.35 - 0.70. If the constant A could be looked upon qualitatively as representing the strength of sorptions, then the increase in A with the increase in temperature is in accordance with the thermodynamic expectation[45].

3.3.5G Application of statistical models of Langmuir and Volmer

The statistical model equations of Langmuir and Volmer[52] derived initially for ideal systems, are often applied[26,52] to the real systems to yield information on the extent of deviation occuring in such systems due to surface heterogeneity, multilayer formations and mutual interactions between sorbed molecules. Tables 3.8 lists the tests of applicability of these equations Figs. 3.19 and 3.20 show the typical plots of KL and lnKv respectively at different temperatures. Almost all the KL and lnKL (not shown) plots were found to be linear with some slope even upto a coverage of 0.7-0.9. This indicates that the sorbed NH_3 molecules approximate to localized sorption with some elements of molecule-molecule interactions. Kv plots (not shown) at lower temperature (323 K) were linear and parallel to x-axis, indicating the sorption at lower temperature follows mobile sorption model without molecule-molecule interaction. As the sorption temperature increases the Kv plots deviated from linearity, indicating complex nature of sorption.

All the lnKv plots show non-linearity indicating non-applicability of mobile sorption model with molecule-molecule interaction. In conclusion ammonia sorption in omega zeolites follows localized sorption model with molecule - molecule interaction. Similar plots were obtained in the case of CO_2 and NH_3 sorption in cation exchanged Y zeolite[47,48].

3.3.5H Chemical affinity and the selectivity of sorbed phases

When a gas is transferred reversibly and isothermally from the gas phase at a standard pressure Po (760 Torr) into an infinite amount of sorbent-sorbate mixture over which the equilibrium pressure is P, a decrease in chemical potential takes place. Neglecting the nonideality of the sorbate, the chemical affinity may be expressed as[22,52]

$$\Delta\mu = RT \ln (P/P_o) \text{ ---------- } (3)$$

Table 3.8 : Test of isotherm equations[26]

Isotherm Equation	Plot against θ	Result if model is applicable
(i) $p = K_L(\theta/1-\theta)$	$p(1-\theta/\theta) = K_L$	K_L is independent of θ
(ii) $p = K_{BW}(\theta/1-\theta)\exp(b\theta)$	$\ln p(1-\theta/\theta) = \ln K_L$	Straight line with slope = b and intercept = $\ln K_{BW}$
(iii) $p = K_V(\theta/1-\theta)\exp(\theta/1-\theta)$	$p(1-\theta/\theta)\exp(-\theta/1-\theta) = K_V$	K_V is independent of θ
(iv) $p = K_{VW}(\theta/1-\theta)\exp(\theta/1-\theta-\alpha\theta)$	$\ln p(1-\theta/\theta)\exp(-\theta/1-\theta) = \text{in } K_V$	Straight line with slope = -α and intercept = $\ln K_{VW}$

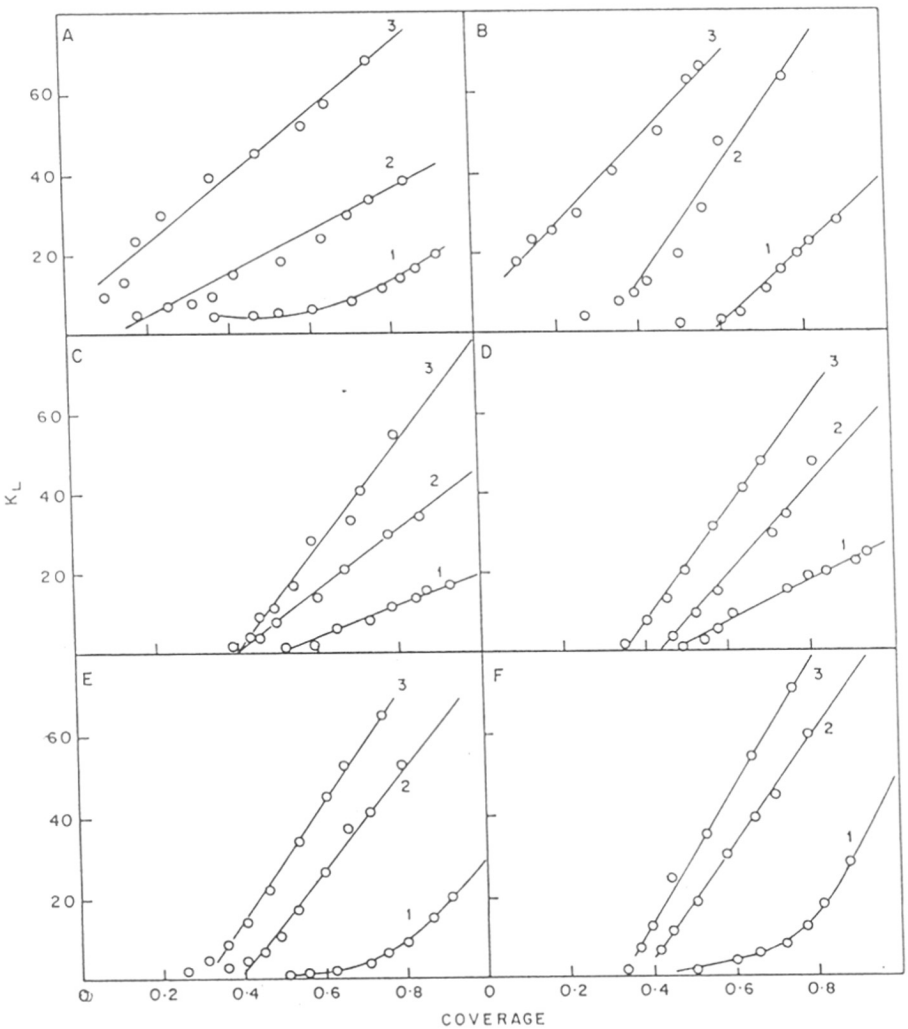

FIG. 3.19 : PLOTS OF K_L WITH COVERAGE OF AMMONIA SORPTION IN (A) Na-Al-OMEGA, (B) Na-Ga-OMEGA, (C) H-Al-OMEGA, (D) H-Ga-OMEGA, (E) La-Al-OMEGA AND (F) La-Ga-OMEGA AT (1) 323 K, (2) 423 K AND (3) 523 K

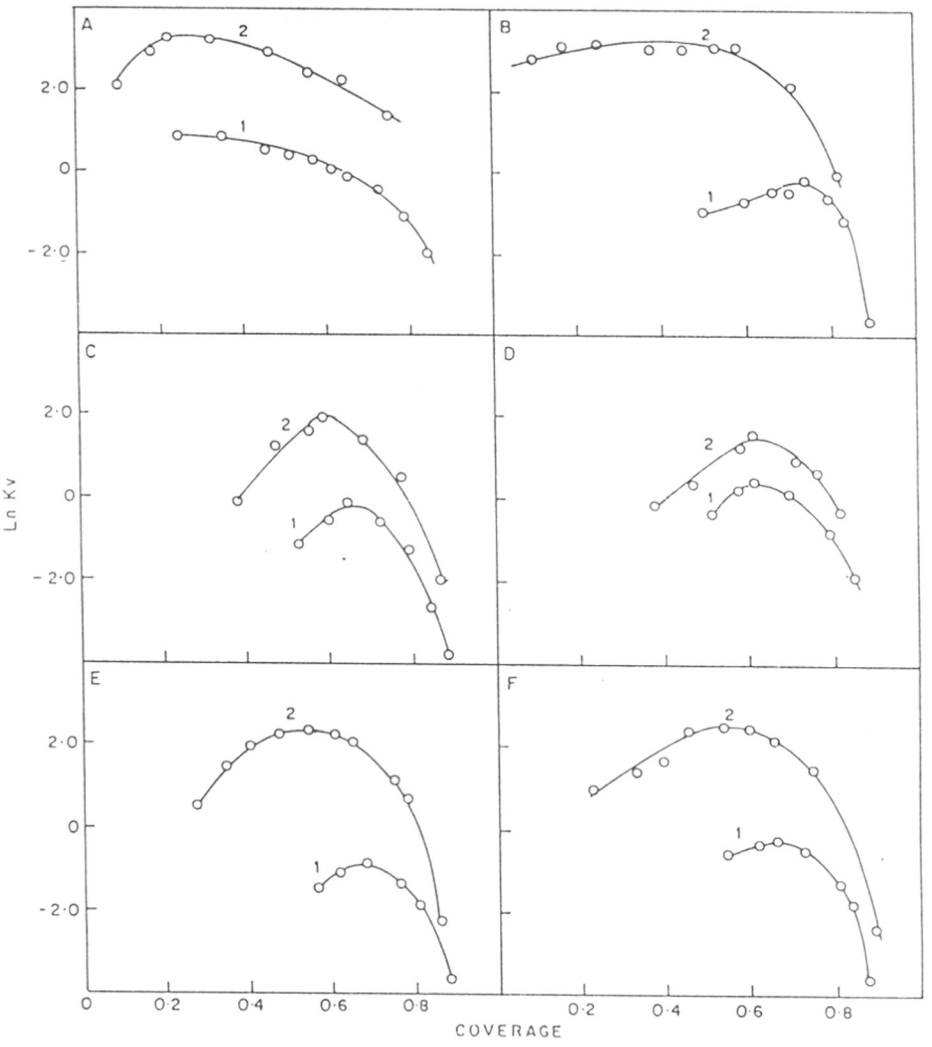

FIG. 3.20 : PLOTS OF LnKv WITH COVERAGE OF AMMONIA IN (A) Na-Al-OMEGA, (B) Na-Ga-OMEGA, (C) H-Al-OMEGA, (D) H-Ga-OMEGA, (E) La-Al-OMEGA AND (F) La-Ga-OMEGA AT (1) 323 K AND (2) 523 K

The value of $\Delta\mu$ may be taken as the quantitative measure of chemical affinity of the sorbate for the sorbent. The plots of $-\Delta\mu$ against the amount sorbed also serve as useful criteria for the comparison of sorption affinities of probe molecules in the lattices of various modified zeolites. The typical plots of $-\Delta\mu$ against the amount sorbed are shown in Figs. 3.21 and 3.22. It is clearly seen from Fig. 3.21 and 3.22 that a decrease in chemical affinity is comparatively sharper at higher temperature as compared to that at lower temperature. The decrease in chemical affinity with the coverage is in accordance with the thermodynamic expectation.

At higher temperature (523 K) Na-gallium omega shows higher chemical potential than Na-aluminium omega over entire coverage. The chemical potential for other cation exchanged forms are higher than the corresponding sodium form zeolite. At lower temperature (323 K) the chemical affinity sequence follows the order La-Ga-omega > Na-Ga-omega > H-Ga-omega in case of gallium isomorph and the sequence La-Al-omega > H-Al-omega > Na-Al-omega in case of Al isomorph. In the higher coverage region the chemical affinity sequence becomes more complicated. The affinity curves, in general, indicate that gallium zeolites exhibit lower chemical affinity than their aluminium analogs.

3.3.5I Isosteric Heats (Qst) of Ammonia sorption

Isosteric heats of ammonia sorption, Qst are computed from the shift of sorption equilibrium with temperature at constant sorbate loading in accordance with the Clausius-Clapeyron relationship as follows[22,52]

$$-\Delta H = Qst = R\,[(T_2T_1)/(T_2-T_1)]\,\ln\,(P_2/P_1) \text{ ---- (4)}$$

If Qst is temperature independent, the plots of ln(P) against 1/T are expected to be linear within experimental error. These isosteres were found to be almost linear in the present studies. Fig. 3.23 shows the variations in Qst (obtained from the slopes of the linear isosteres) with the amount of ammonia sorbed in various omega zeolites. Fig. 3.23 shows wide variation in Qst from 40 kJ, $mole^{-1}$ to 75 kJ, $mole^{-1}$. The zeolite Na-Al-omega shows the lowest Qst values of ammonia sorption

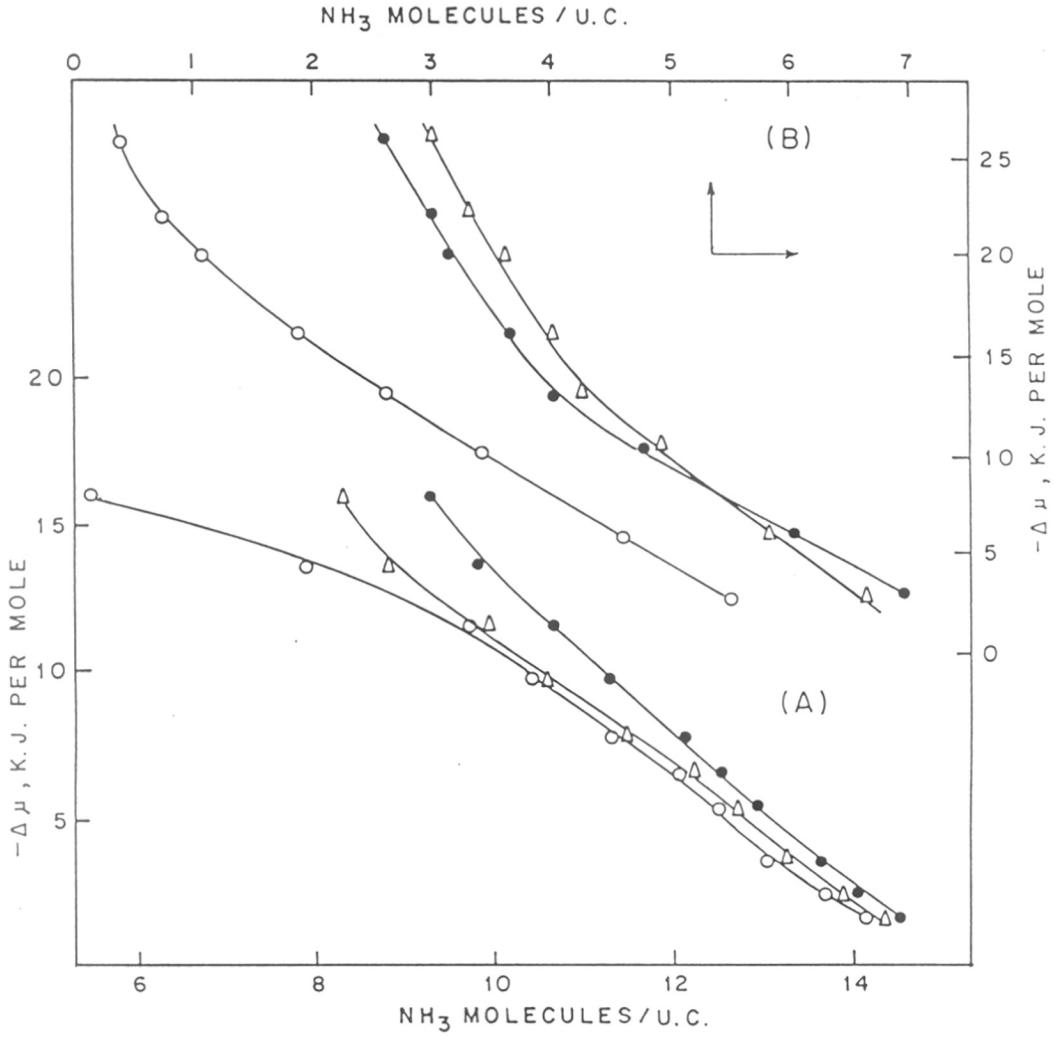

FIG.3.21: CHEMICAL AFFINITY FOR NH_3 SORPTION WITH THE COVERAGE FOR ○ Na-Al-OMEGA, Δ H-Al-OMEGA, ● La-Al-OMEGA AT (A) 323 K AND (B) 523 K

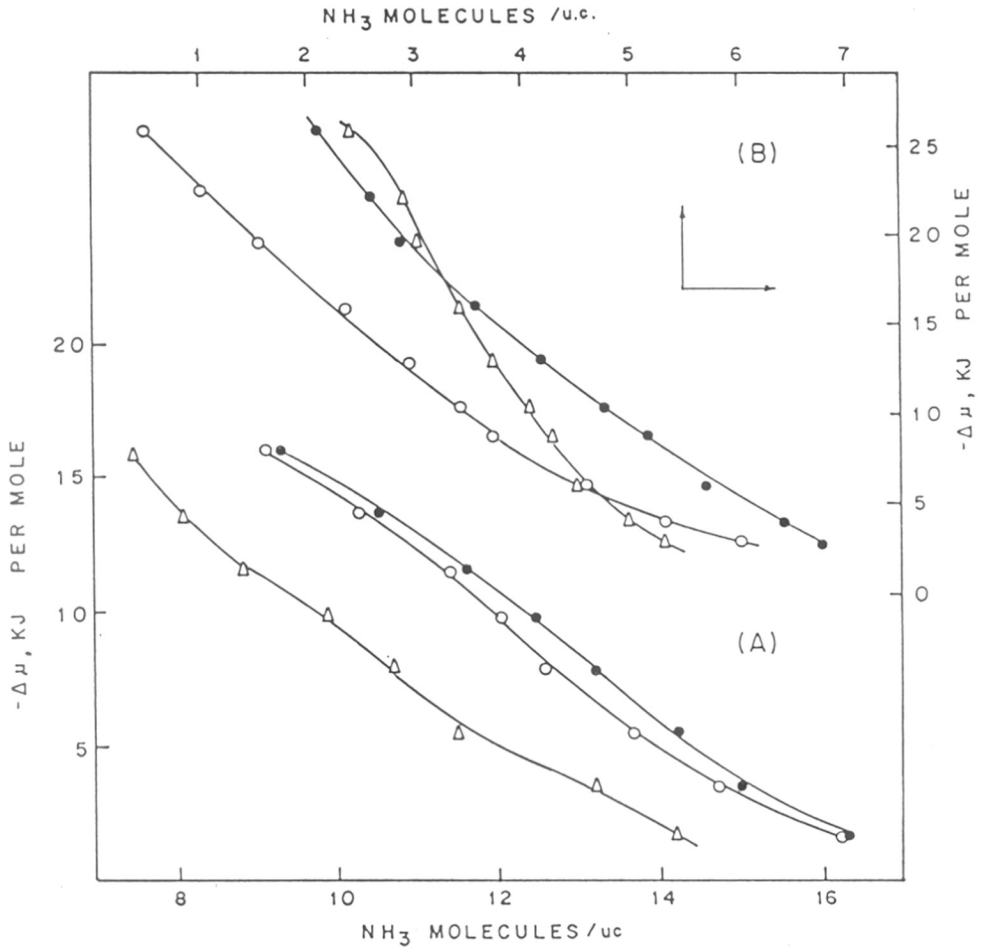

FIG.3·22:CHEMICAL AFFINITY FOR NH_3 SORPTION WITH THE COVERAGE FOR o Na-Ga-OMEGA, Δ H-Ga-OMEGA, • La-Ga-OMEGA AT (A) 323 K AND (B) 523 K

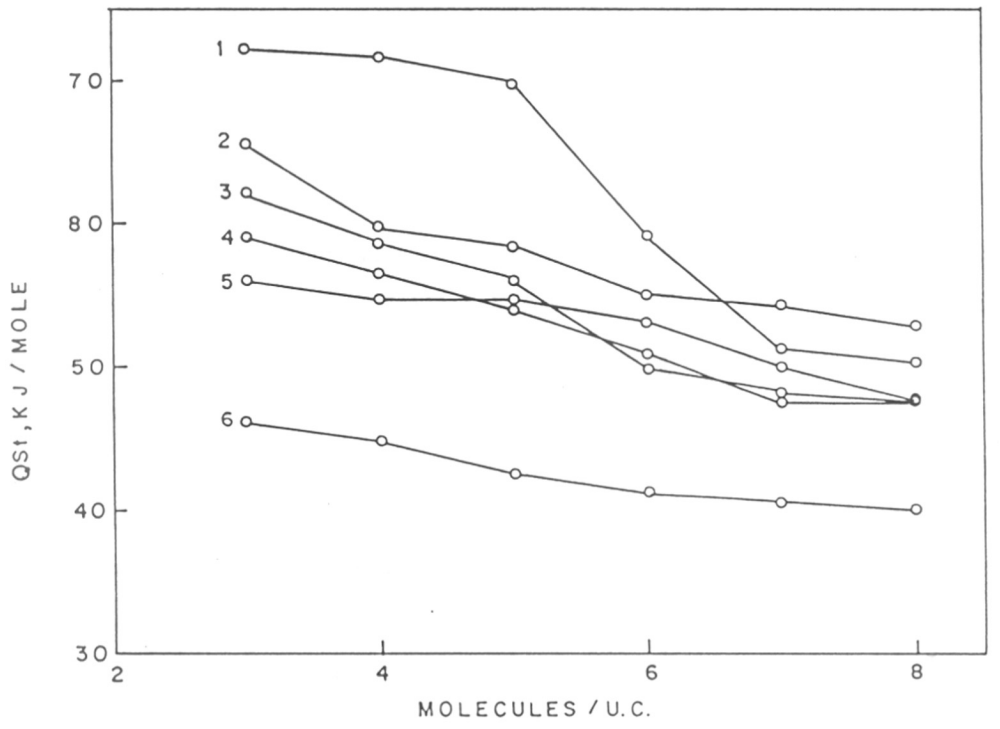

FIG.3·23:ISOSTERIC HEATS (Q st) OF NH_3 SORPTION IN (1) H-Al-OMEGA, (2) La-Al-OMEGA, (3) La-Ga-OMEGA, (4) H-Ga-OMEGA, (5) Na-Ga-OMEGA AND (6) Na-Al-OMEGA

over the entire coverage ranging between 40-45 kJ $mole^{-1}$. It is also seen from the Fig. 3.23 that Na-Al-omega offers the most homogeneous surface having a very narow range of the strength of sorption centers. In the lower coverage region (3 molecules $u.c.^{-1}$) the Qst sequence is H-Al-omega > La-Al-omega > La-Ga-omega > H-Ga-omega > Na-Ga-omega > Na-Al-omega. In higher coverage region (8 molecules $u.c.^{-1}$.) the Qst sequence becomes La-Al-omega > H-Al-omega > Na-Ga-omega > La-Ga-omega > H-Ga-omega > Na-Al-omega.

All the Qst curves show a steady increase in Qst accompanied by smooth humps. As the ammonia molecules are sorbed perhaps they interact with sorption centers of increasing energy. Usually isosteric heat of sorption takes care of two types of interactions i.e. (i) Sorbate-sorbent interaction in the lower coverage region and (ii) sorbate-sorbate interaction in the higher coverage region. In the middle coverage region both the interactions are operative and the magnitude of 'Qst' value determines their individual contributions. The humps usually observed in Qst curves are the consequence of the resultant of these interactions. Logically omega samples containing protons or lanthanum ions are expected to show higher Qst than those containing sodium which is in agreement in the studies. The indirect methods like this for the evaluation of Qst is expected to be reasonably accurate. The wide variation in Qst with the coverage in all the zeolites indicate surface heterogeneity in all the samples. In case of cation exchanged beta samples[44] 'Qst' showed decrease with the increase in ammonia coverage.

CONCLUSION

XRD profiles and thermo analytical data show that NH_4-Ga-isomorph of omega possesses considerably lower thermal stability. The thermal stability is also enhanced to some extent by La exchange whereas the protonic forms seem to be responsible for lowering the thermal stability. The protonic form of aluminum is comparatively more stable than that of protonic form of Ga-omega. FTIR spectra in framework region show highly crystalline nature of all synthesized samples. It also reveals higher thermal stability of Al compared to Ga-omega zeolite. Spectra in hydroxyl stretching region and of chemisorbed pyridine show both Brönsted and Lewis acidity which are stronger in Al-omega than in Ga-omega zeolite. Thus, FTIR spectra clearly shows that Ga cations are occupying in framework position in Ga-omega zeolite. Thermo analytical data revealed two or three different stages of weight loss in TG curves. Both surface area and micropore volume estimated from low temperature nitrogen sorption increased on proton exchange and decreased in the lanthanum exchange zeolite. The equilibrium sorption uptakes were found to be lower in gallium isomorphs than those in aluminum isomorphs. The type-I ammonia sorption isotherms showed that the hold-up capacity is highest in lanthanum exchange omega followed by protonic form. The ammonia sorption isotherm data were satisfactorily represented by applying Langmuir, BET, Dubinin equations. However, Freundlich and Sips equation showed limited applicability to the ammonia sorption data. Statistical models of Langmuir and Volmer indicated that ammonia sorption in omega zeolite broadly follow localized sorption model with molecule-molecule interaction. The chemical potential for cation exchanged forms are higher than the corresponding sodium forms of zeolites. Na-Al-omega offered the most homogeneous surface for NH_3 sorption whereas the other cationic forms showed heterogeneous character of the surface. The proton form of Al-omega showed highest value of isosteric heat (around 72 kJ mol^{-1}) for ammonia sorption. The sequence of isosteric heat follows H-Al-omega > La-Al-omega > La-Ga-omega > H-Ga-omega > Na-Ga-omega > Na-Al-omega.

REFERENCES :

1. Tsitsishvili G.V. and Andronikashvili T.G., "Molecular Sieve Zeolites-II", Advan. Chem. Ser., 102, Amer. Chem. Soc., Washington D.C., p. 217 (1971).
2. Ballivet D., Pichat P. and Barthomeuf D., "Molecular Sieves-II", Advan. Chem. Ser., **121**, Amer. Chem. Soc., Washington D.C., p. 469 (1973).
3. Tsistishvili G.V., "Molecular Sieves", Advan. Chem. Ser., **121**, Amer. Chem. Soc. Washington D.C., p. 291 (1973).
4. Yates D.J.C., "Molecular Sieves", Soc. Chem. Ind., London, p. 334 (1968).
5. Ward J.W., "Molecular Sieves Zeolites-I", Advan. Chem. Ser. 101, Amer. Chem. Soc., Washington D.C., p. 380 (1971).
6. Jacobs P.A. and Heylen C.F., J. Catal., **34**, 267 (1974).
7. Kladnig W. J., Phy. Chem. **79**, 262, (1975).
8. Vogt V.F., Wolf H., Bremer H, Rubinstein A.M., Klyachko A.L., Brueva J.R. and Mishin I.V., Z. Anorg. Alleg. Chem., **439**, 153 (1978).
9. Breck D.W., "Zeolite Molecular Sieves, Structure, Chemistry and Use", Wiley Interscience, New York, ibid, p. 495 (1974).
10. Kiosky J.R., Goyette W.J. and Nottermann T.M., J. Catal. **52**, 25 (1978).
11. Beglaryn A.A. and Ramanovskii B.V., Int. Chem. Engg., **15**, 613 (1975).
12. Mapes J.E. and Eischens R.P., J. Phy. Chem. **58**, 1059 (1954).
13. Mamoru Ai., J. Catal. **52**, 16 (1978).

14. Lisovskii A.E., Kozhurov A.J., Feizullaeva Sh.E. and Alkhozov T.G., Kinetics and Catalysis, **19**, 477 (1978).

15. Steinberg K.H., Bremer H. and Falke P., Z. Phy. Chemie. Leipzig, **257**, 151 (1976).

16. Barrer R.M. and Bratt G.C., J. Phys. Chem. Solids, **12**, 130, 146 (1959).

17. Barrer R.M. and Gibbons R.M., Trans. Faraday Soc., **59**, 2569, 2875 (1963); ibid, **61**, 948 (1965).

18. Tsutsumi K., Hong QuiKoh, Hagiwara S. and Takahashi H., Bull. Chem. Soc. Japan, **48**, 3576 (1975).

19. Masuda T., Taniguchi H., Tsutsumi K. and Takahashi H., Bull. Chem. Soc. Japan, **51**, 1965, 1970 (1978).

20. Masuda T., Taniguchi H., Tsutsumi K. and Takahashi H., Bull. Chem. Soc. Japan, **52**, 2849 (1979).

21. Masuda T., Taniguchi H., Tsutsumi K. and Takahashi H., J. Japan Petro. Inst., **22**, 67 (1979).

22. Coughlan B. and Kilmartin S., J. Chem. Soc., Faraday Trans.-1, **71**, 1809, 1818 (1975).

23. Coughlan B. and Larkin P.M. Chem. and Ind., 275 (1976).

24. Coughlan B. and Larkin P.M., Proc. Irish Acad. Roy. Inst. Chem., Centenary Issue, 388 (1977).

25. Coughlan B. and Shaw R.G., Proc. Roy. Irish Acad., 76B, 191-239 (1976).

26. Coughlan B. and McEntee J.J., Proc. Roy. Irish Acad., 76B, 473-533 (1976).

27. Coughlan B. and McCann W.A., J. Chem. Soc., Faraday Trans.-1, **75**, 1969, 1984 (1979).

28. Galli E., Cryst. Struct. Commun. **3**, 339 (1974).

29. Rinaldi, R., Pluth, J.J. and Smith, J.V., Acta. Crystallogr. B, **31**, 1603 (1975).

30. Weeks, T.J. Jr., Kimak, D.G., Bujalski, R.L. and Bolton A.P., J. Chem. Soc. Faraday Trans., **72**, 575 (1976).

31. Flanigen, E.M., French Patent 1, 548, 382 (1968).

32. Chauvin B., Fajula, Figueras F., Gueguen C. and Bousquet J., Catal. **111**, 94 (1988).

33. Mirajkar S.P., Eapen M.J., Tamhankar S.S., Rao, B.S. and Shiralkar V.P., J. of Inclu. Phen. **16**, 139 (1993).

34. Araya A., Barber T.J., Lowe B.M., Sinclair D.M. and Varma A., Zeolites **4**, 263 (1984).

35. Breck D.W., Zeolite Molecular Sieves, Structure, Chemistry and Use. John Wiley Interscience, New York, 364 (1974).

36. Perrotta A.J., Kibby C., Mitchell B.R. and Tucci E.R., J. of Catal. **55**, 240 (1978).

37. Szostak R., Molecular Sieves : Principles of Synthesis and Identification, Van Nostrand Reinhold, p. 320 (1989).

38. Chiche B.H., Fajula F. and Garrone E., J. Cat. **146**, 460 (1994).

39. Maubert A., Datartre R., Menorval L.C. and Figueras F., Zeolites, **13**, 587 (1993).

40. Jacobs P.A. and von Ballmoos, J. Phy. Chem., **86**, 3050 (1982).

41. Perry E.P., J. Catal. **2**, 371 (1963).

42. Kiselev, A.V., Discuss Faraday Soc., **40**, 205 (1965).

43. Dubinin, M.M., Radushkevich, L.V., Proc. Akad. Sci. USSR **55**, 327 (1974).

44. Reddy K.S.N., Eapen M.J., Soni H.S. and Shiralkar V.P., J. Phys. Chem. **96**, 7923 (1992).

45. Joshi P.N. and Shiralkar V.P., J. Phys. Chem. **97**, 619 (1993).

46. Kulkarni S.J. and Kulkarni S.B., Indian J. Chem., **28A**, 6 (1989).

47. Shiralkar V.P. and Kulkarni S.B., Zeolites, **4**, 329 (1984).

48. Rao G.N., Joshi P.N., Kotasthane A.N. and Shiralkar V.P., J. Phys. Chem. **94**, 8589 (1990).

49. Shiralkar V.P. and Kulkarni S.B., J. Colloid and Interface Sci., **108**, 1 (1985).

50. Mirajkar S.P., Thangaraj A. and Shiralkar V.P., J. Phys. Chem. **96**, 3073 (1992).

51. Sips R.J., Chem. Phys. **16**, 491 (1948).

52. Barrer R.M. and Coughlan B., Molecular Sieves Soc. Chem. Ind. London, p. 141, 233, 241, (1968).

Chapter IV

Catalysis

4.1 INTRODUCTION

a) Studies on alkylation of phenol with methanol

The selectivity of zeolites in catalytic applications is controlled by chemical and geometrical factors. The chemical factors relate to the type of active functions present in zeolite framework such as strength and density of the acid sites, metal, metal oxide sites etc., while the geometrical factor relates to the size and connectivity of the channel system.

The transformation of hydrocarbons over zeolites (large pore) provides an illustration to the influence of the acidic function, together with metal or oxide function. However, the geometrical factor is an important property, since it allows the design of the catalyst exhibiting shape selective property. Shape selectivity can direct the selectivity in the desired product by controlling the diffusivity of the reactant or product through the pores of the zeolite. Therefore, in order to design active and selective catalyst based on zeolites one needs to know the parameters that control the acid strength and chemical environment of the sites influencing the catalytic properties.

The wide range of applications of zeolites may be seen from the fact that the catalytic properties can be varied in almost limitless fashion, namely by appropriate choice of mode of preparation including isomorphous substitution[1-3] or by subsequent modification of the zeolites (e.g. ion exchange, metal impregnation, steaming and acid leaching). The shape selectivity can operate only when the reaction occurs within the zeolite pores, however, it is uncertain whether reaction takes place on both the inner and outer surfaces or, on the other hand, only on the outer surface. Examples are known in which the molecular dimensions would certainly permit reactions within the zeolite framework, but the course of reaction is apparently not determined by shape selectivity, but by other parameters such as thermodynamics of the reaction.

One such reaction is alkylation of phenol with methanol. The products of the reaction are mainly cresols and anisole. Cresols are important intermediates for producing phosphate plasticizers, phenolic resins and antioxidants in the chemical industries with increasing demand of the development of new synthesis process of cresols. The alkylation of aromatic nucleus[4,5,6,7-11] or of the side chain[5,12-15] of alkylbenzene are competing reactions which have been extensively studied.

However, alkylation reactions of arenes containing functional groups like -OH, N, NH_2 are more complex than the alkylation of alkylbenzene, because of the attack at the nucleus as well as at the functional group. For example, in the case of phenol not only carbon (C-) but also oxygen (O-) alkylation is possible[6,16-19]. Even in medium pore zeolites this reaction does not follow the shape selectivity as observed in other alkylations. An excellent review on this topic has been written by Jacobs et al[6].

b) **Conversion of n-hexane over the zeolite omega**

Conversion of n-paraffins to aromatics and isoparaffins are the general reactions involved in reforming processes to increase the octane number (an engine knocking characteristic) of gasoline[20-24].

Generally, in the reforming process, higher paraffins (C_6-C_{11}) are converted into the aromatics over bifunctional catalysts such as, platinum on alumina. The aromatization of paraffins over these catalysts is possible only when at least 6-carbon atoms are present in the molecule, preferably, in a chain. However, the aromatization of lighter paraffins (C_3 to C_5) has been reported over medium pore, high silica pentasil zeolites, such as, ZSM-5[25,26]. The reaction is believed to take place through oligomerization and cyclization steps[27]. The enhancement of aromatization by zinc and gallium promoters in ZSM-5 samples was reported by Ono *et al.*[28], as early as 1987. Kannai and Kawta[29] have reported the aromatization of n-hexane over gallo-silicate and gallo-alumino-silicate samples of the MFI (ZSM-5) system and concluded that the protonic forms of these silicates are more active in the aromatization than the protonic form of pure ZSM-5 or Ga_2O_3 impregnated ZSM-5. Perrotta *et al.*[30] have shown that the conversion of n-hexane on zeolite omega has more cracking activity than the corresponding forms of faujasite.

Zeolite omega is a synthetic counterpart of the mineral mazzite[31-33]. The aluminosilicate framework consists of columns of gmelinite cages bridged by oxygen atoms to give a 12-membered cylindrical main channel system along the crystallographic c-axis. Structurally both aluminium omega and gallium omega zeolites are similar.

In this chapter, the catalytic reactions over omega zeolites in the phenol alkylation and n-hexane conversion are reported and correlated with the characterization data to orient structural features and acidic functions of the zeolites.

4.2 EXPERIMENTAL

Synthesis and characterization of the catalysts used in the study are discussed in detail in Chapter II and III. The unit cell composition of the catalysts used in the phenol alkylation and n-hexane conversion studies are tabulated in Table 4.1.

The powdered catalysts are pressed, pelleted, crushed and sieved to obtain 10 - 20 mesh particles. All the reactions are carried out at atmospheric pressure in a fixed bed downflow, integral reactor shown in Fig. 4.1. For phenol alkylation reaction, about 3 g of the catalyst (10-20 mesh) was positioned in a cylindrical silica reactor (1.5 X 30 cm), provided with the thermowell in the center. The catalyst (10-20 mesh) was packed in such a way that the thermowell top was at the center of the bed. The zone below and above the catalyst bed was filled with inert porcelein beads to serve as preheater. The reactor was placed in a constant temperature zone of an electrically heated furnace. The catalyst was activated at 773K for 8 h in a flow of dry air before use. The catalyst was then flushed with dry nitrogen and cooled to the desired reaction temperature.

For n-hexane reaction studies, 2 g of sample (10-20 mesh) after the activation of catalyst in air at high temperature (773 K); the temperature of the reactor was brought down to 373 K in inert atmosphere of nitrogen. Then the reactor temperature was raised to the 773 K in presence of hydrogen and maintained for atleast 2 h and then brought to reaction temperature. The liquid reactants were injected using a syringe feed pump (SAGE Instruments, model 352, USA) at the required rate.

The reaction products were passed through a condenser cooled by chilled water. The condensed liquid product was collected periodically. The liquid products obtained during the alkylation of phenol were analyzed in a gas chromatograph (Shimadzu, model GC 15A), using a glass packed column of 3 % OV 225 on chromosorb AW (6'X1/8" i.d.) and the gaseous products were analyzed using a porapack Q column (6'X1/8" i.d.). Phenol conversion (α phenol) is calculated as the sum of the alkylated products and others formed in the reaction. The products of n-hexane reaction were analyzed using a capillary column (50 m x 0.25 mm) having silicon gum as the stationary phase on chromatograph (HP 5880). The products were also analyzed by GC- Mass spectrometer (Shimadzu, model QP-2000), equipped with fused silica capillary column (50 m X 0.25 mm; crosslinked methyl silicon gum).

Table 4.1 Chemical composition of the catalysts used in the catalytic studies

S.No.	Catalyst	Unit cell composition
1.	H-Al-omega (98.65)*	$Na_{0.08}\ H_{6.52}\ [(AlO_2)_{6.6}\ (SiO_2)_{29.4}]$
2.	H-Al-omega (45.40)	$Na_{3.60}\ H_{3.00}\ [(AlO_2)_{6.6}\ (SiO_2)_{29.4}]$
3.	H-Al-omega (31.00)	$Na_{4.55}\ H_{2.05}\ [(AlO_2)_{6.6}\ (SiO_2)_{29.4}]$
4.	H-Al-omega (24.50)	$Na_{4.98}\ H_{1.62}\ [(AlO_2)_{6.6}\ (SiO_2)_{29.4}]$
5.	La-Al-omega (62.2)	$Na_{2.5}\ H_{0.05}\ La_{1.35}\ [(AlO_2)_{6.6}\ (SiO_2)_{29.4}]$
6.	H-ZSM-5 (99.0)	$Na_{0.05}\ H_{4.97}\ [(AlO_2)_{5.02}\ (SiO_2)_{90.98}]$
7.	H-Ga-omega (99.3)	$Na_{0.05}\ H_{6.91}\ [(GaO_2)_{6.96}\ (SiO_2)_{29.04}]$
8.	0.1% Pt-H-Al-omega (98.65)	$0.1\%\ Pt\ Na_{0.08}\ H_{6.52}\ [(AlO_2)_{6.6}\ (SiO_2)_{29.4}]$
9.	0.1% Pt-H-Ga-omega (99.3)	$0.1\%\ Pt\ [Na_{0.05}\ H_{6.91}\ [(GaO_2)_{6.96}\ (SiO_2)_{29.04}]$
10.	2% Ga_2O_3 - Pt-H-Al-omega (98.65)	$2\%\ Ga_2O_3, 0.1\%\ Pt\ [Na_{0.08}\ H_{6.52}\ [(AlO_2)_{6.6}\ (SiO_2)_{29.4}]$
11.	3% Ga_2O_3 - Pt-H-Al-omega (98.65)	$3\%\ Ga_2O_3, 0.1\%\ Pt\ [Na_{0.08}\ H_{6.52}\ [(AlO_2)_{6.6}\ (SiO_2)_{29.4}]$

* Values within the parantheses signify percent exchange of cations.

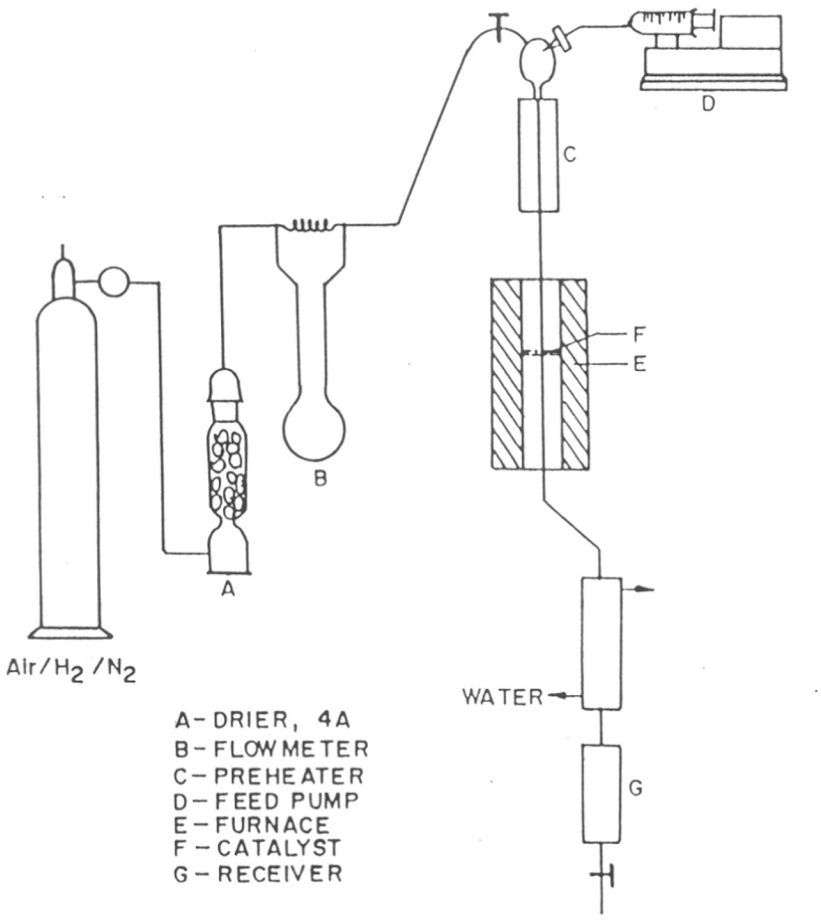

FIG. 4·1 : FIXED BED, DOWN-FLOW REACTOR USED IN THIS STUDY

4.3 RESULTS AND DISCUSSION

4.3.1a. Phenol alkylation

AR grade phenol and methanol were used without further purification. The alkylation of phenol with methanol is studied to evaluate catalytic activity of the zeolite omega samples synthesized and characterized as described in Chapter II and III. From the analysis of the products using GC and GC-MS, the following reaction mechanisms were proposed (Fig. 4.2), main reactions being 1 and 2. Influence of reaction parameters on the product distribution and the various reactions taking place are discussed.

4.3.2a. Mechanism of phenol alkylation

Venuto *et al.*[34,35] reported a decreased reactivity of phenol for the alkylation with ethene on zeolite pore which is opposite to the nucleophilicities. The competitive adsorption measurement showed that adsorption of phenol was more than benzene and ethene[36]. The operation of a Rideal type mechanism[36,37] was proposed based on these studies. An aromatic compound adsorbed on a Brönsted site will be positively charged as poorly susceptible to an electrophilic attack. Such an electrophilic aromatic substitution reaction can be viewed as the reaction of an adsorbed ethyl cation formed from ethene with a free aromatic radical.

It was also reported[38] that phenol is more active on Y and pentasil zeolite in the methanol alkylation than benzene. Therefore, it is evident that more polar alkylating fragments compete more favourably with phenol by adsorption thereby increasing the acidity. This is also indirectly proved by an increase in phenol conversion at higher methanol to phenol ratio.

The reaction mechanism on omega is also similar to that of the Y-type zeolite except for the unidimensional channel system in omega where, the diffusion limitations are more (Fig. 4.2). The secondary reactions are more controlled by the reaction parameters. The reaction scheme presented is discussed in the light of the reaction parameters or reaction conditions.

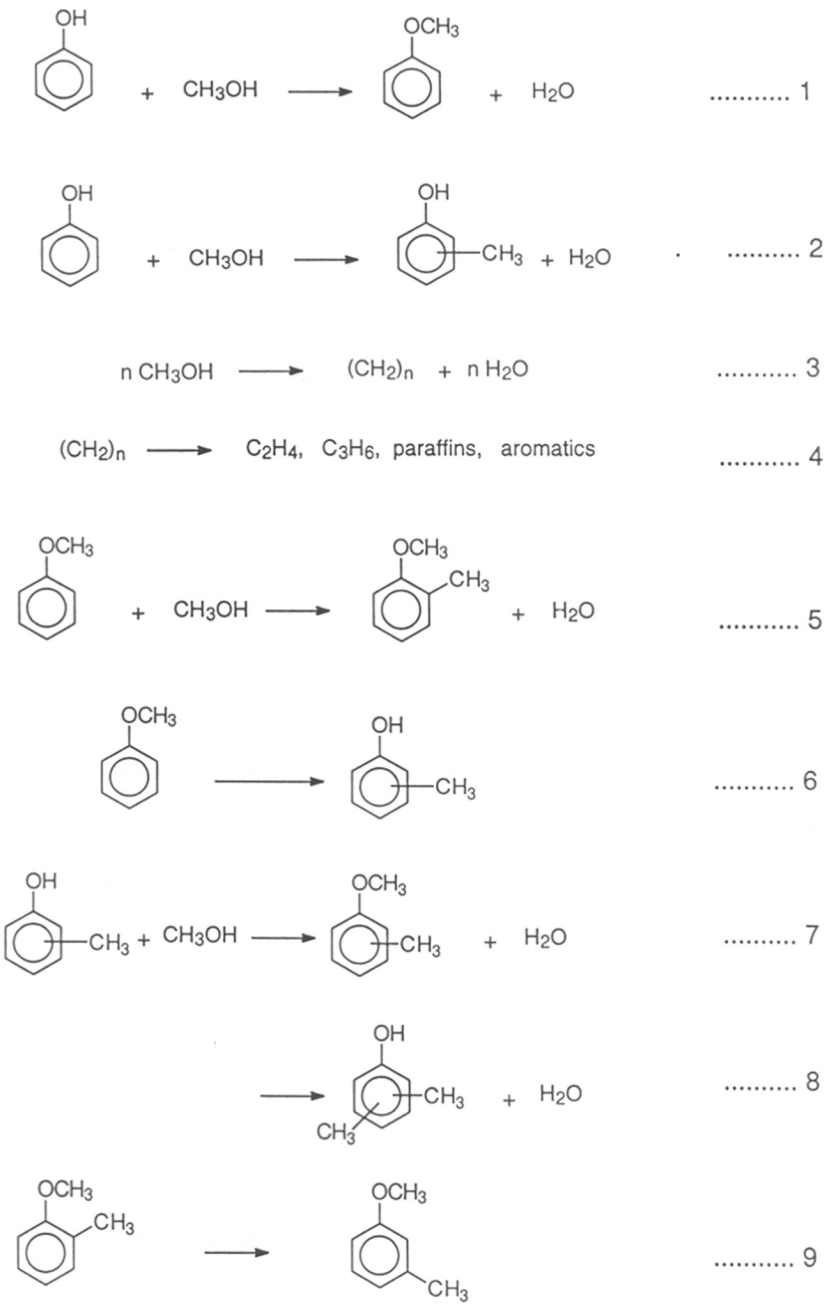

FIG.4.2 METHYLATION OF PHENOL WITH METHANOL OVER ZEOLITE OMEGA.

4.3.3a. Effect of temperature on the activity of H-Al-Omega.

Data summarized in Table 4.2 represent the distribution of products at different temperatures. Methanol conversion is complete at all temperatures. Anisole formation is maximum at low temperature. The cresols increase with the increase of temperature, however, at very high temperatures there is a decrease in formation of cresols. Among the cresols, o-cresol is maximum. Eventhough the alkylations are ortho-para directive and statistically the o/p value is in the order of 2/1, the ortho-concentration is very high in this study. At higher temperature considerable amount of m-cresol formation is observed. Xylenol formation is also increasing with temperature. The catalyst was deactivated over a period of 24 h, however, the original activity was restored by heating in air flow at 823 K.

The results can be explained on the basis of the primary products formed in the alkylation reactions, which are anisole and cresols. Anisole is formed by the O-alkylation while, cresols are formed by the C-alkylation, mainly due to the Brönsted acid sites. At low temperature, the conversion of phenol is low and the only products observed are anisole and cresols. As the temperature is increased, the conversion of phenol also increased, methyl anisole and xylenols are also observed. This suggests that, at higher temperature, the successive alkylation of anisole and cresol is occuring. At high temperature m-cresol is also observed. According to an electrophilic aromatic substitution m-cresol is not a primary product. The formation of m-cresol is by the isomerization of p-cresol on the acidic site of the catalyst as a secondary reaction. Normally, stronger acid sites catalyze the C-alkylation[38-40]. It is well known that the pentasil zeolites are having stronger acid sites than faujasite and omega zeolite. The data published by Balsama *et al.*[41] confirmed that over ZSM-5 C-alkylated products are higher than on faujasite. Thus the C-alkylation is favoured more by Brönsted acid sites. However, according to the literature, the low anisole selectivity in ZSM-5 is attributed to the less anisole stability in the 10-membered ring than in the large pore zeolites[38]. Some of the authors reported[39,41-43] high anisole selectivity even in pentasil zeolite, which may be due to extraframework aluminium or the impregnated phosphorous oxide to reduce surface acidity. Formation of cresols can also be due to secondary reactions as per the reaction Scheme 6 (Fig. 4.2).

Table 4.2 Effect of temperature on alkylation of phenol with methanol over H-Al-omega.

Product (wt.%)	Temperature, K				
	573	623	673	723	773
Non aromatics	1.23	1.05	1.45	1.99	3.24
Dimethyl ether	3.23	1.05	-	-	-
Anisole	7.13	10.82	6.05	4.15	0.50
o-Cresol	4.05	7.24	9.24	6.82	3.86
Phenol	83.36	74.19	72.17	70.74	78.91
p-Cresol	0.30	1.60	1.05	0.56	0.71
m-Cresol	-	0.20	1.00	0.89	1.40
Methyl Anisole	0.50	1.64	2.84	3.08	1.48
Xylenols	0.10	0.56	2.15	2.31	2.06
Others	0.10	1.65	4.05	9.46	7.84
α Phenol	14.20	23.80	29.20	29.8	16.8
Phenol to alkylates	11.20	21.90	24.20	20.30	11.8
O/C alkylation	1.74	1.06	0.49	0.62	0.17

Reaction conditions : Pressure = Atmospheric

Activation temperature = 823 K; Methanol:Phenol (mole ratio) = 1; WHSV = 1.3 h^{-1}; TOS = 4 h.

At higher temperatures, some of the anisole formed is converted into cresol by isomerization. When the reaction temperature is decreased, the anisole to cresol ratio is found to increase. At higher temperature, p-cresol is isomerized to m-cresol. All the catalyst deactivated with time, however, the deactivation is faster at higher temperatures. This is due to the simultaneous methanol reaction to hydrocarbons giving mostly aromatics as per the reaction scheme.

4.3.4a Influence of mole ratio

The influence of an increasing methanol/phenol ratio on the product selectivity and more particularly on the anisole/cresol ratio is shown in the Table 4.3. There is a decreasing tendency with increasing mole ratio which is expected and can be explained due to the presence of more alkylating agent. Anisole can be converted to cresol by rearrangement on acid catalyst and in addition with more alkylating agent present, methyl anisole and cresols are formed by C-alkylation in higher amounts.

The deactivation is faster at higher mole ratio because of methanol reaction which is taking place on the catalyst as per the reaction scheme. A similar type of observation has been made by Balsama *et al.*[41] The selectivity to alkylated products is more at low methanol to phenol mole ratios.

4.3.5a Influence of space velocity

The data in Table 4.4 indicates the product pattern with a change in space velocity. If the cresol formation is also a primary reaction then the ratio of anisole to cresol should not vary much. This observation is supported by the data presented in Table 4.4. The slight changes in the values may be due to the secondary reactions taking place. At higher space velocity the conversion of phenol is less and the secondary reaction of methanol is reduced. The deactivation is fast at high space velocities.

4.3.6a Alkylation of phenol over catalyst with different sodium levels.

In order to evaluate the influence of acidity in the alkylation reaction a series of samples having different degrees of exchange of protons in the Na-omega samples are prepared. The data obtained are summarized in Table 4.5. The conversion of phenol decreases with increase of sodium content in the zeolite. This is due to the lowering of acidity. However, the selectivity to alkylation

Table 4.3 Effect of Phenol to methanol mole ratio in phenol alkylation over H-Al-omega.

Product (wt.%)	Phenol to Methanol mole ratio				
	1:1	1:2	1:3	2:1	3:1
Non Aromatics	1.45	4.15	6.85	0.85	0.35
Dimethyl Ether	-	-	-	-	-
Anisole	6.05	9.72	11.35	4.65	3.25
o-Cresol	9.24	14.67	17.28	7.62	4.75
Phenol	72.17	55.03	44.67	78.03	85.50
p-Cresol	1.05	3.85	4.15	0.85	0.75
m-Cresol	1.00	1.45	2.65	0.65	0.40
Methyl anisole	2.84	4.85	5.65	1.50	0.90
Xylenols	2.15	3.43	4.90	1.05	0.50
Others	4.05	2.85	2.50	4.80	3.60
α Phenol	29.20	37.10	44.25	21.20	16.80
Phenol to alkylates	24.20	34.20	41.70	16.90	11.50
O/C alkylation	0.48	0.46	0.43	0.49	0.52

Reaction conditions : Temperature = 673 K; Pressure = Atmospheric ;

Activation temperature = 823 K; Methanol:Phenol (mole ratio) = 1 ; WHSV = 1.3 h^{-1} ; TOS = 4 h.

Table 4.4 Effect of space velocity on the alkylation of phenol with methanol over H-Al-omega.

Product (wt.%)	Space velocity (h^{-1})			
	0.65	1.37	1.94	3.24
Non Aromatics	1.05	1.45	2.25	3.02
Methyl alcohol	-	-	0.15	0.40
Anisole	6.95	6.05	4.25	3.69
o-Cresol	9.82	9.24	3.56	2.80
p-Cresol	0.90	1.05	0.75	0.85
m-Cresol	1.15	1.00	0.82	0.40
Phenol	68.78	72.17	81.85	85.59
Methyl anisole	3.15	2.84	1.85	0.90
Xylenols	2.75	2.15	1.65	0.65
Others	5.45	4.05	2.87	1.70
α phenol	28.43	29.20	14.20	9.80
Phenol to alkylates	21.30	24.20	10.86	7.90
O/C alkylation	0.50	0.49	0.61	0.48

Reaction conditions : Temperature = 673 K; Pressure = Atmospheric ;

Activation temperature = 823 K; Methanol:Phenol (mole ratio) = 1 ; TOS = 4 h.

Table 4.5 Effect of percent proton exchange (H^+) on alkylation of phenol with methanol over Na-Al-omega zeolite.

Product (wt.%)	% exchange			
	98.5	45.4	31.0	24.5
Non aromatics	1.45	1.05	0.05	0.05
Dimethyl ether	-	1.85	2.90	3.60
Methyl alcohol	-	0.15	0.70	1.50
Anisole	6.05	5.45	4.07	4.11
o-Cresol	9.24	8.41	10.60	6.29
Phenol	72.17	73.03	72.96	80.17
p-Cresol	1.05	3.93	4.14	2.90
m-Cresol	1.00	3.02	2.73	1.13
Methyl anisole	2.84	-	-	-
Xylenols	2.15	-	-	-
Others	4.05	3.11	1.85	0.25
α-Phenol	29.20	21.86	19.25	13.10
α-Methyl alcohol	100.0	99.80	99.70	98.50
Methyl alkylation	69.80	54.40	56.50	39.20
O/C alkylation	0.49	0.35	0.23	0.40

Reaction conditions : Temperature = 673 K; Pressure = Atmospheric ;

Activation temperature = 723 K; WHSV = 1.3 h^{-1}; Phenol : methanol (mole ratio) = 1 ; TOS = 4 h

product increases at around 69 % proton exchange and the products are anisole and cresols. On very high protonic form, most of the decomposed products like C_2-C_4 olefins and other hydrocarbon products are formed. This is due to a higher acidity of catalyst which favours the competitive methanol reaction than the alkylation. The formation of xylenols and methyl anisoles are also observed at higher protonic exchanges. At higher sodium content, the acidity of the zeolite decreases, hence, the conversion and the total alkylation activity decreases. The secondary reactions like the successive alkylation of anisole and cresol are also reduced. Further, the transformation of anisole to cresol is also decreased. With 30-40 % Na exchange, activity remained for a longer cycle length (> 40 h).

4.3.7a Alkylation over gallosilicate zeolite

The activity of gallosilicate omega is studied in the alkylation of phenol with methanol as alkylating agent. Experimental procedure is identical to that described for the aluminum omega zeolite.

The experiment was carried out at 673 k and the results are summarized in Table 4.6. The catalyst deactivated in a period of 5 h. Even though the initial activity is very low compared to Al zeolite, the product pattern in the initial stages have shown very low anisole to cresol ratio compared to the studies on the aluminum zeolite. As the catalyst deactivates, the ratio of anisole/cresol also increases (initially it was 0.12 which increases to 0.6).

Xylenols and methyl anisoles are not observed in the product. However, unreacted methanol is observed in the product. The results suggest low activity inspite of XRD patterns being similar to that of Al-omega zeolite.

To investigate into the lower activity of Ga- analog compared to Al-analog, both Al- and Ga-omega were subjected to calcination in air at different temperatures and at each temperature the XRD pattern was recorded for the crystallinity. From Figs. 3.1 and 3.2 in Chapter III, it is noticed that upto 823 K, there is no appreciable loss in crystallinity in case of Al-omega zeolite. However, gallium sample indicated a loss of almost 46% crystallinity even at 773 k. The sorption studies as observed in Chapter III also indicate that Ga-omega samples have lower sorption

Table 4.6 Alkylation of phenol with methanol over H-Ga-omega.

TOS (h)	0.5*	1.0*	1.5	2.0	2.5	3.5	4.5
Non Aromatics	4.10	3.77	1.02	0.72	0.55	0.45	0.34
Methanol	0.16	0.60	8.24	9.28	9.23	9.77	8.47
Anisole	0.25	0.48	0.96	0.81	0.68	0.55	0.44
o-Cresol	1.08	0.94	0.77	0.60	0.48	0.42	0.34
Phenol	93.34	92.98	86.84	86.92	87.80	87.75	89.48
p-Cresol	0.59	0.49	0.22	0.15	-	-	-
m-Cresol	0.48	0.16	-	-	-	-	-
Methyl anisole	-	0.23	1.28	0.98	0.78	0.62	0.48
Xylenols	-	0.35	0.67	0.54	0.48	0.44	0.45
Others	-	-	-	-	-	-	-
α-Phenol	2.25	2.70	3.35	2.70	2.25	1.95	1.85
Phenol to alkylates	2.09	2.25	3.20	2.50	2.00	1.67	1.39
O/C alkylation	0.12	0.28	0.17	0.67	0.70	0.63	0.55

* The gas analysis indicates major C_2 - C_4 hydrocarbons, $C_2 > 70\%$.

Reaction conditions : Temperature = 673 K; Pressure = Atmospheric ;

Activation temperature = 723 K; WHSV = 1.3 h^{-1}; Phenol : methanol (mole ratio) = 1.

capacities. This can be attributed to the occlusion of octahedral species inside the zeolite channels or pores. In general, the low activity may be due to the poor thermal stability and occlusion of octahedral species in the channel and pores of H-Ga-omega analog.

A comparison of activity of H-Al-omega, La-exchanged sample made with Al-omega and H-Ga-omega samples is presented in Table 4.7. The La-exchanged sample showed different product pattern than that of H-Al-omega. No anisole formation is observed. The catalytic activity of La-exchanged sample is less than the H-Al-omega but more than gallosilicate omega zeolite. The absence of anisole formation in La-Al-omega is due to the additional acidity created by the rare earth ion which is attributed to its polarization and liberating H^+ ions.

The product pattern in Table 4.8 explains the activity of H-Al-omega, H-ZSM-5 and is compared with HY zeolite reported by Balsama *et al.*[41] From the Table 4.8, it is clear that omega zeolite, even though, a wide pore zeolite, the behavior is not entirely similar to that of faujasite due to difference in crystal structure. The alkylation activity is more in Y zeolite as compared to omega, but the O-alkylation is high in omega and H-ZSM-5 zeolites. The monomolecular reactions like anisole transformation to cresol is more in ZSM-5 due to high acid strength and due to the ease of the 1,2 methyl shift reactions because of its pore geometry. Further, the higher acid strength of ZSM-5 facilitates the isomerization of o-cresol to m-cresol, which is less in omega. The O/C alkylation is always high in wide pore zeolites due to the lower acid strength of both the wide pore zeolites.

4.3.1b Conversion of n-hexane over zeolite omega

The typical reactions that take place during the conversion of n-hexane can be summarized as follows:

1. **Dehydrogenation**

$$C_6H_{14} \xrightarrow{-H_2} C_6H_{12}$$

2. **Cracking**

$$C_6H_{14} \longrightarrow C_3H_6 + C_3H_8$$

$$C_6H_{14} \longrightarrow C_2H_4 + C_4H_{10}$$

Table 4.7 Comparative studies on alkylation of phenol with methanol over H-Al-omega, La-Al-omega and H-Ga-omega.

Product (Wt., %)	Zeolites		
	H-Al-omega	La-Al-omega	H-Ga-omega
Non-aromatics	1.45	3.60	0.45
Dimethyl ether	-	-	5.77
Anisole	6.05	-	0.55
o-Cresol	9.25	5.49	0.42
Phenol	72.17	81.71	91.15
p-Cresol	1.04	2.65	-
m-Cresol	1.00	1.32	-
Methyl anisole	2.84	-	0.62
Xylenols	2.15	0.78	0.44
Others	4.05	4.45	0.60
α-phenol	29.2	14.80	4.80
Phenol to alkylates	24.2	9.5	2.12
O/C alkylation	0.49	-	0.63

Reaction conditions : Temperature = 673 K; Pressure = Atmospheric ;

Activation temperature = 723 K; WHSV = 1.3 h^{-1}; Phenol : methanol (mole ratio) = 1 ; TOS = 4 h

Table 4.8 Comparative study on alkylation of phenol with methanol over H-Al-omega, H-ZSM-5 and H-Y*

Product (Wt., %)	Zeolites		
	H-Al-omega	H-ZSM-5	H-Y*
Non-aromatics	1.45	1.30	-
Dimethyl ether	-	-	-
Anisole	6.05	1.30	4.12
o-Cresol	9.25	14.81	19.13
Phenol	72.17	74.34	48.96
p-Cresol	1.04	2.10	6.43
m-Cresol	1.00	1.25	6.50
Methyl anisole	2.84	-	1.40
Xylenols	2.15	2.25	13.24
Others	4.05	2.65	0.22
α-phenol	29.2	21.74	45.5
Phenol to alkylates	24.2	18.50	33.5
O/C alkylation	0.49	0.16	0.38

Reaction conditions : Temperature = 673 K; Pressure = Atmospheric

Activation temperature = 723 K; WHSV = 1.3 h^{-1}; Phenol : methanol (mole ratio) = 1 ; TOS = 4 h

*Reaction temperature 523 K.

3. **Isomerization**

C_6H_{14} ---------> 

C_6H_{14} ---------> 

C_6H_{14} ---------> 

C_6H_{14} ---------> 

4. **Cyclization**

C_6H_{14} $\xrightarrow{-H_2}$ $C_5H_9CH_3$ (Methyl cyclopentane)

C_6H_{14} $\xrightarrow{-H_2}$ C_6H_{12} (Cyclohexane)

5. **Aromatization**

C_6H_{14} $\xrightarrow{-4H_2}$ C_6H_6 (Benzene)

n-Hexane produces cracked products according to reaction (2) which is governed by the acidity of the catalyst. ZSM-5 being highly acidic gives more of these lower hydrocarbons, while the isomerization reaction (3) is more easier over mildly acidic catalysts. Reactions (4) and (5) are the cyclization reactions which are favoured by metal functions. However, the aromatization reaction is highly favoured over ZSM-5 at temperatures above 753 K.

4.3.2b Reaction mechanism

The formation of C_1-C_6 paraffins and olefins can be explained as follows[44] ,

$C_6H_{14} + H^+B^- \rightarrow C_6H_{15}^+B^-$

$\rightarrow H_2 + C_6H_{13}^+B^-$ 1

$\rightarrow CH_4 + C_5H_{11}^+B^-$ 2

$\rightarrow C_2H_6 + C_4H_9^+B^-$ 3

$\rightarrow C_3H_8 + C_3H_7^+B^-$ 4

$\rightarrow C_4H_{10} + C_2H_5^+B^-$ 5

The initial process involves the protonation of n-hexane on the Brönsted acid site to form a $C_6H_{15}^+$ carbonium ion. This carbonium ion decomposes to form either hydrogen and a n-hexane carbenium ion [$C_6H_{13}^+$] or a smaller paraffin [$C_{6-n}H_{2(6-n)+2}$], where n changes from 2 to 5 and a small carbenium ion [$C_nH_{2n+1}]^+$, which replaces the proton on the Brönsted base.

Depending on the probabilities of the various steps, the carbenium ions in equations 1 to 5 can either desorb as an olefin or participate in bimolecular reactions. The general form of a bimolecular reaction between a carbenium ion and a gas phase feed molecule can be written as

$$C_6H_{14} + [C_nH_{2n+1}]^+B^- \longrightarrow C_mH_{2m+2}^* + [C_kH_{2k+1}]^+B^- (n \neq m) \qquad 6$$

Where $2 \leqslant n \leqslant 6$, $2 \leqslant m \leqslant 6$, and $2 \leqslant k < 6$.

The chain transfer process involves the rearrangement of the adsorbed carbenium ion before disproportionation or desorption occurs. When such rearrangement is followed by hydride transfer from n-hexane to the rearranged carbenium ion, isomeric paraffins are produced according to general expression

$$C_6H_{14} + i\text{-}[C_nH_{2n+1}]^+B^- \longrightarrow i\text{-}C_nH_{2n+2} + [C_6H_{13}]^+B^-$$

After hydride transfer from n-hexane, the carbenium ion $[C_6H_{13}]^+B^-$ is formed, which on undergoing a number of hydride shifts leads to the formation of a variety of C_6 - isomers. In the last step or in the chain termination step, the desorption of the carbonium ion takes place as an olefin after ß-scission or remains on the surface to form coke.

As already mentioned, omega is a large pore zeolite with unidimensional pores. The aluminosilicate framework consists of a column of gmelinite cages bridged by oxygen atoms to give a 12-membered cylindrical main channel system along with the crystallographic c-axis. Due to this unidimentional character of the pores in omega and the quasi-inaccessibility of the gmelinite cage, omega shows very high sensitivity for coking and deactivates rapidly in most of the catalytic reactions[45,46].

The activity of zeolite omega and its gallium analog in the transformation of n-hexane has been studied as a function of reaction parameters and the results are discussed in the light of structural and physicochemical characteristics.

Minachev and Esakov[47], Guisnet and Perot[48], have established that activity and selectivity in alkane hydroconversion over a bifunctional catalyst depends on the balance between the hydrogenation and the acidic functions. Guisnet and Perot[48] have also reported that a platinum content

of 0.5 wt.% is the optimum concentration of the metal function for the hydrogenation and dehydrogenation activities in platinum loaded mordenite and Y. However, when the acidic function is not sufficiently balanced, the selectivity for cracking products increases.

The unit cell composition of the catalyst used in the present n-hexane conversion studies are tabulated in Table 4.1. AR grade n-hexane is used as reactant in the present study.

4.3.3b Influence of temperature and platinum impregnation over Al-omega

The results of the conversion of n-hexane over H-Al-omega and Pt-H-Al-omega at 523 and 723 K are presented in Table 4.9. The data reveal that C_2-C_5 and isomeric C_6 hydrocarbons are the major products over H-Al-omega. The deactivation of the catalyst is very fast with significant deactivation in just 3 h (Fig. 4.3). Coq *et al.*[46] have also reported such a rapid deactivation during the hydroconversion of n-hexane over omega in the absence of platinum. When the sample was impregnated with 0.1% platinum, there was a remarkable change in the product pattern with maximum conversion to C_6 isomeric products. The deactivation of the catalyst was not entirely suppressed, though it was significantly reduced. A decrease in the conversion of n-hexane with an increase in platinum loading was observed[46]. Even at a conversion level as low as 2% the reaction rate decreased drastically on Pt loading. They attributed it to the presence of platinum particles inside the channels of the zeolite, slowing down the diffusion of reactants.

A comparison of the activity of H-Al-omega at two different temperatures is also included in Table 4.9. At the higher temperature (723 K) the conversion is more and the cracking activity is also enhanced by a factor of about 3.5, while the isomerization activity is decreased. Unlike in the case of the medium pore zeolites such as ZSM-5, cyclic products and aromatics are not found to be formed to any significant extent.

4.3.4b Influence of space velocity

The results of the studies on the influence of the space velocity in the range 1.3 to 3.33 h^{-1} on product distribution in the case of Pt-H-Al-omega are presented in Fig.4.4. At higher space velo-

Table 4.9 Product distribution during hydroconversion of n-Hexane

Product breakup Wt %	Catalyst H-Al-omega (523 K)	H-Al-omega (723 K)	Pt-H-Al-omega 523 K	Pt-H-Al-omega (723 K)
C_1	0.01	0.93	0.01	0.58
$C_2+C_2^=$	0.06	2.30	0.06	4.27
$C_3+C_3^=$	2.75	15.49	2.15	25.10
iC_4	2.70	2.57	4.50	4.18
nC_4	0.99	1.41	0.90	2.99
$C_4^=$	0.01	0.28	0.01	1.14
iC_5	1.62	0.97	3.37	1.95
nC_5	0.68	0.35	0.80	0.80
$22DMC_4$	0.80	0.10	3.49	0.12
$23DMC_4$	1.19	0.19	3.50	0.39
2 MP	3.48	0.64	11.44	1.37
3 MP	2.13	0.59	6.96	1.00
n-Hexane	83.47	73.19	62.50	54.51
MCP	0.04	0.11	0.08	0.12
Aromatics	.03	0.10	0.10	0.84
Others	0.04	0.18	0.12	0.64
% n-Hexane	16.53	26.21	37.50	45.49

Reaction Conditions : Temp = 523 and 723 K; Press = Atmospheric
WHSV = 1.32 hr^{-1}; H_2/HC (mole) = 1
Activation Temp = 773 K; TOS = 30 min.

Others include C_5 and higher hydrocarbons.

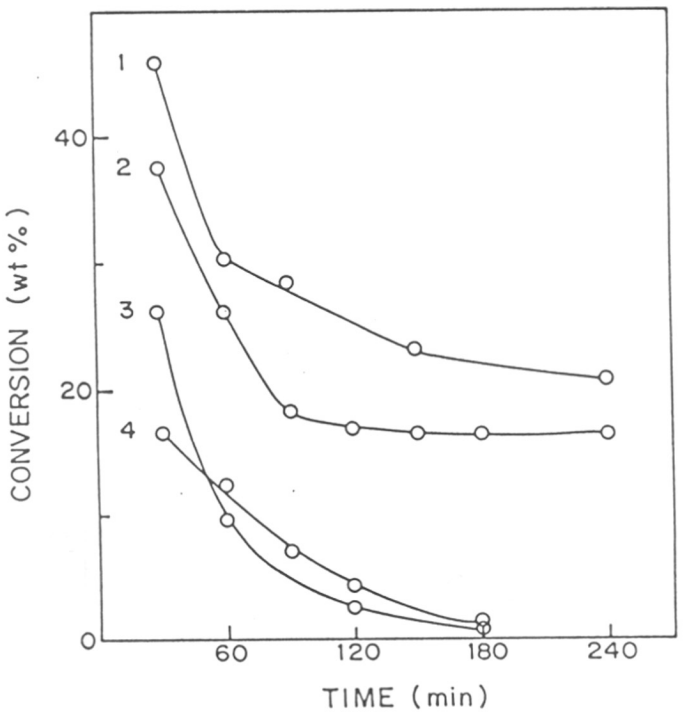

FIG. 4·3 : INFLUENCE OF TEMPERATURE AND DURATION OF RUN ON n-HEXANE CONVERSION
1) Pt-H-Al-OMEGA(723K), 2) Pt-H-Al-OMEGA(523K), 3) H-Al-OMEGA(723K) AND 4) H-Al-OMEGA(523K)

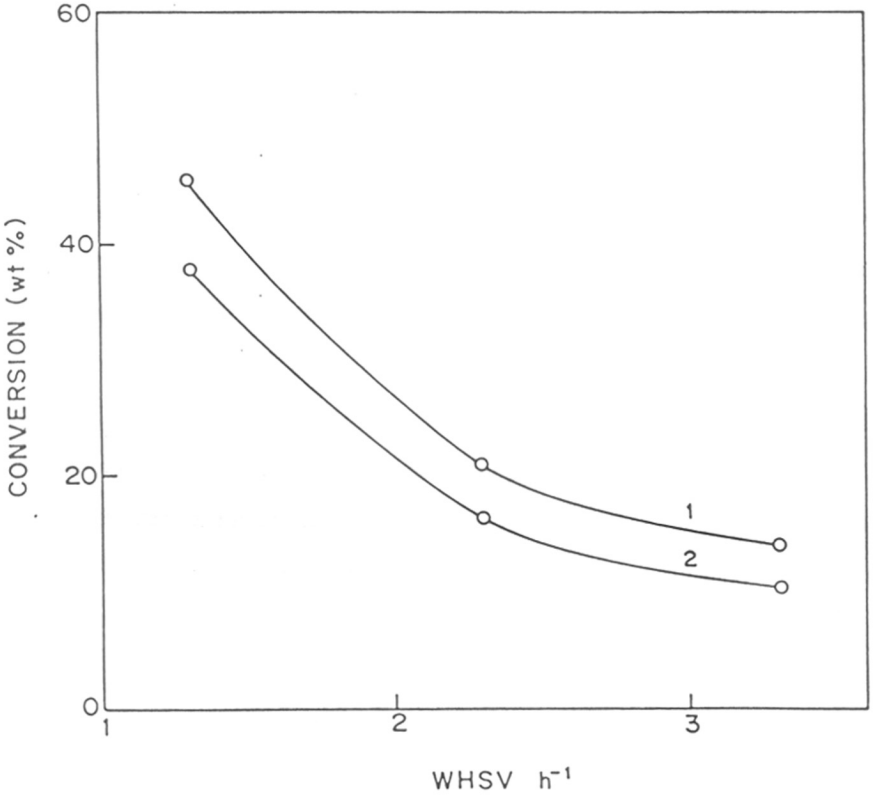

FIG.4·4: EFFECT OF WHSV ON CONVERSION OF n-HEXANE AT 1) 723K AND 2) 523 K

cities, the conversion is reduced at both the temperatures. As expected, the cracking and isomerization activities are also low. At lower space velocities, conversion of n-hexane is more. The deactivation is more rapid at higher space velocities.

4.3.5b Influence of temperature and platinum impregnation over Ga-omega

Conversion of n-hexane over H-Ga-omega and Pt-H-Ga-omega with metal to silicon ratio equal to that of Al-omega at 523 and 723 K are presented in Table 4.10. The decrease in the activity of H-Ga-omega at both the temperatures (Fig. 4.5) is due to fast deactivation as explained earlier for H-Al-omega. From Fig. 4.5, it is observed that by the impregnation of 0.1% Pt a remarkable change in the activity is observed. It is observed (Table 4.10) that H-Ga-omega produces more cracked products and Pt-H-Ga-omega produces more isomeric products. The conversion of n-hexane is low at the lower temperature (523 K) and even though an increase in activity is observed at higher temperature, it is still less than that of Al-omega. The sorption studies also showed (explained in chapter III) lower sorption values for H-Ga-omega. Irrespective of the conversion level, both Al- and Ga-omega samples have shown isomerization activities at the lower temperature, whereas, only Ga-omega shows high isomerization activity even at the higher temperature. This is probably due to the decrease in the acidity due to the deposition of Ga-oxide on the surface or due to the inherent lower acidity of the gallosilicate when compared to the aluminosilicate. The activity of the gallosilicate zeolite could be restored only if the regeneration is carried out in a controlled manner by heating upto 723 K for a long duration (> 10 h). At higher temperatures of calcination the original activity could not be restored due to the loss of crystallinity resulting in the blockage of pores/channels by the dislodged species. In order to verify the thermal effects, calcination of the samples were done at different temperatures and the XRD patterns were recorded (in Fig. 3.2 and Table 3.2, Chapter III).

4.3.6b Influence of Ga_2O_3 loading over Pt-H-Al-omega

For further studies, more samples of Pt-H-Al-omega zeolites with addition of gallium oxide (2%, 3%) were prepared. n-Hexane conversion at two different temperatures (523 and 723 K) were studied and the results are presented in Tables 4.11 and 4.12. The sample with 2% Ga_2O_3 content

Table 4.10 Product distribution during hydroconversion of n-Hexane

Product breakup Wt %	Catalyst H-Ga-omega (523 K)	H-Ga-omega (723 K)	Pt-H-Ga-omega 523 K	Pt-H-Ga-omega (723 K)
C_1	-	0.62	-	0.65
$C_2+C_2^=$	0.01	2,52	0.01	2.56
$C_3+C_3^=$	0.11	9.71	0.16	8.35
iC_4	0.14	2.04	0.45	1.79
nC_4	0.07	1.39	0.10	1.16
$C_4^=$	-	1.12	0.01	0.85
iC_5	0.11	0.68	0.10	0.58
nC_5	0.16	0.34	0.31	0.27
$22DMC_4$	0.02	0.15	0.58	0.10
$23DMC_4$	0.13	0.10	0.25	0.52
2 MP	0.36	0.47	0.56	9.74
3 MP	0.48	0.52	0.83	5.95
n-Hexane	98.24	79.51	96.48	67.03
MCP	0.13	0.13	0.10	0.13
Aromatics	.03	0.15	-	0.14
Others	0.01	0.55	0.06	0.18
∠ n-Hexane	1.76	20.49	3.52	32.97

Reaction Conditions : Temp = 523 and 723 K, Press = Atmospheric
WHSV = 1.32 hr^{-1}; H_2/HC (mole) = 1
Activation Temp = 773 K; TOS = 30 min.

Others include C_5 and higher hydrocarbons.

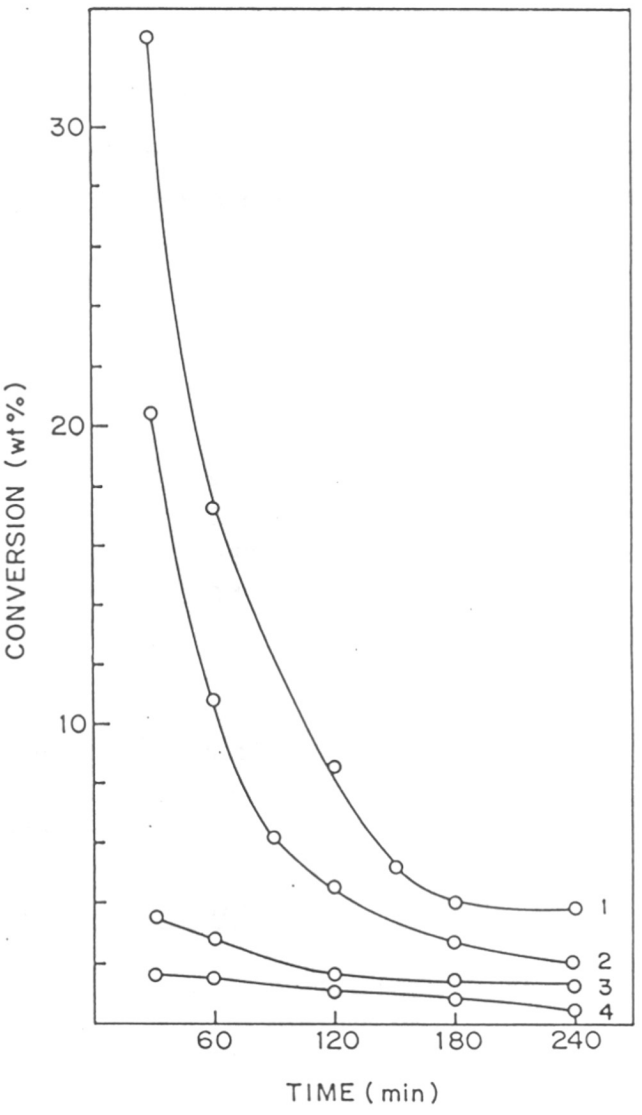

FIG.4·5 : INFLUENCE OF TEMPERATURE AND DURATION OF RUN ON n-HEXANE CONVERSION :
1) Pt-H-Ga-OMEGA(723K), 2) H-Ga-OMEGA (723K),
3) Pt-H-Ga-OMEGA (523K) , 4) H-Ga-OMEGA (523 K)

Table 4.11 Product distribution during hydroconversion of n-Hexane

Product breakup Wt %	Catalyst Pt-H-Al-omega	Pt-H-Al-omega (2% Ga_2O_3)	Pt-H-Al-omega (3% Ga_2O_3)
C_1	0.01	0.05	0.06
$C_2+C_2^=$	0.06	0.52	0.37
$C_3+C_3^=$	2.14	7.20	6.79
iC_4	4.50	9.80	6.50
nC_4	0.92	3.40	2.78
$C_4^=$	0.01	0.40	0.20
iC_5	3.37	5.60	3.79
nC_5	0.80	2.97	1.57
$22DMC_4$	3.49	3.62	1.93
$23DMC_4$	3.50	3.09	1.99
2 MP	11.44	10.82	6.27
3 MP	6.96	6.60	3.72
n-Hexane	62.50	45.50	63.82
MCP	0.08	0.10	0.03
Aromatics	0.10	0.05	0.03
Others	0.12	0.18	0.15
$\mathcal{C}$ n-Hexane	37.50	54.50	36.18

Reaction Conditions : Temp = 523 K; Press = Atmospheric
WHSV = 1.32 hr^{-1}; H_2/HC (mole) = 1
Activation Temp = 773 K; TOS = 30 min.

Others include C_5 and higher hydrocarbons.

Table 4.12 Product distribution during hydroconversion of n-Hexane

Product breakup Wt %	Catalyst Pt-H-Al-omega (723 K)	Pt-H-Al-omega (2% Ga_2O_3) (723 K)	Pt-H-Al-omega (3% Ga_2O_3) 723 K
C_1	0.58	1.06	0.70
$C_2+C_2^=$	4.27	7.65	3.25
$C_3+C_3^=$	25.10	29.50	15.62
iC_4	4.18	4.34	1.85
nC_4	2.99	3.92	1.97
$C_4^=$	1.14	0.70	1.86
iC_5	1.95	2.28	1.15
nC_5	0.80	1.23	1.06
$22DMC_4$	0.12	0.30	0.39
$23DMC_4$	0.39	0.67	0.89
2 MP	1.37	2.61	4.24
3 MP	1.00	1.77	2.75
n-Hexane	54.51	42.08	61.97
MCP	0.12	0.11	0.12
Aromatics	0.84	0.97	0.90
Others	0.64	0.81	1.28
C_6- n-Hexane	45.49	57.92	38.03

Reaction Conditions : Temp = 723 K; Press = Atmospheric
WHSV = 1.32 hr^{-1}; H_2/HC (mole) = 1
Activation Temp = 773 K; TOS = 30 min.

Others include C_5 and higher hydrocarbons.

showed higher conversions at both the temperatures. The increase in the conversion is attributed to the increase in Lewis acid sites formed during the reduction of the gallium oxide. Such creation of Lewis sites in Ga_2O_3 supported on H-ZSM-5 has already been postulated by earlier workers[29,49,50]. The sample containing 3% Ga_2O_3 showed lower activity as compared to the former, which may be due to the blockage pores and channels at the higher Ga_2O_3 loading. At lower temperatures, the isomerization activity is comparable to the cracking activity; but at higher temperatures the major reaction is cracking. Both the catalysts deactivated within 12 to 14 h. After regeneration at 773 K, the initial activity could be restored.

A comparative study of n-hexane hydroconversion over different zeolites is carried out at 523 and 723 K is presented in Tables 4.13 and 4.14 respectively. From n-hexane hydroconversion studies it is observed that H-Al-omega deactivates fast and is sensitive to coke formation. The impregnation of 0.1 wt.% platinum brings about a remarkable change in the product pattern and stability. A similar effect on the addition of platinum is also noticed in the case of H-Ga-omega, though to a smaller extent. The addition of 2% Ga_2O_3 in Pt-H-Al-omega increases the activity of H-Al-omega. This is probably, due to the creation of Lewis acid sites by Ga_2O_3. However, more Ga_2O_3 loading (3 %) decreases the activity probably due to partial blockage of the pores and channels by more amount of Ga_2O_3.

Table 4.13 Product distribution during hydroconversion of n-Hexane

Product breakup Wt %	Catalyst Pt-H-Al-omega	Pt-H-Al-omega (2% Ga_2O_3)	Pt-H-Al-omega (3% Ga_2O_3)	Pt-H-Ga-omega
C_1	0.01	0.05	0.06	-
$C_2+C_2^=$	0.06	0.52	0.37	0.01
$C_3+C_3^=$	2.14	7.20	6.79	0.16
iC_4	4.50	9.80	6.50	0.45
nC_4	0.92	3.40	2.78	0.10
$C_4^=$	0.01	0.40	0.20	0.01
iC_5	3.37	5.60	3.79	0.10
nC_5	0.80	2.97	1.57	0.31
$22DMC_4$	3.49	3.62	1.93	0.58
$23DMC_4$	3.50	3.09	1.99	0.25
2 MP	11.44	10.82	6.27	0.56
3 MP	6.96	6.60	3.72	0.83
n-Hexane	62.50	45.50	63.82	96.48
MCP	0.08	0.10	0.03	0.10
Aromatics	0.10	0.05	0.03	-
Others	0.12	0.18	0.15	0.06
-(- n-Hexane	37.50	54.50	36.18	3.52

Reaction Conditions : Temp = 523 K; Press = Atmospheric
WHSV = 1.32 hr^{-1}; H_2/HC (mole) = 1
Activation Temp = 773 K; TOS = 30 min.

Others include C_5 and higher hydrocarbons.

Table 4.14 Product distribution during hydroconversion of n-Hexane

Product breakup Wt %	Catalyst Pt-H-Al-omega	Pt-H-Al-omega (2% Ga_2O_3)	Pt-H-Al-omega (3% Ga_2O_3)	Pt-H-Ga-omega
C_1	0.58	1.06	0.70	0.65
$C_2+C_2^=$	4.27	7.65	3.25	2.56
$C_3+C_3^=$	25.10	29.50	15.62	8.35
iC_4	4.18	4.34	1.85	1.79
nC_4	2.99	3.92	1.97	1.16
$C_4^=$	1.14	0.70	1.86	0.85
iC_5	1.95	2.28	1.15	0.58
nC_5	0.80	1.23	1.06	0.27
$22DMC_4$	0.12	0.30	0.39	0.10
$23DMC_4$	0.39	0.67	0.89	0.52
2 MP	1.37	2.61	4.24	9.74
3 MP	1.00	1.77	2.75	5.95
n-Hexane	54.51	42.08	61.97	67.03
MCP	0.12	0.11	0.12	0.13
Aromatics	0.84	0.97	0.90	0.14
Others	0.64	0.81	1.28	0.18
$\mathcal{C}$ n-Hexane	45.49	57.92	38.03	32.97

Reaction Conditions : Temp = 723 K; Press = Atmospheric
WHSV = 1.32 hr^{-1}; H_2/HC (mole) = 1
Activation Temp = 773 K; TOS = 30 min.

Others include C_5 and higher hydrocarbons.

4.4 CONCLUSION

In the alkylation of phenol with methanol over different omega zeolite samples, it is seen that the temperature around 673 K was optimum, more acidic catalysts like H-Al-omega and La-Al-omega samples indicated higher activity than different degree of Na- exchanged Al-omega and H-Ga-omega samples.

In n-hexane conversion reaction H-Al-omega and H-Ga-omega deactivate fast and are sensitive to coke formation. The impregnation of 0.1% platinum brings about a remarkable change in the product pattern and stability of the zeolite. Addition of 2% Ga_2O_3 in Pt-H-Al-omega increases the activity. At lower temperature, isomeric products are higher and at high temperature, the decomposition is more.

REFERENCES

1. Tielen, M., Geelen, M. and Jacobs P.A., in "Proc. ZEOCAT Symp., Siofok, Hungary, 1985 Acta Physica et Chemica, 31, 1 (1985).
2. Weitkamp J., Beyer H., Borbely G., Cortes-Corberan V., and Ernst S., Chem.-Ing.-Tech., **58**, 969 (1986).
3. Jansen J., Biron E., and van Bekkum H., Stud. Surf. Sci. Catal. **37**, 133 (1988).
4. Hoelderich W.F. and Galli E., Ger. Chem. Eng., **8**, 337 (1985).
5. Hoelderich W.F., Hesse M. and Naeumann F., Angew. Int. Edit., **27**, 226 (1988).
6. Jacobs, P.A., Jacobs, J.M. and Parton R., in "Proc. Int. Symp. on Zeolites as Catalysts, Sorbents and Detergent Builders," Wurburg, FRG, 1988, Elsevier, Amsterdam 163, (1989).
7. Lewis P.J. and Dwyer F.G., Oil Gas J., **75**, 55 (1977).
8. Dwyer, F.G., in "Chemical Industries, Vol.5" (Ed. W.R. Moser), Marcel Dekker, New York p. 39 (1981).
9. Keading, W.W., Barile G.C. and Wu M.M., Catal. Rev.-Sci.Eng., **26**, 597 (1984).
10. Chen, F.R., Coudurier G. and Naccache C., Stud. Surf. Sci. Catal. **28**, 733, (1986).
11. Fraenkel D., Cherniavsky M., Ittah B. and Levy M., J. Catal. **101**, 273, (1986).
12. Yashima T., Sato, K., Hayasaka T. and Hara N., J. Catal. **26**, 303 (1972).
13. Unland M.L. and Barker G.E. in "Chemical Industries Vol.5", (Ed. W.R. Moser), Marcel Dekker, New York p. 39, (1981).
14. Garces J.M., Vrieland G.E., Bates S.I. and Scheidt F.M., Stud. Surf. Sci. Catal., **20**, 67 (1985).

15. Lacroix C., Deluzarche A., Kiennemann A. and Boyer A., Zeolites, **4**, 109 (1984).

16. Chantal P.D., Kaliaguine S. and Grandmaison J.L., Appl. Catal. **18**, 133, (1985) and Stud. Surf. Sci. Catal., **19**, 93 (1984).

17. Namba S., Yashima T., Itaba Y. and Hara N., Stud. Surf. Sci. Catal. **5**, 105 (1980).

18. Balsama S., Beltrame P., Beltrame P.L., Carniti P., Forni L. and Zuretti G., Appl. Catal. **13**, 161 (1984).

19. Dakuchaeva T.G., Kozhevnikow S.A., Sibarov D.A. and Timofeev V.F., Neftekhimiya (1985).

20. Dobres R.M. and Baker R.W., Catalysis (Ed. P.H. Emmett), 6, Reinhold, New York (1958).

21. Weisz P.R., Adv. Catal., **13**, 137 (1962).

22. Sinfelt J.H., Adv. Chem. Eng. **5**, 37 (1964).

23. Ciapetta F.G., Wallace D.N., Catal. Rev., **5**, 67 (1971).

24. Sterba M.J., Haensel V., Ind. Eng. Chem. Prod. Res. Dev., **15**, 2 (1976).

25. Scire S., Maggiore R., Galvango S., Crisafulli and Salarino L., React. Kinet. Catal. Lett. **40No.2**, 349 (1989).

26. Maggiore R., Scire S., Craisafulli G., Toscano, and Galvango S, React. Kinet. Catal. **41No.1**, 153 (1990).

27. Sirokman G., Sendoda Y. and Ono Y., Zeolite **6**(301), 299 (1986).

28. Ono Y., Catal. Rev. Sci. Eng., **34**(3), 179 (1992).

29. Kanai J. and Kawata N., App. Catal. **55**, 115 (1989).

30. Perrotta A.J., Kibby C., Mitchell B.R. and Tucci E.R., J. Catal. **55**, 240 (1978).

31. Barrer R.M. and Villigier H.Z., Kristallogr. **128**, 352 (1969).

32. Galli E., Cryst. Struct. Commun., **3**, 339 (1974).

33. Rinaldi R., Pluth J.J. and Smith J.V., Acta. Crystallogr. **B 31**, 1603 (1975).

34. Venuto, P.B., Hamilton L.A., Landis P.S. and Wise J.J., J. Catal. **5**, 81 (1966).

35. Venuto P.B., Hamilton L.A., Landis P.S. and Wise J.J., J. Catal., **5**, 484 (1966).

36. Venuto P.B. and Wu L.E., J. Catal., **15**, 205 (1969).

37. Venuto P.B. and Landis P.S., Adv. Catal., **18**, 259 (1968).

38. Parton R.F., Jacobs J.M., Van Ooteghem H. and Jacobs P.A., Int. Symp. on Zeolites as Catalysts and Detergent Builders, Wurzburg (1988).

39. Pierantozzi R. and Nordquist A.F., Appl. Catal., **21**, 263 (1986).

40. Corma A., Garcia H. and Primo J., J. Chem. Res. (S), 40, (1988).

41. Balsama S., Beltrame P., Beltrame P.L., Carniti P., Forni L. and Zuretti G., Appl. Catal., **13**, 161 (1984).

42. Marczewski M., Perot G. and Guisnet M., Stud. Surf. Sci. Catal., **41**, 273 (1988).

43. Haung F.Y. and Yang S.M., Hua Hsuech, **44**, 6 (1986).

44. Gorten W.A., Wojciechowski., J. Catal. **140**, 262 (1993).

45. Chauvin B., Fajula F., Figueras F., Gueguen C. and Bousquet J., J. Catal. **111**, 94, 105 (1988).

46. Coq B., Figueras F. and Rajaofanova V., J. Catal. **114**, 321 (1988).

47. Minachev Kh.M. and Isakov Ya. I., "Zeolite Chemistry and Catalysis" (J.A. Rabo, Ed.) p. 552, ACS Monograph 171, Amer. Chem. Soc., Washington DC, (1976).

48. Guisnet M. and Perot G., "Zeolites : Science and Technology" (Ribeiro F.R., Rodrigues A.E., Rollman L.D. and Naccache C., (Eds.), 397, Nijhoft, The Hague (1984).

49. Price G.L. and Kanazirev, J. Catal. **126**, 267 (1990).

50. Dooley K.M., Guidry T.F. and Price G.L., J. Catal. **157**, 66 (1995).

Chapter V

Summary

SUMMARY

Wide pore zeolites are extensively used in petroleum and petrochemical industry. In recent years much work on wide pore zeolites like Y and mordnite in the synthesis of fine chemicals is reported. Zeolite omega is a synthetic counterpart of the mineral mazzite. The aluminosilicate framework consists of columns of gmelinite cages bridged by oxygen atoms to give a 12 membered cylindrical main channel system along the crystallographic c axis with a diameter of 7.4Å. The topology of zeolite omega consists of one dimensional channel structure. The silica alumina ratio of omega zeolite varies from 5-10. The Na form is thermally stable, however, the protonic form of Al-omega is stable upto 823 K. Due to the high alumina content and more acidic nature like faujasite with wide pore, omega zeolite is a potential material for catalytic purpose. Hence detailed study was undertaken in the synthesis, modification, characterization and catalytic applications.

Zeolite Al-omega was synthesized hydrothermally using TMAOH (25 wt. % methanol) between temp. range 383 to 413 K. The crystallization kinetics was studied to obtain the apparent activation energies of the nucleation process and crystal growth process. The crystallization kinetics curve at different temperatures show sigmoidal or S shape in nature indicating different rates of crystallization at different times. The curves show that the kinetics of crystallization depends on the temperature. The crystallization was treated as first order reaction as the major part of the crystallization curve is almost linear. Since nucleation is the rate determining step, the activation energy of nucleation is calculated from the Arrhenius equation which expresses the temperature dependance of the rate of nucleation. The value for apparent activation energy of nucleation (En) is 82.9 KJ mol^{-1} and that of crystallization (Ec) is 65.6 KJ mol^{-1}.

The gallosilicate analog was synthesized with the same oxide mole composition except that gallium nitrate was used in place of sodium aluminate. In order to maintain the sodium content equivalent to that in the sodium aluminate, additional quantity of sodium hydroxide was added during the synthesis. The incorporation of Ga in the omega framework was confirmed by chemical analysis, XRD, framework IR and solid state MAS NMR spectra.

From XRD, the lowering of 2Θ values for the XRD reflections in Ga-omega as compared to those in Al-omega was observed. The unit cell volume obtained from XRD data for Ga-omega (2225 $Å^3$) was found to be atleast marginally higher than that (2210 $Å^3$) for Al-omega zeolite. The IR spectra of Ga-omega show a lower wavenumber for all the structure-sensitive vibrations, due to incorporation of heavier Ga atoms, as compared to those of Al-omega. The ^{71}Ga MAS NMR spectrum confirms the tetrahedral coordination of Ga^{3+} species in the omega framework. Al-omega exhibited spherical crystallites (3 μm), whereas a cylindrical morphology (3.5 - 8.0 μm) was obtained for Ga-omega. Chemical analysis shows that the sodium occupancy in Ga omega (90%) is higher than that in Al-omega (79%). The sodium form of Al and Ga-omega are stable upto a temperature around 1173 K. Sorption uptakes were found to be higher for Al-omega than for Ga-omega.

XRD profiles and thermo analytical data show that NH_4-Ga-isomorph of omega possesses considerably lower thermal stability. The thermal stability is also enhanced to some extent by La exchange;whereas the protonic forms seems to be responsible for lowering the thermal stability. The protonic form of aluminum is comparatively more stable than that of protonic form of Ga-omega. FTIR spectra in framework region show highly crystalline nature of all synthesized samples. It is also revealed higher thermal stability of Al compared to Ga-omega zeolite. Spectra in hydroxyl stretching region and of chemisorbed pyridine show both Brönsted and Lewis acidity which are stronger in Al-omega than in Ga-omega zeolite. Thus, FTIR spectra clearly shows that Ga cations are occupying in framework position in Ga-omega zeolite. Thermo analytical data revealed two or three different stages of weight loss in TG curves. Both surface area and micropore volume

estimated from low temperature nitrogen sorption increased on proton exchange and decreased in the lanthanum exchange zeolite. The equilibrium sorption uptakes were found to be lower in gallium isomorphs than those in aluminum isomorphs. The type-I ammonia sorption isotherms showed that the hold-up capacity is highest in lanthanum exchange omega followed by protonic form. The ammonia sorption isotherm data were satisfactorily represented by applying Langmuir, BET, Dubinin equations. However, Freundlich and Sips equations showed limited applicability to the ammonia sorption data. Statistical models of Langmuir and Volmer indicated that ammonia sorption in omega zeolite broadly follow localized sorption model with molecule-molecule interaction. The chemical potential for cation exchanged forms are higher than the corresponding sodium forms of zeolites. Na-Al-omega offered the most homogeneous surface for NH_3 sorption whereas the other cationic forms showed heterogeneous character of the surface. The proton form of Al-omega showed highest value of isosteric heat (around 72 kJ mol^{-1}) for ammonia sorption. The sequence of isosteric heat follows H-Al-omega > La-Al-omega > La-Ga-omega > H-Ga-omega > Na-Ga-omega > Na-Al-omega.

The catalytic activity of both Al-and Ga-omega zeolites in the alkylation of phenol using methanol and hydroconversion of n-hexane reactions are studied. The alkylation was studied to evaluate the effect of reaction parameters on the product distribution. Temperature around 673 K was optimum for this reaction. Higher temperature increased gaseous products due to methanol reaction whereas at lower temperature phenol conversion was low. More acidic catalysts like protonic Al-omega zeolite and La-Al-omega zeolite indicated only alkylation of the nucleus. There is no para selectivity in the reaction products. o-Cresol is about 60% of the total cresols. m-Cresol is formed by 1) the isomerization of the primary product p-cresol and 2) by the rearrangement of anisole. Usually ratio of O/C alkylation is high. Some of these secondary reactions like meta cresol formation is noticed depending on the experimental conditions. At high methanol to phenol ratio and at high temperatures methyl anisole and xylenols are also observed. The catalyst deactivated in short time. However, the Ga-analog did not show much of the catalytic activity. The sequence of phenol alkylation activity is H-Al-omega > La-Al-omega > Na-Al-omega > H-Ga-omega.

In n-hexane conversion reaction H-Al-omega and H-Ga-omega are sensitive to coke formation and deactivate fast. Impregnation of 0.1 % platinum in both H-Al-omega and H-Ga-omega brings about remarkable change in the product pattern and stability of the zeolite catalysts. The H-Pt-Al-omega shows higher activity than H-Pt-Ga-omega over the entire range of reaction temperature studied. Irrespective of the conversion level both Al- and Ga-omega samples have shown isomerization activities at lower temperature, whereas only Ga-omega shows high isomerization activity even at high temperature. Addition of 2% Ga_2O_3 in Pt-H-Al-omega sample showed higher activity and stability. The activity sequence for n-hexane conversion reaction is 2% Ga_2O_3 Pt-H-Al-omega > Pt-H-Al-omega > Pt-H-Ga-omega > H-Al-omega > H-Ga-omega.

In general, from the above studies, it is observed that H-Al-omega is more active than La-Al-omega and H-Ga-omega zeolite, which is in broad agreement with thermal, FTIR, sorption kinetics with different probe molecules and ammonia sorption isotherm analysis.

LIST OF PUBLICATIONS AND PATENTS

Publications :

(1) Hydrothermal Synthesis of Al- and Ga- Substituted Omega Zeolite,
Mirajkar S.P., Eapen M.J., Tamhankar S.S., Rao B.S. and Shiralkar V.P., J. Inc. Phen., **16**, 139 (1993).

(2) Sorption Properties of Titanosilicate Molecular Sieves,
Mirajkar S.P., Thangaraj A. and Shiralkar V.P., Phys. Chem. **96**, 3073 (1992).

(3) Sorption of Ammonia in Cation Exchanged Omega Zeolite and Gallium Analog,
Mirajkar S.P., Eapen M.J., Rao B.S. and Shiralkar V.P. (Communicated).

(4) Physico-chemical Properties of Al- and Ga-Analog of Zeolite Omega,
Mirajkar S.P., Hegde S.G., Ramaswamy V., Shiralkar V.P. and Rao B.S. (Communicated).

Patent :

A process for the "Preparation of Novel Omega Type Gallosilicate Composite Material", Ratnasamy P., Shiralkar V.P., Mirajkar S.P., Rao B.S. and Eapen M.J., IND. PAT. APPL. No. 24/DEL/92.